

Aus dem Max-Planck-Institut für Hirnforschung

# Reizabhängige Synchronisation im Sehsystem der Katze

Dissertation  
zur Erlangung des Doktorgrades  
der Naturwissenschaften

vorgelegt beim Fachbereich Physik  
der Johann-Wolfgang-Goethe-Universität  
in Frankfurt am Main

von  
Tilmann Kluge  
aus Hameln

Frankfurt 2004  
(DF1)

Vom Fachbereich Physik der Johann-Wolfgang-Goethe-Universität  
als Dissertation angenommen.

Dekan: Prof. Dr. Dörner

Gutachter: Prof. Dr. Ronald Tetzlaff  
Prof. Dr. Wolf Singer

Datum der Disputation: 04. Juni 2004

# TABLE OF CONTENTS

CHAPTER 1: INTRODUCTION .....	1
CHAPTER 2: NEUROPHYSIOLOGICAL BACKGROUND .....	7
2.1.Introduction .....	7
2.2.The Neuron .....	8
2.3.The Visual System of the Cat .....	9
2.4.Binding Problem and Neuronal Synchronization .....	14
CHAPTER 3: MATERIALS AND METHODS .....	19
3.1.Preparation .....	19
3.2.Data Acquisition .....	21
3.3.Stimuli .....	22
3.3.1.The Tuning Curve Stimulus .....	23
3.3.2.Random Dot Stimulus with Changing Stimulus Coherence .....	25
3.3.3.The Shape-From-Motion Stimulus .....	26
3.4.Indices for Quantification of the Tuning curve .....	30
3.4.4.Preferred Direction and Direction index .....	30
3.4.5.Tuning Width Index .....	32
3.5.Analysis of Spike Signals .....	33
3.5.6.Quantification of Firing Rates .....	33
3.5.7.Cross Correlation Analysis .....	34
3.6. Analysis of the Local Field Potential .....	38
3.6.8.Power Spectrum of the LFP .....	39
3.6.9.Spike-Triggered Average .....	40
3.6.10.Spike-Field-Coherence .....	41
3.7.Statistical Analysis .....	43
3.7.11.Normal distribution .....	43
3.7.12.The t-Test .....	45
3.7.13.Analysis of Variance (ANOVA) .....	46
3.7.14.Fisher's Protected Least Significant Difference Test .....	48
CHAPTER 4: INCOHERENT MOTION IN AREAS 17 AND PMLS .....	49
4.1.Introduction .....	49
4.2.Tuning Behavior of Spatially Incoherent Stimuli .....	55
4.2.1.Introduction .....	55
4.2.2.Results .....	56
Area 17 .....	56
Area PMLS .....	59
4.2.3.Discussion .....	61
4.3.Effects of Visual Noise on Firing Rates	

in Areas 17 and PMLS .....	66
4.3.4.Introduction .....	66
4.3.5.Results .....	67
Area 17 .....	68
Area PMLS .....	71
Stimulation in the null direction .....	73
4.3.6.Discussion .....	74
4.4.Synchrony in Incoherent Stimuli .....	78
4.4.7.Introduction .....	78
4.4.8.Results .....	79
Area 17 .....	79
Area PMLS .....	82
4.4.9.Discussion .....	86
4.5.Power Spectra of the Local Field Potential .....	94
4.5.10.Introduction .....	94
4.5.11.Results .....	95
Area 17 .....	95
Area PMLS .....	98
4.5.12.Discussion .....	101
4.6.Spike Field Coherence .....	105
4.6.13.Introduction .....	105
4.6.14.Results .....	105
Area 17 .....	105
Area PMLS .....	109
4.6.15. Discussion .....	113
4.7.Summarizing Discussion .....	115
4.8.Conclusions .....	123
CHAPTER 5: ANALYSIS OF SHAPE-FROM-MOTION STIMULI IN AREA PMLS .....	125
5.1.Introduction .....	125
5.2.Results .....	129
5.2.1.Shape-From-Motion Tuning Curve .....	129
5.2.2.Processing of Contours in Shape-From-Motion Stimuli .....	133
Effects of static random dot backgrounds on firing rates .....	134
Effects of moving RD backgrounds .....	136
Effect of masking .....	138
Effects of visual noise .....	140
SFM bar with different directions of dot motion .....	140
5.3.Discussion .....	143
Response strength without background .....	143
Effects of static random dot backgrounds on firing rates .....	144
Effects of moving RD backgrounds .....	145
Effects of visual noise .....	147
Effect of masking .....	149
SFM bars with different directions of dot motion .....	150
SFM tuning curve stimulus .....	151

5.4.Conclusion .....	154
CHAPTER 6: OUTLOOK .....	155
CHAPTER 7: BIBLIOGRAPHY .....	161
CHAPTER 8: LIST OF FIGURES .....	175
CHAPTER 9: LIST OF ABBREVIATIONS .....	177



# ZUSAMMENFASSUNG

---

Die vorliegende Arbeit soll einen Beitrag zur Erforschung der Verarbeitungsmechanismen des Gehirns leisten. Die Erregung des komplexen Systems "Hirn" liefert Antworten, deren Analyse zu einem besseren Verständnis dieser Informationsverarbeitung führt. Zu diesem Zweck wurde das Gehirn mit unterschiedlichen visuellen Stimuli angeregt und die hirnelektrischen Signale gemessen, die von Nervenzellgruppen (Multiunits) im visuellen Kortex der Katze ausgesandt wurden. Die verwendeten Stimuli waren ein Streifenmuster sowie eine Zufallspunktverteilung, deren Kohärenz beliebig geändert werden konnte. Darüber hinaus wurden die Antworten auf eine Vielzahl von Stimuli analysiert, die nur aufgrund des Bewegungskontrastes zwischen punktdefiniertem Objekt und Hintergrund zu erkennen sind (Shape-from-Motion- (SFM-) Stimuli). Die aufgenommenen Daten wurden mit Hilfe einer umfangreichen Signalanalyse untersucht. So wurden in Abhängigkeit von der Stimulusbedingung die Anzahl der Nervenimpulse pro Zeiteinheit (Feuerraten), Synchronisation, Frequenzverteilung sowie Kopplung von Aktionspotenzialen und LFP-Daten analysiert.

Die Experimente im ersten Teil dieser Arbeit untersuchten den Einfluss von Kohärenz auf die Verarbeitung von Bewegungsinformation im primären visuellen Areal (A17) und im posteromedialen lateralen suprasylvischen Sulcus (Area PMLS) der Katze. Es konnte gezeigt werden, dass Multiunits in A17 und PMLS sowohl auf Streifenmuster als auch auf Zufallspunktverteilungen antworten und dass die Stärke der Antwort als eine Funktion der Stimulusrichtung variiert. Die Vorzugsrichtung ist in beiden Arealen weitgehend unabhängig von der Art des verwendeten Stimulus, was darauf hindeutet, dass die Stimulusrichtung für Streifenmuster und Zufallspunktmuster in diesen Arealen durch einen einheitlichen Mechanismus bestimmt wird.

Bei einer Abnahme der Stimuluskohärenz zeigen die Multiunits eine Abnahme der Feuerrate, wobei im Vergleich zu PMLS in A17 eine stärkere Abnahme der Kohärenz nötig ist, um die gleiche Abnahme der Feuerrate zu erreichen. Dieses Ergebnis konnte durch die unterschiedlichen Größen der rezeptiven Felder der beiden Areale erklärt werden und ist ein weiterer Hinweis darauf, dass eine wichtige Funktion von PMLS in der Analyse von Bewegung und räumlich verteilter Information liegt. Da beide Areale keine signifikante Änderungen der Feuerrate bei Inkohärenzniveaus von mehr als 50% zeigten, scheinen sie nicht in der Lage zu sein, die Bewegungsrichtung eines inkohärenten Zufallspunktmusters nahe der psychophysischen Detektionsschwelle von 95% auf der Basis von Feuerraten zu erkennen.

Die Korrelation der Aktionspotenziale unterschiedlicher Multiunits zeigte bereits bei einer geringen Abnahme der Stimuluskohärenz eine monotone Verbreiterung des zentralen Maximums in den Korrelogrammen beider Areale. Die Stärke der Synchronisation hingegen war kaum beeinflusst. Darüberhinaus kam es zu einer Verschiebung der Leistung im lokalen Feldpotential (LFP) von hohen hin zu niedrigen Frequenzbereichen. Diese Verschiebung wurde auch für die Kopplung zwischen LFP und Ak-

tionspotenzialen nachgewiesen. Diese Resultate unterstützen die Theorie, dass präzise Synchronisation und hochfrequente Oszillationen ein Mechanismus für die Bindung kohärenter Objekte sind. Sie zeigen darüber hinaus, dass Synchronisation auch nicht kohärente Stimuli binden kann und dass die Verschiebung im LFP hin zu niedrigeren Frequenzen wichtig für die Integration verteilter Information über einen größeren visuellen Raum sein kann. Da bei hohen Inkohärenzniveaus keine präzise Synchronisation mehr nachgewiesen werden konnte, kann jedoch auch die Synchronisation nicht als alleiniger Mechanismus zum Erkennen einer Bewegungsrichtung eines inkohärenten Zufallspunktmusters herangezogen werden.

In den Experimenten im zweiten Teil dieser Arbeit wurde untersucht, wie das Gehirn SFM-Stimuli verarbeitet. Die Auswertungen der Feuerraten haben gezeigt, dass Multiunits in PMLS sowohl auf helligkeitsdefinierte Kontrastbalken als auch auf SFM-Balken reagieren. Die Stärke der Antwort hängt von der Kombination von Stimulus und Hintergrund und von der relativen Bewegungsrichtung zueinander ab. Während ähnliche Feuerraten für Balken mit hohem Kontrast relativ zum Hintergrund und für punktdefinierte Balken gefunden wurde, die sich über einen dunklen Hintergrund bewegten, führte ein statischer Zufallspunkthintergrund zu einer starken Abnahme der von dem SFM-Balken hervorgerufenen Antwort. Ein in die Gegenrichtung bewegter Hintergrund sowie ein reduziertes Kohärenzniveau des Zufallspunkthintergrundes führten dazu, dass die Multiunits auf den SFM-Balken nicht mehr mit einer Zunahme der Feuerraten reagierten. Um die hemmende Wirkung des Hintergrundes aufzuheben, musste der Hintergrund auf einer Fläche des visuellen Feldes, die der Größe des rezeptiven Feldes entsprach, abgedeckt werden. Dieses Ergebnis zeigt, dass die Feuerraten für diese Art Stimulus nicht wesentlich von Arealen außerhalb des rezeptiven Feldes beeinflusst werden.

Zur weiteren Analyse der Fähigkeit von PMLS, SFM-Balken nur aufgrund des Bewegungskontrastes zwischen punktdefiniertem Objekt und Hintergrund zu erkennen, wurde mit Hilfe von zwei Tuningkurven-Stimuli, bei denen sich die Bewegungsrichtung der Punkte innerhalb des Balkens um  $90^\circ$  unterschied, die Vorzugsrichtung der Multiunits bestimmt. Die Auswertung ergab, dass sich die gemessene Vorzugsrichtung der Multiunit um  $45^\circ$  drehte, obwohl sich die Bewegungsrichtung des Balkens selbst nicht änderte. Darüber hinaus wurden verschiedene SFM-Stimuli untersucht, die alle dieselbe Bewegungsrichtung des Balkens, jedoch unterschiedliche Bewegungsrichtungen der Punkte innerhalb des Balkens aufwiesen. Wenn PMLS die Bewegung des SFM-Objekts statt der Bewegung der einzelnen Punkte verarbeitet, sollte die Feuerrate für alle diese Bedingungen identisch sein. Die Ergebnisse zeigen jedoch, dass sich die durch die verschiedenen SFM-Stimuli hervorgerufenen Feuerraten verringerten, je weiter sich die Punkte, die den Balken bildeten, von der Bewegungsrichtung des Balkens – und damit von der Vorzugsrichtung der Multiunit – weg bewegten. Durch dieses Ergebnis konnte gezeigt werden, dass Multiunits in PMLS nicht in der Lage sind, die Richtung von kinetisch definierten Balken zu analysieren und statt dessen nur die Bewegung der einzelnen Komponenten erfassen.



## INHALTSANGABE

---

Unser visuelles System ermöglicht eine schnelle, flexible und zuverlässige Wahrnehmung der uns umgebenden Welt. Dies alles wird von einem komplexen, dynamischen neuronalen Netzwerk vollbracht. Wie genau diese Verarbeitung vonstatten geht und wie hirnelektrische Aktivitäten von räumlich weit entfernten Arealen des Gehirns koordiniert und Informationen über Objekte gebunden werden, ist nach wie vor ungeklärt. Die Suche nach dem zugrunde liegenden Mechanismus ist daher eine der großen Herausforderungen für die heutige Wissenschaft geworden (Überblick siehe Ausgabe 1 von Neuron 24, 1999).

Obwohl die physikalischen Eigenschaften des einzelnen Neurons heute zu weiten Teilen gut bekannt sind, ist im Vergleich dazu das Wissen über die Verarbeitungsmechanismen des Gehirns deutlich geringer. Besonders die Grundlagen höherer kognitiver Funktionen sind weitgehend unbekannt. Antworten auf Fragen nach diesen Verarbeitungsmechanismen liefern überwiegend Experimente, in denen die neuronale Antwort auf ein definiertes Eingangssignal gemessen wird.

In dieser experimentellen Arbeit wurden die von *Multiunits* bei visueller Stimulation ausgesandten hirnelektrischen Signale gemessen. Die Experimente wurden am visuellen Kortex der Katze durchgeführt. Zur visuellen Stimulation wurden dem Tier definierte

*Multiunits*: Als Multiunit wird eine Gruppe von 5 bis 20 Neuronen bezeichnet, deren Signal sich bei Extrazellulärmessungen an der Elektrode überlagert.

Muster auf einem Monitor gezeigt. Die verwendeten Stimuli waren ein *Streifenmuster* sowie eine Zufallspunktverteilung, deren *Kohärenz* beliebig geändert werden konnte. Das zu messende Signal wurde mit extrazellulären Ableitmethoden als eine Funktion der Zeit aufgezeichnet und anschließend parallel in zwei getrennten Frequenzbereichen von 1 kHz bis 10 kHz (Aktionspotenziale) und von 1 Hz bis 100 Hz (*lokales Feldpotential*, LFP) digitalisiert. Die aufgenommenen Daten wurden in Abhängigkeit von verschiedenen Stimulusbedingungen in Hinblick auf Feuerraten, Synchronisation, Frequenzverteilung sowie Kopplung von Aktionspotenzialen und LFP-Daten analysiert.

Die Experimente im ersten Teil dieser Arbeit (Kapitel 4) untersuchten den Einfluss von Kohärenz auf die Verarbeitung von Bewegungsinformation in zwei wichtigen visuellen Arealen der Katze: dem primären visuellen Areal (A17) und dem posteromedialen lateralen suprasylvischen Sulcus (Area PMLS). In einem ersten Schritt wurde die *Richtungsselektivität* der gemessenen Multiunits bestimmt. Um die aus dieser Messung resultierenden *Tuningkurven* quantifizieren zu können, wurden die Vorzugsrichtung und ein Richtungsparameter berechnet. Zusätzlich wurde im Rahmen dieser Arbeit ein Parameter zur Quantifizierung der Breite der Tuningkurve neu entwickelt. Die drei Maße sind in Gleichung 3-1 bis 3-3 definiert.

Die Ergebnisse der Auswertung zeigen, dass Multiunits in A17 und PMLS sowohl auf Streifenmuster als auch auf Zufallspunktverteilungen antworten und dass die Stärke der Antwort als eine Funktion der Stimulusrichtung variiert. Dieses Ergebnis stimmt mit früheren Studien überein [125, 14, 73]. Weiterhin wird gezeigt, dass die Vorzugsrichtung in beiden Arealen weitgehend unabhängig von der Art des verwendeten Stimulus ist. Für A17 stimmt auch dieses Resultat mit früheren Arbeiten überein [15]. Für PMLS hingegen ist in der Literatur eine größere Differenz zu finden [73]. Dieser Unterschied wird auf eine ungenauere Berechnung der Vorzugsrichtung in der zitierten Literatur zurückgeführt, was ausführlich in Kapitel 4.2.3 diskutiert wird.

Die Breite der Tuningkurven in den zwei Arealen A17 und PMLS ist für das Streifenmuster und das Zufallspunktmuster unterschiedlich. In beiden Arealen ruft das Zufallspunktmuster eine breitere Tuningkurve hervor als das Streifenmuster. Dies kann auf Unterschiede im Frequenzraum der beiden Stimuli zurückgeführt

**Streifenmuster:** Äquidistante Streifen, deren Helligkeit kontinuierlich zwischen hell (Weiß) und dunkel (Schwarz) wechselt, bewegen sich in einer definierten Richtung über den Bildschirm. Die Breite der Streifen sowie die Geschwindigkeit der Bewegung wird an das zu messende Areal angepasst.

**Kohärenz:** Maß für die Gleichförmigkeit der Bewegung des Zufallspunktmusters. Die Kohärenz des Stimulus wird durch Ausblenden und anschließendes Einblenden von Punkten an zufällig neu ausgewählter Position verändert. Die übrigen Punkte bewegten sich gleichmäßig in eine definierte Richtung. Der Kohärenzlevel in Prozent entspricht der Anzahl an versetzten Punkten.

**lokales Feldpotential:** Analoges, über einen größeren Hirnbereich gemittelt Signal, grob vergleichbar dem EEG.

**Richtungsselektivität:** Viele Zellen im visuellen Kortex reagieren nur auf eine bestimmte Bewegungsrichtung eines Stimulus. Die Stärke dieser Richtungsabhängigkeit der neuronalen Antwort wird als Richtungsselektivität bezeichnet, die Richtung der größten Aktivität als Vorzugsrichtung der Zelle.

**Tuningkurven:** Ergebnis der Messung der Richtungsselektivität. Dazu wird ein Stimulus in verschiedene Richtungen bewegt und die Antwort der Zelle als Funktion dieser Richtung gemessen.

werden und ist ausführlich in Kapitel 4.2.3 beschrieben. Trotz unterschiedlicher Tuningbreiten weisen beide Stimulusarten ein ausreichend schmales Tuningverhalten auf, so dass eine Vorzugsrichtung berechnet werden konnte. Die Unterschiede in der Vorzugsrichtung zwischen Streifenmuster und Zufallspunktmuster sind klein genug, um in den folgenden Experimenten dieselbe Bewegungsrichtung für beide Stimuli zu verwenden.

Da beide Areale eine ähnliche Vorzugsrichtung für die beiden Stimuli aufweisen, liegt die Vermutung nahe, dass die Stimulusrichtung für Streifenmuster und Zufallspunktmuster durch den selben Mechanismus bestimmt wird. Ein solcher gemeinsamer Mechanismus war für A17 schon von Skottun et al. [126] vorgeschlagen worden. Die Ergebnisse dieser Arbeit erlauben nun, dies auch für PMLS zu postulieren. Der hohe Korrelationskoeffizient der Richtungsindizes für Streifenmuster und Zufallspunktmuster in PMLS sind ein zusätzlicher Hinweis auf einen solchen einheitlichen Mechanismus.

Nach der Bestimmung der Stimulationsrichtung wurde in einem nächsten Experiment die Abhängigkeit der Feuerrate von der Kohärenz des Punktzufallsmusters untersucht. Multiunits in A17 und PMLS zeigen eine deutliche Abnahme der Feuerrate bei einer Abnahme der Stimuluskohärenz. Allerdings sind in den beiden Arealen unterschiedliche Kohärenzniveaus nötig, um die Feuerrate zu reduzieren. Während in PMLS schon bei 5% Inkohärenz eine Abnahme der Feuerrate gemessen wird, sind in A17 mehr als 20% Inkohärenz nötig. Dieses Ergebnis kann auf die unterschiedlichen Größen der *rezeptiven Felder* der beiden Areale zurückgeführt werden. Die Wahrscheinlichkeit, einen inkohärenten Punkt innerhalb eines rezeptiven Feldes zu finden, verringert sich mit der Größe des Feldes. Daher führen die kleinen rezeptiven Felder in A17 zu einer „Blindheit“ für inkohärente Punkte bei geringem Inkohärenzlevel, wohingegen die großen Felder in PMLS schon diese wenigen inkohärenten Punkte detektieren können. Berücksichtigt man die unterschiedlichen Größen der rezeptiven Felder, zeigen beide Areale eine vergleichbare Abnahme der Feuerraten mit abnehmender Stimuluskohärenz. Dieses Ergebnis, das ausführlich in Kapitel 4.3.3 diskutiert ist, ist ein weiterer deutlicher Hinweis darauf, dass eine wichtige Funktion von PMLS in der Analyse von Bewegung und räumlich verteilter Information liegt [110]. Während A17 vornehm-

*Rezeptives Feld:* Bereich der Netzhaut, von der aus ein Stimulus die Antwort einer Zelle im Kortex beeinflusst.

lich als ein lokaler Detektor für Orientierung und Richtung fungiert, kann PMLS zusätzliche Information über großflächigere, inkohärente Stimuli zur Verfügung stellen.

Trotz dieser Abnahme der Feuerraten scheinen beide Areale nicht in der Lage zu sein, die Bewegungsrichtung eines inkohärenten Zufallspunktmusters nahe der Wahrnehmungsschwelle auf der Basis von Feuerraten zu erkennen. Psychophysische Experimente haben gezeigt, dass Katzen die Bewegungsrichtung innerhalb eines Zufallspunktmusters bei einer Inkohärenz von 95% detektieren können [98]. Die Resultate der vorliegenden Arbeit zeigen jedoch in beiden Arealen keine signifikanten Änderungen der Feuerrate bei Inkohärenzniveaus von mehr als 50%. Feuerraten in A17 und PMLS können daher nicht als alleiniger Mechanismus für das zuverlässige Erkennen einer Bewegung innerhalb eines stark inkohärenten Musters herangezogen werden. Es kann jedoch nicht ausgeschlossen werden, dass für Bewegung nahe der Wahrnehmungsschwelle ein Bewusstseinszustand mit einem aktiven Mechanismus erforderlich ist und daher unter Anästhesie keine Änderung der Feuerraten gemessen werden kann.

Um Änderungen in der zeitlichen Struktur der aufgenommenen Aktionspotenziale zu untersuchen, wurden diese Signale einer Korrelationsanalyse unterzogen. Zur weiteren Quantifizierung wurden die Korrelogramme mit verschiedenen mathematischen Funktionen beschrieben. Gleichzeitig wurden von den LFP-Signalen Leistungsdichtespektren berechnet und die Leistung über dem Alpha-Frequenzband (6 Hz bis 18 Hz) und Gamma-Frequenzband (30 Hz bis 60 Hz) summiert. Zur Korrelation der Aktionspotenziale und LFP-Daten wurde die sogenannte Spike-Feld-Kohärenz eingeführt. Details zur Berechnung dieser Maße sind in Kapitel 3.6.3 beschrieben.

Die Ergebnisse der Korrelationsanalyse, der Analyse der Leistungsdichtespektren und der Kopplung zwischen Aktionspotenzialen und LFP-Daten ergeben ein einheitliches Bild: Eine Abnahme der Stimuluskohärenz führt zu einer Verringerung der Synchronisationspräzision und zu einer Abnahme der Leistung in den hohen sowie einer Zunahme der Leistung in den niedrigen Frequenzbereichen des LFP.

In Übereinstimmung mit früheren Studien wurden in dieser Arbeit für das Streifenmuster schmale zentrale Maxima in den Korrelogrammen der Multiunits für A17 [42, 28, 31, 124] und PMLS [28]

gefunden. Zusätzlich traten in A17 für diesen Stimulus in den Aktionspotenzialen hochfrequente Oszillationen im Bereich von 40 Hz auf. Auch dieses Resultat unterstützt Ergebnisse früherer Studien [63]. Hochfrequente Anteile wurden auch im Leistungsdichtespektrum des LFP gefunden. Diese Anteile waren in PMLS deutlich schwächer ausgeprägt als in A17. Darüber hinaus zeigte die Spike-Feld-Kohärenz in beiden Arealen eine starke Kopplung zwischen dem Spike-Signal und den hohen Frequenzen im LFP.

Das kohärente Zufallspunktmuster führte zu einer Verbreiterung des zentralen Maximums in den Korrelogrammen beider Areale. Eine Verringerung der Kohärenz führte zusätzlich zu einer monotonen Zunahme der Breite dieses Maximums. Diese Abnahme der Synchronisationspräzision zeigte sich bereits bei geringer Reduzierung der Stimuluskohärenzen. Allerdings zeigte PMLS diese inkohärenzinduzierte Abnahme der Synchronisationspräzision nur, wenn die Stimulation mit einem Streifenmuster ein deutliches, schmales zentrales Maximum im Korrelogramm zeigte. Die Stärke der Synchronisation, d.h. das Verhältnis der Anzahl korrelierter und unkorrelierter Spikes, war hingegen kaum durch unterschiedliche Inkohärenzlevel beeinflusst. Hochfrequente Oszillationen, wie sie für A17 für das Streifenmuster gefunden wurden, waren für das Zufallspunktmuster in beiden Arealen nicht vorhanden.

Auch im Leistungsdichtespektrum des LFP nahmen die hochfrequenten Anteile im Frequenzband von 30 Hz bis 70 Hz mit abnehmender Stimuluskohärenz ab, während die niederfrequenten Anteile zunahmen. Die Abnahme der hohen Frequenzen war in A17 deutlich stärker ausgeprägt als in PMLS. Zusätzlich zeigte die Spike-Feld-Kohärenz für A17 mit abnehmender Stimuluskohärenz eine Abnahme der Kopplung zwischen Aktionspotenzialen und hohen LFP-Frequenzen, während die Kopplung zwischen Spikes und den niedrigen Frequenzkomponenten im LFP zunahm. Der Anstieg der Kopplung zwischen den Aktionspotenzialen und den niedrigen LFP-Frequenzen mit abnehmender Stimuluskohärenz wurde auch in PMLS gefunden. Zusätzlich trat in den Korrelogrammen der Aktionspotenzialen in PMLS für einen Inkohärenzlevel von mehr als 5% eine Alpha-Oszillation im Bereich zwischen 8 Hz und 16 Hz auf. Die Frequenz dieser Oszillation veränderte sich bei zunehmender Inkohärenz ebenso wenig wie die Amplitude relativ zum zentralen Maximum. Diese Alpha-Oszillationen in den Aktionspotenzialen wurden in A17 nicht gemessen.

Präzise Synchronisation und hochfrequente Oszillationen gelten als ein Mechanismus für die Bindung kohärenter Objekte (Überblick in [123]). Die Resultate, die in dieser Arbeit für das Synchronisationsverhalten bei Stimulation mit einem Streifenmuster gefunden wurden, unterstützen diese Theorie. Darüber hinaus zeigen die Ergebnisse, dass Synchronisation auch Objekte in einem nicht kohärenten Stimulus binden kann. Synchronisation ist somit auch wichtig für die Analyse von nicht kohärenten Mustern, die über einen größeren visuellen Raum verteilt sind. Die Ergebnisse zeigen auch, dass durch Synchronisation zusätzliche Information zu den aus Feuerraten gewonnenen Daten bereit gestellt werden kann. Während die von Multiunits in A17 hervorgerufenen Feuerraten nicht in der Lage sind, geringe Inkohärenzen zu detektieren, kann Synchronisation diese erreichen, indem die Information, die zu dem gleichen Ensemble von inhomogen verteilten Punkten gehört, gebunden wird.

Im Unterschied zu A17 waren in PMLS Änderungen in der Synchronisation nur für starke Änderungen im Kohärenzniveau signifikant. Dem gegenüber zeigten Feuerraten zuverlässig schon kleine Änderungen in der Stimuluskohärenz an. Dieses Ergebnis ist ein weiteres Indiz dafür, dass Synchronisation in frühen Stationen des visuellen Pfades in einen mehr feurratenbasierten Code in späteren Stationen der visuellen Hierarchie übersetzt wird.

Es darf spekuliert werden, dass das Auftreten der niederfrequenten Oszillationen sowohl in den Aktionspotenzialen als auch in den LFP-Daten in PMLS wichtig für die Integration verteilter Informationen ist. Im Vergleich zu Gamma-Oszillationen könnten diese niederfrequenten Oszillationen die Integration über einen größeren Bereich des visuellen Raums ermöglichen. Während das Streifenmuster lokal analysiert werden kann, benötigt das Zufallspunktmuster Integration über einen größeren Bereich des visuellen Feldes. Ansteigende Inkohärenz würde diesen Effekt noch verstärken. Unterstützt wird diese Hypothese sowohl durch Ergebnisse von Slice-Präparationen als auch durch elektrophysiologische Studien *in vivo*. Diese haben gezeigt, dass die Ausdehnung kortikaler Anregungen von der Applikationsfrequenz der Anregung abhängt [18] und dass niederfrequente Oszillationen über eine längere kortikale Distanz hinweg synchronisiert bleiben können [13, 55].

Einige Autoren halten die langsamen Alpha-Rhythmen auch für *Top-down-Prozesse* [134] und interareale Verbindungen über eine längere kortikale Distanz hinweg [133] für entscheidend. Während Gamma-Frequenzen für *Bottom-up-Prozesse* und das Erkennen neuer Stimuli wichtig sind, wurden niedrige Frequenzkomponenten dem Fluss von Top-down-Information zugeordnet. Dies wird ausführlich in Abschnitt 4.4.3 dieser Dissertationsarbeit diskutiert.

Es kann nicht ausgeschlossen werden, dass der Anstieg der niedrigen Frequenzkomponenten auch auf Anästhesie zurückzuführen ist. Diese wird gestützt durch eine Studie bei Brecht et al. [10], in welcher niederfrequente Oszillationen häufiger im anästhesierten als im wachen Tier gefunden wurden. Allerdings deuten die starke Kopplung zwischen Spikes und niedrigen Frequenzen bei zunehmender Inkohärenz, der monotone Anstieg der niederfrequenten Komponenten im LFP sowie die Tatsache, dass das kohärente Zufallspunktmuster keine starken Alpha-Oszillationen und Alpha-Komponenten im LFP zeigt, auf eine funktionelle, integrative Funktion hin. Weitere Experimente werden nötig sein, um die Rolle dieser langsamen Oszillationen bei inkohärenten Stimuli abschließend beantworten zu können.

In den Experimenten im zweiten Teil dieser Arbeit (Kapitel 5) wurde untersucht, wie das Gehirn *Shape-from-Motion-* (SFM-) Stimuli verarbeitet. Die Auswertungen der Feuerraten haben gezeigt, dass Multiunits in PMLS sowohl auf helligkeitsdefinierte Kontrastbalken als auch auf SFM-Balken reagieren. Die Stärke der Antwort hängt von der Kombination von Stimulus und Hintergrund und von der relativen Bewegungsrichtung zueinander ab.

Für Balken mit hohem und niedrigem Kontrast relativ zum Hintergrund sowie für punktdefinierte Balken, die sich über einen dunklen Hintergrund bewegten, wurden vergleichbare Feuerraten gefunden. Dies Ergebnis unterstreicht weiter die integrative Eigenschaft von Area PMLS. Während ein Kontrastbalken ein räumlich kohärenter Stimulus ohne Diskontinuitäten ist, verlangt die Analyse eines Balkens, der aus Zufallspunkten zusammengesetzt ist, die Integration eines nicht kontinuierlichen Stimulus über einen größeren Bereich des visuellen Feldes. Diese Ergebnisse stimmen gut mit den Resultaten aus Kapitel 4.3 überein, dass Feuerraten für ein großes Zufallspunktmuster und ein Streifenmuster vergleichbar sind. Beide Resultate deuten also darauf hin, dass PMLS als ein primäres Bewegungsareal zuverlässig auf die Bewegung aller Arten von Sti-

*Top-down-Prozesse:* Anatomisch: Prozesse, die durch Feed-back-Verbindungen von höheren zu niedrigeren Arealen vermittelt werden; kognitiv ein hypothesen- oder erwartungsgesteuertes Verhalten.

*Bottom-up-Prozesse:* Anatomisch: Prozesse, die durch Feed-forward-Verbindungen von niedrigeren zu höheren Arealen vermittelt werden; kognitiv ein stimulusgesteuertes Verhalten.

*Shape-from-Motion-Stimulus:* Ein aus vielen kleinen Punkten bestehender Stimulus, in dem ein Objekt allein durch Bewegungskontrast zwischen den Punkten definiert wird.

multi reagiert. Die Fähigkeit, einen nicht kontinuierlichen Stimulus wie einen punktdefinierten Balken zu integrieren, macht PMLS zu einem guten Kandidaten für die Verarbeitung von bewegungsdefinierten Konturen.

In einem nächsten Schritt wurde der Einfluss eines statischen Punkthintergrundes auf die Feuerraten der verschiedenen Stimuli untersucht. Die Ergebnisse zeigen, dass ein solcher Hintergrund keinerlei Effekt auf die von einem helligkeitsdefinierten Balken hoher Lichtstärke hervorgerufene Feuerrate hatte. Wenn allerdings die Lichtstärke des Balkens so angepasst wurde, dass sie mit der durchschnittlichen Lichtstärke des Punkthintergrundes übereinstimmte, reduzierte der Hintergrund die vom Balken induzierte Feuerrate um mehr als 50%. Eine Reduzierung um 75% trat auf, wenn der punktdefinierte Balken über den statischen Punkthintergrund bewegt und damit zu einem SFM-Balken wurde. Der neuronale Mechanismus, welcher dieser Reduktion der Feuerraten zugrunde liegt, bleibt leider weiter unklar. Mögliche Mechanismen sind *laterale Inhibition* sowie ein Mechanismus ähnlich dem Mechanismus, der das Erkennen von illusionären Konturen, wie z.B. bei einem *Kanizsa-Dreieck* erlaubt.

Im Gegensatz zu einem statischen Punkthintergrund, der die Feuerraten für einen helligkeitsdefinierten Balken nicht beeinflusst, führte ein Zufallspunkthintergrund, der sich entgegen der Vorzugsrichtung der Multiunit bewegte, zu einer starken Abnahme der Feuerraten. Dieser Effekt war für den SFM-Balken deutlich ausgeprägter: Während ein statischer Zufallspunkthintergrund bereits einen hemmenden Einfluss auf die Feuerraten hatte, führte der sich bewegende Hintergrund zu einer beinahe völligen Auslöschung der Antwort. Dieses Ergebnis kann durch die Annahme erklärt werden, dass PMLS nur die stärkste Richtung des Stimulus innerhalb des rezeptiven Feldes anzeigt. Im Falle des bewegten Hintergrundes ist dann die Bewegung des Hintergrundmusters diese stärkste Bewegung.

Um die Reizstärke des bewegten, punktdefinierten Balkens zu testen, wurde dieser Balken über einen statischen Punkthintergrund bewegt, in den die bereits in den Kohärenzexperimenten beschriebene Inkohärenz von 5%, 10% bzw. 20% eingeführt wurde. Schon 5% Inkohärenz reichten aus, die Antwort auf einen SFM-Balken vollständig zu unterdrücken. Dieses Ergebnis war überraschend, da die geringen Inkohärenzniveaus die Wahrnehmung des SFM-Bal-

*laterale Inhibition:* Mechanismus zur Kontrastverstärkung, für den Neurone andere Neurone mit räumlich benachbarten rezeptiven Feldern hemmen.

*Kanizsa-Dreieck:* Das Kanizsa-Dreieck besteht lediglich aus drei „Pac-Men“ in den Ecken eines illusionären Dreiecks. Obwohl keinerlei weitere Verbindungen existieren, nehmen die meisten Beobachter klar definierte Linien eines Dreiecks wahr.



kens für einen menschlichen Beobachter nach subjektiver Beurteilung kaum beeinflussen. Zusätzlich wurde in den vorhergehenden Kapiteln gezeigt, dass geringe Inkohärenz in einem sich bewegenden Zufallspunktmuster nur zu kleinen Änderungen in der Feuerrate von Multiunits in PMLS führte. Verglichen mit dem größeren Stimulus des vorherigen Kapitels muss die Information über die Bewegung des wesentlich schmaleren SFM-Balkens jedoch aus einem viel kleineren Teil des rezeptiven Feldes gewonnen werden. Das könnte zu dem schwächeren Bewegungssignal geführt haben.

Um die Stärke der hemmenden Wirkung des entgegen der Vorzugsrichtung bewegten Punkthintergrundes zu untersuchen, wurden Teile dieses Hintergrundes durch eine quadratische Maske mit einer Seitenlänge gleich der Breite des SFM-Balkens ausgeblendet. Diese Maskengröße führte nicht zu einer signifikanten Änderung der Feuerrate verglichen mit der Stimulusbedingung ohne Maskierung. Da PMLS große rezeptive Felder besitzt [96], war die Größe dieser Maske nicht ausreichend, um das exzitatorische rezeptive Feld genügend abzudecken und damit den hemmenden Effekt des Hintergrundes auszuschalten. Wurde die Maske auf die Größe des rezeptiven Feldes vergrößert, verschwand der hemmende Einfluss des Hintergrundes. Die Feuerraten entsprachen nun denen, die bei Bewegung über einen Hintergrund hervorgerufen wurden, der dem Muster der verwendeten Maske entsprach. Das Ergebnis zeigt, dass im Gegensatz zu Studien mit anderen Stimuli [45, 11] die Feuerrate für SFM-Stimuli nicht wesentlich durch die Bewegung des Hintergrundes außerhalb des rezeptiven Feldes beeinflusst wird.

Zur weiteren Analyse der Fähigkeit von PMLS, SFM-Balken nur aufgrund des Bewegungskontrastes zwischen punktdefiniertem Objekt und Hintergrund zu erkennen, wurden je Multiunit zwei Tuningkurven gemessen. Für die Messung der einen Tuningkurve bewegten sich sowohl die Kontur als auch die Punkte innerhalb des Balkens in dieselbe Richtung, für die zweite Tuningkurve bildeten sie einen Winkel von  $90^\circ$ . Die Tuningkurven wurden wie für den ersten Teil der Arbeit beschrieben ausgewertet. Die Auswertung ergab, dass sich die mit den zwei Tuningkurven gemessene Vorzugsrichtung der Multiunit um  $45^\circ$  drehte, obwohl sich die Bewegungsrichtung des Balkens selbst nicht änderte. Durch dieses Ergebnis konnte gezeigt werden, dass Multiunits in PMLS die Bewegungsrichtung der Komponenten eines SFM-Balkens und nicht die Bewegung des Objektes selbst verarbeiten.

Um weitere Hinweise für diese Hypothese zu gewinnen, wurden verschiedene SFM-Balken verwendet, die alle dieselbe Bewegungsrichtung, jedoch unterschiedliche Bewegungsrichtungen der Punkte innerhalb des Balkens aufwiesen. Wenn PMLS die Bewegung der einzelnen Punkte statt der Bewegung des Balkens verarbeitet, sollte die Feuerrate für alle diese Bedingungen verschieden sein. Die Ergebnisse zeigen, dass sich die durch die verschiedenen SFM-Stimuli hervorgerufenen Feuerraten verringerten, je mehr sich die Richtung der Punkte, die den Balken bildeten, von der Bewegungsrichtung des Balkens – und damit von der Vorzugsrichtung der Multiunit – unterschieden. Zusammen mit den Resultaten der SFM-Tuningkurve zeigen diese Ergebnisse, dass PMLS nicht in der Lage ist, die Richtung von kinetisch definierten Balken zu analysieren, und statt dessen nur die Bewegung der einzelnen Komponenten erfasst.

Wenn PMLS in der Katze nun nicht das Areal ist, das SFM-Stimuli detektiert, bleibt die Frage, wo im visuellen Kortex dieser Stimulus verarbeitet wird. Es wurde gezeigt, dass Katzen in der Lage sind, SFM-Stimuli zu erkennen [110]. Basierend auf fMRI-Experimenten am Menschen kann spekuliert werden, dass erst höhere Areale im visuellen Pfad diese Aufgabe übernehmen. Leider sind homologe Areale weder zu Area KO noch zu Area IT bekannt, die im Menschen [23, 94, 143] bzw. in Affen [114] für die Verarbeitung von bewegungsdefinierten Konturen und Objekten entscheidend sind. Analog zum Affen könnte auch in der Katze das Bewegungssignal in PMLS detektiert und dann in den ventralen Pfad des visuellen Systems geleitet werden. Dort würden diese Signale weiter verarbeitet, um die nötigen Informationen für die Verarbeitung von SFM-Stimuli bereit zu stellen. Dies würde auch erklären, warum Läsionen in PMLS zu einer starken Störung beim Erkennen von dreidimensionalen SFM-Zylindern führen [110]. Um die Frage zu beantworten, wo und wie im visuellen Kortex der Katze SFM-Stimuli verarbeitet werden, sind weitere Experimente – auch in anderen Hirnarealen als den hier untersuchten – nötig.

## CHAPTER 1    **Introduction**

---

Our visual system provides us with a rapid, flexible and reliable perception of the surrounding world. The brain easily processes our three dimensional reality and lets us react in an appropriate way. Its speed is incredibly high given the huge amount of information processed every second. All this is accomplished by a highly complex, dynamic network of neurons. Roughly 10 billion nerve cells each containing an average number of 10,000 synapses are working together in order to perform this highly demanding task. Exactly how the brain is doing this still remains an unsolved question. The first link between neural communication and electrical signals was made in 1791 by Luigi Galvani who showed that frog muscles can be electrically stimulated. It took another 130 years, before impulses from nerve cells could be measured directly by amplifying the electrical signal coming from extracellular microelectrodes.

Despite a waste amount of interdisciplinary research over the last decades, our knowledge about the functional mechanism of this highly complex system is still in its infancy. One reason for this might lie in the fact that most fundamental research has been done on the molecular level rather than on the system level. Although the physics of a single neuron is well understood, much less is known about the underlying physical mechanisms of larger areas of the brain or even the brain as a whole. Especially higher cognitive func-

tions are still not within reach. To this day, the attempts to understand the whole brain from its single parts, neurons and synapses, have not proven successful.

Compared to the knowledge about a single neuron and its molecular mechanisms, our knowledge about the integrative properties of the brain develops rather slowly. By now it is widely accepted that information processing in the brain is a highly parallel process, where even simple tasks require the parallel activation of large cortical areas. The processing, storage and representation of information is therefore not restricted to a local area but is distributed over wide regions of the brain as well as over a large number of neurons. This rises the question of how these populations of neurons work together and, more importantly, how they manage to coordinate their activity. The highly parallel processing of sensory information most likely needs some form of integrative mechanism [123] in order to bind distributed information about the same object. Finding this mechanism that allows to coordinate activity of different regions of the brain has drawn a lot of attention. The answer to this so called *binding problem* has become one of the major landmarks in all areas of brain sciences, including neurobiology, neurophysiology, neuronal computation and physics (for review see issue 1 of *Neuron* 24, 1999). The different mechanisms proposed to solve this problem shall be described in the chapter *Neurophysiological Background*.

The visual system is a sensory system that needs to solve the binding problem fast and efficiently. The process of figure-ground segregation, necessary for the analysis of visual scenes, is one example, where higher cognitive processing can only be performed after background and figure have been bound to form separate entities. This segregation process can roughly be divided into two separate stages. First, objects are to be analyzed with respect to special features such as orientation of edges or direction of movement. This processing starts already at the retina where orientation is represented by colinearly aligned receptive fields of ganglion cells that project onto the same cortical neurons. Second, these elementary features have to be bound to give a representation of the respective objects within the brain.

The feature binding underlies certain rules. These rules were first described in the 1920s and 1930s by the so called Gestalt-physiologists like Wertheimer [148], Köhler [59] or Koffka [62]. They rejected the earlier idea that perception is made up from local sensory

units by simply concatenating elements to form shapes. They postulated that perception cannot be reduced to the analysis of isolated parts or a piecewise relation between them. Perception rather has its own intrinsic structure and emergent properties not shared by their single structural parts. For instance, the line shown in Fig. 1-1 can be easily perceived as such although it consists of single points. The rules governing this binding are called “*Gestalt criteria*”. One of these criteria, the *Common Fate*, states that single objects, all moving into the same direction at the same speed, are perceived as one moving ensemble instead of many single objects [95]. This Gestalt criterion is sketched in Fig. 1-2. When all dots have the same color, the U in the figure is visible only if the dots that make up the letter are moving into a common direction. Static dots are not distinguishable from the background. This Gestalt criterion shall play an important rule throughout this thesis.

When one looks at the brain as a physical system, it quickly becomes apparent that it is one of the most complex, highly non linear physical systems known. Most of today’s knowledge about the underlying mechanisms of this system comes from experiments that try to extract the underlying mechanism from neuronal responses of the brain to a defined input signal. The sensory systems of the brain are best suited for this approach. In these systems, a defined input signal can easily be applied many times without significant perturbations. This thesis shall therefore focus on the visual system of the cat. The results of the experiments shall help to gain a better understanding of the underlying processing mechanism of the brain by analyzing a certain output signal  $y_i(t)$  for a given input signal  $x_i(t)$ . The input signal  $x_i(t)$  shall be a defined visual stimulus, e.g., a white dot on a dark background on a monitor seen by the cat. The input will elicit a response of electrical impulses in the retina. These impulses will then travel along the visual pathway through many processing stages in the visual system of the brain. The measured output signal  $y_i(t)$  shall be the electrical impulses elicited by a single nerve cell or by a small assembly of nerve cells (multiunit) in different locations of the visual systems. The functional relation between these output signals and the input signal shall help to gain a better understanding of the transfer properties of the cat brain. Many experiments using different input signals shall be performed.



**Figure 1-1: Gestalt criterion**

Although the shape is made up of single dots, the object is perceived as a line. This is one example of a Gestalt criterion stating that the perception of an object is governed by the object’s intrinsic properties and not by its single elements.

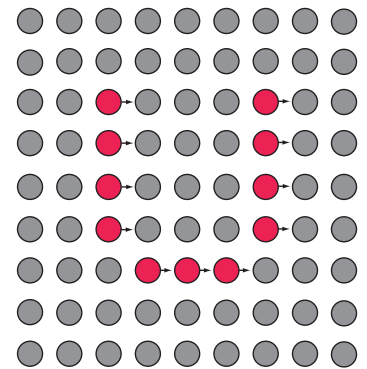


**Figure 1-2: Example of Common Fate**

The figure gives an example for the Gestalt criterion of Common Fate. When all dots would have the same color, the red „U“ in the center would only be visible if the dots forming the letter would move into a common direction. It would become invisible, as soon as the movement of the dots stops.

The electrical impulses of the brain shall be measured using extracellular recording techniques. The signal shall be recorded as a function of time. Bandpass filter shall divide the amplified signal into two different frequency ranges. After collecting the data, a signal analysis shall be performed. Characteristic parameters such as firing rate or the precision of synchronization of neuronal activity between two neurons shall be extracted, calculated and analyzed, in order to draw conclusions on the mechanisms underlying the processing in this complex system. If no parameter are available from the literature, new parameters shall be developed to allow a more accurate description and quantification of the measured signal. The digitized data shall be analyzed depending on many different input stimuli (see *Materials and Methods*) using, e.g., firing rates, correlation analysis or spike field coherence.

This thesis consists of two major parts. In one group of experiments, random dot patterns with different levels of stimulus coherence shall be used to investigate their influence on firing rates and on synchrony of firing activity between two multiunits. These experiments shall be performed in two major visual areas of the cat, the primary visual area (area 17) and the posteromedial lateral suprasylvian area (PMLS). The other group of experiments shall use shape-from-motion (SFM) stimuli as input signal to the visual system. These stimuli are defined by motion contrast, only, and should be bound by the brain according to the „Gestalt criterion“ of *Common Fate*. It shall be investigated, how the brain is processing this type of stimulus.

In particular, it shall be investigated, if firing rates reliably signal the coherence of a stimulus and whether these changes in firing rates can explain the ability and limitations of the brain to perform motion discrimination found in psychophysical experiments. Changes in firing rates shall be measured when the coherence of a random dot stimulus is disturbed by visual noise. In addition, differences between the two areas 17 and PMLS in their ability to signal this motion coherence shall be investigated.

A coherent random dot pattern moving uniformly in one direction should be bound to form an object according to the “Gestalt criterion” of *Common Fate*. The binding hypothesis predicts that this object binding should lead to synchronous firing activity of cells in the visual system. The degree of synchrony shall be determined by cross-correlation analysis. Adding visual noise to the dot pattern could gradually decrease the amount and the precision of synchro-

ny as the coherence of motion and consequently the binding cue decreases. On the other hand, precise synchronization might remain as long as the cortex can discriminate a direction of motion within the random dot pattern and will break down as soon as the noise level will exceed a certain discrimination threshold. Experiments in this thesis shall be designed in order to answer the open question, which of these two mechanisms is utilized by areas 17 and PMLS. By comparing these results with changes of firing rate upon decreasing stimulus coherence, it shall be examined, whether changes in synchrony or changes in firing rate are the more reliable answer to different coherence of stimulus motion.

In additional experiments it shall be investigated, if the increase in width of the central maximum of the correlation function between two multiunits in the two areas will be accompanied by a transition from high to low frequency components in the local field potential (LFP, see *Materials and Methods*). It shall further be investigated, if these shifts within the power spectrum of the LFP are identical for areas 17 and PMLS or if the two areas show different responses to decreasing stimulus coherence. In addition, the correlation between the multiunit responses and the LFP shall be investigated by means of the spike-field coherence.

The hypothesis that multiunits in area PMLS can analyze the direction of motion of a contour that is solely defined by the relative motion of a group of dots against a background dot pattern shall be tested in the second large group of experiments performed in this thesis. The stimulus shall be a group of moving dots that should form a moving bar (SFM bar) according to the „Gestalt Criterion“ of *Common fate*.

If multiunits in area PMLS can analyze the movement of the contour of this shape, the direction of movement of the dots relative to the contour should not make a significant difference for the analysis of the motion direction, as long as the shape itself can be perceived as such. The direction of motion detected by multiunits in area PMLS should always be the direction of motion of the contour.

In order to test this hypothesis, a stimulus built from several SFM bars that differ in their direction of motion for the dots building the bar shall be used as input signal. The neuronal response to this input shall be quantitatively analyzed using several parameters.

## Chapter 1

If multiunits in area PMLS are able to signal the direction of motion of the shape, the parameter describing the preferred direction of these bars should be identical. In order to gain further insight into the processing of motion defined stimuli, different stimulus conditions shall be designed and used to test the influence of different background patterns on firing rates elicited by stimulation with a SFM bar, to test the influence of stimulus noise on the detectability of a SFM bar and to investigate, whether areas outside the receptive field influence the firing rates elicited as a response to a SFM bar.

The experiments may provide answers to some of the open questions concerned with motion discrimination in the visual system of the cat and contribute to the ongoing debate about the importance of firing rate and synchronization for processing in the brain.



## CHAPTER 2    **Neurophysiological Background**

---

### **2.1 Introduction**

The cell is the primitive building block for every biological system. In higher biological systems, many different cells are working together to build functional units. By far, the most complex of these units is the human brain. It is built up from many different types of cells ranging from supporting glia cells to interneurons and huge pyramidal neurons. Nevertheless, the many different kinds of nerve cells forming the brain can be derived from one basic type. In addition to properties every cell needs in order to survive, nerve cells have three unique features that enable them to communicate and thus to build the huge network that mediates behavior and consciousness. First, proteins in the external membrane of neurons permit the influx and efflux of ions which make neurons electrically and chemically excitable. Second, special proteins at particular sites of the cell body, the synapses, endow the cells with specialized secretory properties that allow for the controlled transfer of electrical signals between nerve cells. Third, dendrites as the receptive units and the axon with synaptic terminals as the transmitting unit limit the flow of impulses to one direction.

## 2.2 The Neuron

The human brain consists of at least  $10^{10}$  nerve cells, each having on the order of 10,000 synaptic connections. A nerve cell, or neuron, consists of a cell body, called the soma, and two types of processes, called dendrites and axons (Fig. 2-1). The dendrites are short processes that branch out in a tree-like fashion and receive the action potentials from other neurons to pipeline them to the cell body. In pyramidal neurons one distinguishes two types of dendrites depending on their origin at the soma. Those emerging from the basis of the soma are called *basal dendrites*, those emerging from the tip of the soma are called *apical dendrites*. These apical dendrites often connect different layers of the cortex. The axon, in contrast, takes the impulse from the soma and carries it to other neurons. Axons are usually thinner than dendrites. They have many collaterals that also branch frequently. Axons can grow to an impressive length of up to 3 m and can connect parts of the central nervous system that are far apart.

Nerve cells use electrical signals to communicate. These signals, the *action potentials*, consist of potential changes across the cell membrane caused by current flow through voltage gated ion channels. The action potential is an all-or-none impulse with a fixed amplitude of around 100 mV and a duration of approximately 1 ms. It travels at a rate of 1 to 100 m/s with a constant amplitude to the end of the axon being regenerated at regular intervals along the way. Because of their shape, action potentials are often called spikes. In a simple model, all the incoming action potentials are summed at the soma of the downstream nerve cell. Every time the summed signal exceeds a certain threshold, a new action potential is generated and transmitted through the axon.

The transmission of a signal from one neuron to another occurs at the synapses which are the points of contact between two nerve cells. Most synapses work chemically: The signal coming from the axon triggers a release of transmitter molecules in the synaptic cleft. This transmitter binds to receptor molecules at the dendritic side that in turn activate ion channels in the postsynaptic membrane.

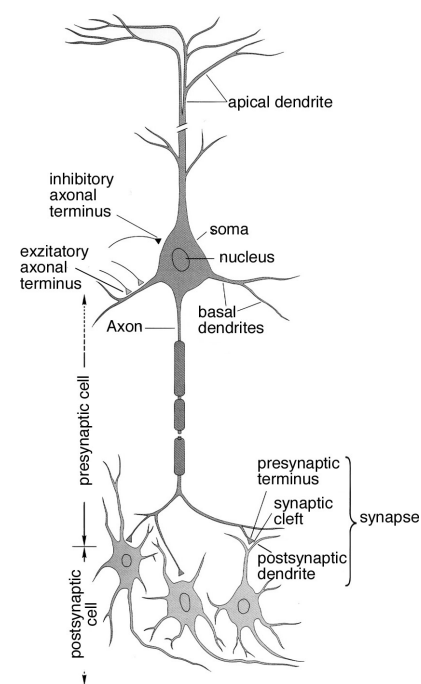


**Figure 2-1: Anatomy of a pyramidal cell**  
 Explanations can be found in the text.  
 Slightly modified after 57

Therefore, synapses can transmit signals only from the axon to the dendrites. The synaptic cleft is between 20 and 30 nm wide. Neurotransmitters are released in packages, called quanta. Each quantum contains several thousands of transmitter molecules.

Synapses can be roughly divided into two types: excitatory or inhibitory. The neurotransmitter as well as the receptor determines the type of a synapse. An excitatory synapse excites the downstream cell, i.e. it adds a positive amount to the membrane potential at the soma until the threshold for generating an action potential is reached. An inhibitory synapse inhibits the cell by decreasing this membrane potential at the soma.

## 2.3 The Visual System of the Cat

Visual perception begins at the retina where incoming light is converted into electrical signals. Already at this early stage a first processing occurs. The signal is then transmitted through the optic nerve to higher areas in the brain for further processing. The cat retina contains two kinds of photoreceptors, *rods* and *cones*. Rods are more sensitive to light than cones and are responsible for black and white perception. Cones, on the other hand, are responsible for the perception of color. The cat retina has two types of cones, each containing a visual pigment with different absorption maxima at 450 nm and 556 nm, respectively. Although even a third type of cone with an absorption maximum at 500 nm was proposed by Sterling [135], color vision in the cat is extremely reduced as compared to monkeys and humans.

Receptors on the retina are not uniformly distributed. A central part contains a maximum density of receptors and ganglion cells. It is called the *area centralis* and is the point of the retina which is in the center of the visual field upon fixation. Consequently, later cortical and subcortical stages in the visual system devote a disproportionately large part of their visual maps to the representation of the *area centralis*.

Photons entering the retina are converted into electrical impulses by the visual pigments in the cones and rods. Bipolar cells transmit these impulses to the ganglion cells. The axons of the ganglion cells form the optic nerve and serve as the output for the retina. The processing of the incoming signals begins already at this stage. Adjacent ganglion cells are synaptically connected such that the output of one cell is being influenced by other ganglion cells. The restricted part of the retina providing input to a cell is called the *receptive field* (RF) of the ganglion cell. An RF contains either an excitatory center and an inhibitory surround or an inhibitory center with an excitatory surround. This mechanism enhances the contrast of the retinal image and in addition enables the cell to work with the extreme differences in brightness found in our environment [57].

Ganglion cells exist in three different functional classes, X, Y and W. The X-type responds to stimulation with a sustained, or tonic, response. They have a high spatial resolution and are used for the analysis of shapes. The Y-type ganglion cell responds in a more transient, or phasic, way and are more used for contrast and motion perception. They do not respond with a continuous firing rate but with a burst-like pattern. W type ganglion cells prefer low velocities and show either tonic or phasic responses.

The axons of the ganglion cells combine to form the optic nerve which leads to the chiasma opticum (Fig. 2-2). The nasal fibers of both eyes cross in order to get a complete representation of one hemifield in one hemisphere. The left visual hemifield is now represented in the right hemisphere and vice versa. However, in the cat, connections terminating in the superior colliculus (SC) do not cross at the chiasma opticum so that all afferents in the SC are originating from the contralateral eye. From the chiasma opticum, 50% of the nerve fibers lead to the lateral geniculate nucleus (LGN), a relay station in the thalamus. The LGN contains a topographic organization, i.e., neighboring points on the retina are represented as neighboring points in the LGN. The remaining 50% of the retinal fibers branch off to the SC and other subcortical thalamic structures like the pulvinar.

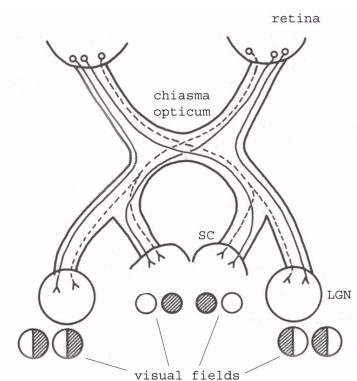


**Figure 2-2: Crossing at the chiasma** Gray represents the part of the visual field represented in one nucleus. In the cat, the whole contralateral visual field is represented in the SC. Taken from 91.

X- and Y-type ganglion cells terminate in different layers of the retinotopically organized LGN. The dorsal layers A and A<sub>1</sub> are innervated mainly from X-cells. In particular, the axons from the contralateral eye terminate in layer A whereas the axons from the ipsilateral eye terminate in layer A<sub>1</sub>. Layer C contains mainly connections from Y and W cells whereas layers C<sub>1</sub> and C<sub>2</sub> are dominated by input from W cells. Cells in the LGN show mostly the same properties as cells in the retina. However, lateral inhibition leads to an increase in center-surround antagonism and a further increase in contrast. In the LGN, the incoming axons are monosynaptically connected to the geniculate cells which in turn connect in a retinotopic projection directly to the primary visual cortex.

30% of the cerebral cortex in cats and 60% in monkeys is used for processing visual information [33, 91]. Within this big portion of the cortex are multiple distinct representations of the retina. Neurons in the LGN project to the primary visual area, also called area 17 or striate cortex. This largest area of the visual system (310-380 mm<sup>2</sup>) is located in the occipital lobe of the brain. It contains a single complete first order representation of the visual field, i.e., neighboring points of the whole hemiretina project to neighboring points of the cortex. 50% of area 17 is devoted to the central 10° of the visual field which gives area 17 the highest cortical magnification factor of 3.6 mm<sup>2</sup>/degree<sup>2</sup> at the area centrales (for details see [141]). The two visual areas 18 and 19 also receive direct input from LGN [87]. Therefore it has been argued that these three areas, area 17, 18 and 19, represent a complex of three primary visual areas, each containing a complete representation of the visual field [91].

In addition to these primary visual areas, visual representations have been described in the lateral suprasylvian (LS) sulcus (areas AMLS, ALLS, PMLS, PLLS, VL and DLS) [96], in areas 20 and 21 and in the anterior ectosylvian sulcus (Fig. 2-3). Besides direct input from the thalamus, these areas receive major input from A17, 18 and 19 and are regarded as higher visual areas.

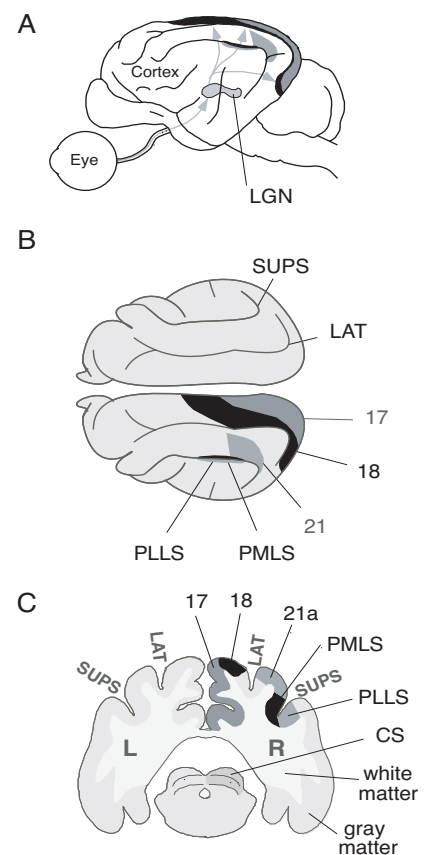


**Figure 2-3: The visual system of the cat**  
**A** Side-view of the cat brain with one eye. Thick lines in the cortex represent the sulci, arrows sketch the visual pathway. **B** View of the cortex from the top. Some important visual areas are shaded. Area PMLS and PLLS are completely hidden within the suprasylvian sulcus and are drawn here for illustration purpose only. **C** Frontal view of the cat cortex. LAT: lateral sulcus, SUPS: suprasylvian sulcus, LGN: Lateral geniculate nucleus.

The cortex is organized in six different layers. Axons from the LGN project to layers IV and VI in area 17. After processing the incoming signal, the output is projected from layer II and III to other visual areas. In addition, cells in layer V project to the SC and pyramidal cells in layer VI make feedback connection to the LGN. Similar to the retina and the LGN, each neuron in the primary visual cortex has a receptive field (RF), i.e., a small region of the retina that is selective for a specific localization of a visual stimulus. In contrast to the RFs of cells in subcortical structures, RFs in early cortical areas show a clear specialization with respect to stimulus orientation, direction of movement or speed of a visual object [52]. The properties of the RFs, for example sensitivity for direction of movement, differ largely between visual areas but also for different cells within the same visual area. However, receptive field properties of neighboring neurons change gradually across the cortical surface, building so-called cortical maps. These cortical maps are formed by vertical columns where cells within one column show similar properties. The presence of such maps has been demonstrated for several parameters characterizing the visual space such as orientation, direction of motion and spatial frequency [70, 147, 145].

Information processing in the brain is highly parallel. Input from the X-system predominantly terminates in area 17 whereas input from the Y-system terminates in area 18. Areas 17 and 18 provide most of the input for area 21a and PMLS, respectively. Through these different input pathways, the functional difference between the X and Y system is projected from the ganglion cells up to the higher visual areas. In contrast to area 21a, area PMLS has a high fraction of direction selective cells that respond to moving stimuli with a relatively high speed. Area PMLS therefore is thought to serve as the major area for the processing of motion whereas area 21a is specialized to the processing of shapes and forms [21].

The two areas 21a and PMLS are considered as the starting points for the two major cortical pathways in the visual system: Area 21a is responsible for analyzing shapes and is therefore the beginning of the “What” path. The major input to this pathway comes

from the X-system. Based on its anatomy, this path is also called the ventral or temporal pathway. Area PMLS, in contrast, is considered to serve as the gateway to the “Where” path, which analyzes motion and depth and rises from the Y-system. This pathway is also called the dorsal or parietal pathway [22]. The receptive fields in area PMLS are larger than those in area 17 and have a strong directional selectivity [129, 103, 45]. As part of the parietal pathway they are proposed to be involved in the analysis of global pattern [53], figure-ground segregation [45] and global motion processing [103]. The lateral suprasylvian area is also an important source for input to both the striatum and the superior colliculus [86].

In addition to input from areas 17, 18 and 19, area PMLS gets direct input from different nuclei of the thalamus (Fig. 2-4) [130, 56]. This includes a direct retino-thalamic pathway via the medial interlaminar nucleus (MIN) and the C-laminae of the lateral geniculate nucleus. In addition, a tecto-thalamic pathway exists via the superior colliculus (SC). The SC projects back to the lateral posterior nucleus (LP), the posterior nucleus (PN) and the C-laminae of the lateral geniculate nucleus. All three nuclei project to the LS cortex. The functional properties of these input pathways to LS are very different including cells with small receptive fields in MIN and LGN, cells with orientation selective RFs in areas 17, 18 and 19 and cells with large RFs and strong direction selectivity in LP and PN thalamic nuclei. Removal of either area 17 or the superior colliculus leads to different changes in the RF properties in area PMLS. Whereas removal of area 17 mainly leads to a reduction of directional selectivity in PMLS cells and an increase of cells responding equally or even better to flashing than to moving stimuli [130], removal of the SC leads mainly to an increased response of LS cells to slow moving stimuli and to static flashed stimuli [127].

This short overview can only give a very simplified picture of the visual system. Almost all areas are mutually interconnected, including connections between both pathways. It is also important to note that, to our knowledge, there exists no area in the visual system that combines all the information from the other visual areas in or-

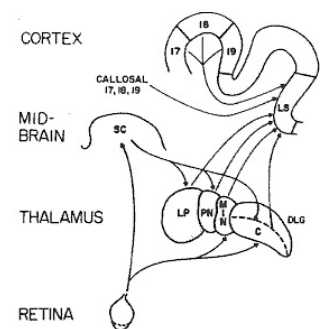


**Figure 2-4: Input to area PMLS**  
Multiple visual pathways connecting to area PMLS. The medial interlaminar nucleus (MIN) and the C laminae of the dorsal lateral geniculate (DLG) project directly to the LS area and form a retino-thalamic pathway. The superior colliculus (SC) projects to the lateral posterior nucleus (LP), the posterior nucleus (PN) and to the C-laminae of the dorsal lateral geniculate, each of which project to the LS area. These projections form the tecto-thalamic pathway. In addition, the LS area receives direct cortical projections from areas 17, 18, 19 and 21a. Taken from 130.

der to serve as a major integration area able to perform high level tasks like object classification, feature binding or feature-ground segregation.

## 2.4 Binding Problem and Neuronal Synchronization

The outside world consists of three dimensional objects of various shapes, colors and sizes. However, the image on the retina consists only of discrete light points representing a two dimensional projection of a three dimensional world. The distinction of objects is lost. In order to distinguish single objects, a mechanism must exist that separates them. This mechanism has to rebuild the relationships between single points on the retina, to integrate the distributed information and to build a consistent representation of objects. The problem of finding this relationship is called the *binding problem*.

In 1962 Hubel and Wiesel [52] found that receptive fields with complex properties are realized by combining information provided by cells with more elementary receptive fields that are on a hierarchically lower level. Ten years after this discovery, in 1972, Horace Barlow postulated a possible solution to the binding problem [5]. He postulated that object recognition is achieved by specialized neurons that code for one and only one feature constellation of a specific object. The so-called “grandmother cells” receive input from neurons that code for elementary properties, like orientation or color. Inputs from these feature-selective cells represent the object which is then detected by “grandmother cells”. According to this model, figure-ground segmentation is achieved through the activation of different grandmother cells, one for each object or constellation of features.

Despite the fact that strong experimental evidence was provided supporting the idea of specialized cells in the primate cortex (for instance see [34]), it was argued that this model imposes serious limitations on the information processing capacities of the brain. The simple feed-forward connection model requires neurons to encode increasingly complex relations among different elementary features. Even though these elementary features characterizing the out-



side world are limited in number, the number of possible combinations of these features is virtually infinite. The fact that even a simple object, e.g., a cup, can appear in a waste number of possible positions, illuminations and colors would require an enormous amount of “grandmother cells”. This would lead to a combinatorial explosion [118, 30]. The number of cells necessary to accomplish the task would quickly exceed even the number of neurons available in the brain.

Furthermore, due to the high specialization of “grandmother cells”, a loss of a single of these cells would lead to the inability to recognize an object under a certain condition. This prediction contradicts experimental findings that parts of the brain can be removed without a complete loss of the ability to perceive a particular form or shape. A further argument contradicting Barlow’s theory is the widely accepted finding that new cortical neurons cannot be built in the adult brain ([102], but see also [144]). Consequently, an enormous number of “empty” “grandmother cells” must be available in order to make learning of new objects or new constellations of objects possible. So far, no experimental evidence for these “sleeping” cells has been presented. In addition, later stages of the visual system that further process the information, do not have available information about features of an object once it was “recognized” by a “grandmother cell”. For example, a green and a red cup represented by two different “grandmother cells” can only be recognized as two separate objects. The information “green” or “red” will not be available for further processing beyond the visual system. Therefore, the approach to solve the binding problem by means of “grandmother cells” raised many problems that eventually lead to the development of new hypotheses.

An alternative approach to the binding problem goes back to an idea first postulated by Donald Hebb in 1949 [51]. In his theory, perception is not achieved by highly specialized single neurons but by assemblies of cells. These cell assemblies consist of a large number of highly interconnected neurons forming a self organizing neural network. This type of coding requires some kind of labeling for the

assemblies so that they can be distinguished by subsequent processing stages. One possibility for labeling different assemblies is through synchronous firing of nerve cells [30, 42, 31]. According to this model, nerve cells that are activated by the same object tend to correlate the times when they fire an action potential. Neurons coding for features belonging to different objects should not show this correlated firing activity. Therefore, relations between object features should be achieved by coordinated activity of an assembly of feature-tuned cells (for reviews see: [44, 123, 122]).

This model of synchronized firing as the coding mechanism has several advantages. The same neuron can contribute to a large number of assemblies and, therefore, code for more than one object. Changes in some features of an object, e.g. color, are coded by incorporating new feature-selective neurons into the assembly. This strategy increases the efficiency of coding and avoids the problem of combinatorial explosion.

Furthermore, processing is distributed over a wide cortical area and does not converge onto one highly specialized single neuron. This distributed processing leads to a less vulnerable system. Since cells do not code for only one specific object, the loss of cells does not lead to the inability to recognize certain objects. In addition, all feature-specific information is available to other brain areas.

The processing speed of a pure rate code is limited by the time needed to reliably assess the average firing rate, i.e. the average spiking activity of a neuron, necessary to distinguish two neuronal responses. In contrast, precise spike timing on a short time scale is a much faster coding mechanism. This code based on the synchronous firing of cells needs a much shorter integration time, i.e., the time needed to reliably distinguish two distinct constellations of object features. It therefore allows for higher processing speeds. In addition to synchronizing their action potentials, cells show an oscillatory modulation of their firing rates [41, 42]. If synchrony occurs on the basis of such a 40 Hz oscillation, a theoretical maximum of up to 40 different assemblies could be formed every second [123].

In order to exploit the high temporal precision of spike timing, neurons have to act as coincidence detectors rather than integrators. In other words, neurons have to be able to distinguish synchronous from non-synchronous incoming spikes on a millisecond time scale and to fire action potentials based on this temporal analysis rather than only integrating incoming signals over time. In which of the two processing modes neurons are operating is still a question of debate [61, 119]. However, there is convincing evidence that neurons can exploit the high precision of temporal patterns of incoming spiking activity [2]. Further evidence comes from the auditory system where neurons do evaluate delays between signals coming from the two ears on a microsecond time scale [65]. A combination of both modes, firing rates and precise spike timing, also seems possible, depending on the task to be accomplished.

In the late 80ies it has been shown by Gray and Singer that cells in the primary visual cortex of the cat coordinate their firing activity combined with an oscillatory pattern in a frequency range of 40 to 60 Hz, the so called  $\gamma$ -band [41]. Gray et al. showed that two cells with non-overlapping receptive fields that are activated by the same moving bar, show synchronized firing activity to a much higher degree than when the same cells were activated by two separate bars [41]. This experiment showed that synchronization between cells can solve a special case of the binding problem, i.e., signal the difference between two separate and one continuous object. Similarly, synchronization and oscillation on an even higher time scale of up to 100 Hz has been found for signal transmission from the retina to the LGN [82, 16]

After these early experiments had shown that internally generated synchronization between neurons reflecting stimulus properties can be found in the visual cortex, subsequent experiments have been designed to test the hypothesis about the role of synchrony in solving the binding problem. It has been shown that not only cells within the primary visual areas tend to synchronize their activity according to the Gestalt criteria but also cells in extrastriate areas, such as the PMLS area, can synchronize their firing activity when stimu-

lated with the same visual object [28]. Furthermore, synchronization can occur between striate and extrastriate areas [28], thus combining different features like shape and motion. Therefore, these experiments showed that synchronization is not solely a local phenomenon but that the cortex is able to maintain synchronization over longer distances. Even over these longer distances, the synchronization occurs without phase shifts between the two cells [28, 88]. Further studies have shown that synchronization could play an important role in the integration of information from different sensory modalities, e.g., between visual and motor areas [107]. Most recent studies showed that the occurrence of synchronization is correlated with the perception of visually ambiguous stimuli. For instance, depending on the exact stimulus condition, two overlaid gratings can be perceived either as two distinct or as a single pattern. It has been shown, that the perception correlates well with the synchronized activity between cells representing the two grating stimuli [17].

## CHAPTER 3    **Materials and Methods**

---

### **3.1 Preparation**

For surgical preparation of the animals, standard techniques were applied. All procedures were in compliance with the German „Tierschutzgesetz“. In the following section, the preparation for recordings from anesthetized animals is described.

After premedication with Atropine (0.1 mg/kg i.m.), anesthesia was induced by Ketamin (Ketanest, 10 mg/kg i.m.) and Xylazine (Rompune, 2.5 mg/kg i.m.) and was maintained with a mixture of 70% N<sub>2</sub>O and 30% O<sub>2</sub>, supplemented by 1% Halothane. After tracheotomy, the animal was placed in a stereotactic head holder. A craniotomy was performed over the cortical area of interest according to stereotactic coordinates and the skull was cemented to a metal rod.

After completion of all surgical procedures, ear and eye bars were removed and the Halothane level was reduced to 0.4% to 0.8% of the total respiration volume. After it was ensured that the level of anesthesia was sufficiently deep to prevent any vegetative reactions to somatic stimulation, the animal was paralyzed with pancuronium bromide (0.2 mg kg<sup>-1</sup> h<sup>-1</sup>). Glucose and electrolytes were supple-

mented intravenously. The electrocardiogram was used to continuously monitor frequency and rhythm of the heartbeat. To ensure a sufficient ventilation, end-tidal CO<sub>2</sub> was kept between 3% and 4% of total respiration volume and the respiration pressure was continuously monitored. Rectal temperature was kept in the range of 37-38°. During the experiments, animals underwent antibiotic treatment with Clamoxyl (50mg/kg i.m.).

The dura was removed prior to insertion of the recording electrodes. After completing the positioning of six to eight electrodes, the skull was closed with hand warm agar and sealed with bone wax. In addition, one electrode was placed in a muscle of the neck to serve as a reference for the electrophysiological recordings.

Atropine 1% and Neosynephrin 5% were used to widen the pupils and to retract the nictitating membrane, respectively. In order to avoid drying of the eyes and to correct for errors of vision due to anesthesia, corneal contact lenses with an artificial pupil of 3 mm diameter were fitted to both eyes. The eyes were refracted for a viewing distance of 57 cm. At this distance a 21 inch computer screen was positioned. As landmarks of the animal's visual field, the area centralis and the blind spot were plotted with a reversible ophthalmoscope.

For recording of neural activity, house made tungsten electrodes were used. The tips were electrolytically sharpened and had a diameter between 10 and 20  $\mu\text{m}$  with a thickness of the electrode's shaft between 125 and 200  $\mu\text{m}$ . The tips were coated with platinum to adjust the impedance to 0.7 to 1.3 M $\Omega$  at 100 Hz.

In area 17, multiunit activity was recorded with two electrode arrays, both being placed in the same hemisphere. The arrays consisted of 4 electrodes with a spacing of 0.2 to 0.3 mm. For area PMLS three arrays were used, two with three and one array with two electrodes, each separated by 0.2 to 0.3 mm.

### 3.2 Data Acquisition

A typical experimental setup for measuring extracellular signals is shown in Fig. 3-1. Microelectrodes were connected to a preamplifier with shielded mini-BNC-cables. The setup measured the potential difference between the tip of the microelectrode and a reference electrode connected to the neck of the animal. Since the recorded signal was on the order of  $10^{-6}$  V to  $10^{-3}$  V, the distance between electrodes and preamplifier was kept as short as possible to avoid artefacts to the very small signal. The house made preamplifier amplified the signal by a factor of 10 so that it could then be fed to a common main amplifier which again amplified the signal by a factor of 1000.

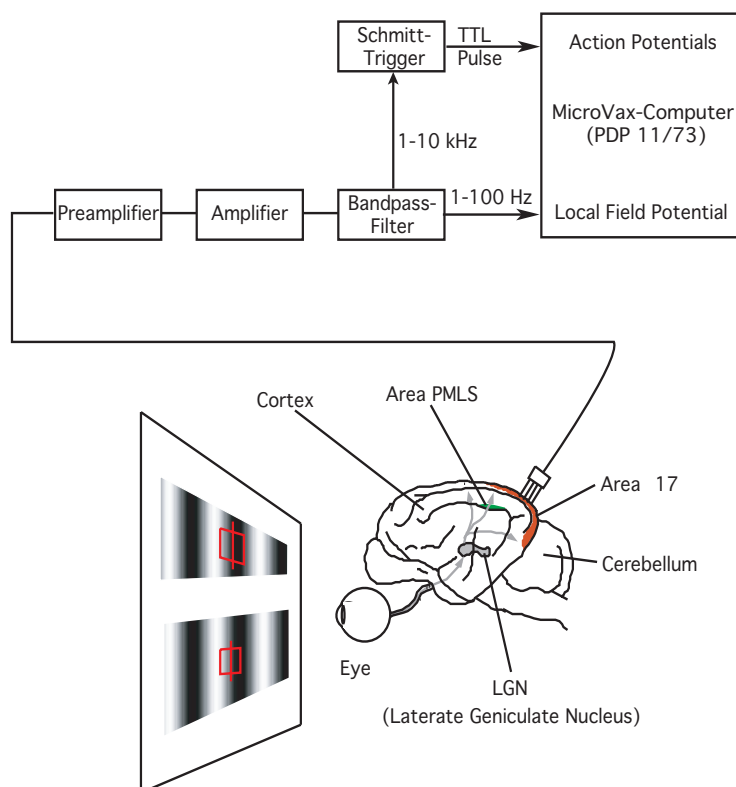


**Figure 3-1: Experimental Setup**

Microelectrodes were connected to a pre- and a main amplifier where the signal was amplified by a factor of 10 and 1000, respectively. For the detection of action potentials ( $< 1$  ms), the amplified signal was filtered by a band pass filter in the range from 1 to 10 kHz. This signal was sent to a Schmitt Trigger where exceeding a threshold produced a TTL-Puls, which was interpreted as the occurrence of an action potential. In addition, LFP was collected and extracted by applying a band pass filter ranging from 1 to 100 Hz. The action potentials as well as the LFP signals were digitized and recorded by a MicroVax-Computer with a digitalization frequency of 1 kHz.

The potential changes measured at the tip of the microelectrode reflected the potential changes in the extracellular medium. Usually, the strongest components of this signal were coming from action potentials generated by nearby cells. For the detection of these short action potentials ( $< 1$  ms), the amplified extracellular signal was filtered by a band pass filter in the range from 1 to 10 kHz. These fil-

ters had a decay of 3 dB per octave (Tektronix, Inc., Beaverton, USA). For the detection of spike events, the amplified and filtered signal was sent to a Schmitt Trigger. The threshold of the Schmitt Trigger was chosen such that the spike signal had to exceed at least twice the noise level. Exceeding the threshold produced a TTL-Puls (TTL: Transistor-Transistor-Logic), which was interpreted as the occurrence of an action potential. The generated TTL pulses were regarded as the train of spiking activity of a group of cells surrounding the tip of the electrode. This spiking activity was called multiunit activity (MUA). The number of cells in one MUA depended on the impedance of the electrode, the diameter of the electrode tip, the shape of the tip, the conductivity of the surrounding brain tissue as well as the choice of the threshold at the Schmitt trigger and were on the order of 25 cells per multi unit.

In addition to the action potential released by individual neurons, the electrodes also recorded the slower potential changes which reflect the dendritic inputs to a small brain area. This signal, called local field potential (LFP), was collected from the same micro-electrode and was extracted by applying a band pass filter ranging from 1 to 100 Hz.

The action potentials as well as the LFP signals were digitized and recorded by a MicroVax-Computer (PDP 11/73) which had a fixed build in digitalization frequency of 1 kHz. In order to have an additional auditory control over the signal, the TTL pulses were sent to a loudspeaker. In addition, the high frequency signal together with the threshold of the Schmitt trigger was displayed on an oscilloscope for visual inspection. Another oscilloscope showed the LFP signal. Averaging the LFP signal over several seconds served as a control to ensure that 50 Hz line noise was not contaminating the signal.

### **3.3 Stimuli**

All visual stimuli were displayed on a 21" computer screen with a horizontal refresh rate of 100 Hz. The monitor was positioned at a distance of 57 cm from the animal's eyes. Receptive fields were



mapped using a hand held lamp (Fig. 3-2). The lamp projected a small rectangular light bar onto the monitor. Once visual responsive neurons were found, i.e. neurons that showed an electrical discharge when the light bar moved over their receptive fields, the size and the position of the receptive field was determined by systematically moving the light bar of the lamp over the monitor. The size of the receptive field was determined as the size of the discharge field of the multi unit sensitive to the luminance defined bar on a black background. These receptive fields were plotted with a computer program and their positions were stored for later analysis. Stimuli were placed such that they covered all receptive fields of the multi units.

### 3.3.1. The Tuning Curve Stimulus

One characteristic property of cells in the early visual areas is their selective response to stimuli moving into a specific direction. Stimuli moving perpendicular or opposite to this direction elicit a reduced or even no response. Cells showing such a selectivity for direction are called *direction selective cells*. The direction eliciting the strongest average response per unit time is called the *preferred direction*, the direction opposite to the preferred direction is called the *null direction* of the cell.

The selectivity of a cell's response with respect to the stimulus direction, i.e. the ratio between the response elicited by stimulation in the preferred and the non-preferred direction, is called the *directional tuning* of the cell (see section 3.4.1 for a more qualitative discussion). Cells that show a strong response only to stimuli moving into the preferred direction and a much weaker response to movements into the non-preferred directions are said to have a strong directional tuning. Cells with a comparable response to all directions of movement are said to have a weak or no directional tuning. The tuning of a cell is measured with a *tuning curve stimulus*. In addition to directional selectivity, cells in the visual system show selective responses with respect to the orientation of a stimulus (*orientational tuning*). For this project it was assumed that in area 17 preferred ori-

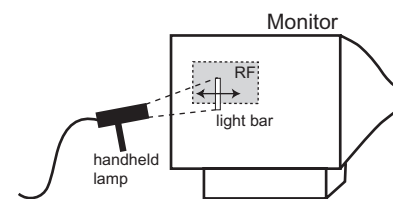


**Figure 3-2: Mapping of receptive fields**  
A hand held lamp projected a small rectangular light bar onto the monitor. Once visual responsive neurons were found the size and the position of the receptive field was determined by systematically moving the light bar of the lamp over the monitor.

entation and direction were perpendicular to each other [141]. Therefore, only the directional selectivity was determined as described in the following paragraph.

The tuning curve stimulus was used to measure the dependence of firing rates on stimulus direction. It is sketched in Fig. 3-3. Identical stimuli moving in different directions were presented inside a quadratic aperture covering the receptive field (RF) of the multi unit. The recorded firing rates were a measure for the response strength of the cell as a function of stimulus direction. For this project, the direction of stimulus movement was varied in 8 steps of  $45^\circ$  each. During the experiments, stimuli were presented in random order to avoid habituation effects. The direction of the strongest response was calculated as described in section 3.4.1.

Directional and orientational selectivity of cells depend on the type of visual stimulus used for the experiment [126]. In addition, the preferred direction can be different for different stimulus conditions like, e.g., the speed of dots in a random dot pattern. Therefore, in order to get accurate results a tuning curve was determined for both types of stimuli that were going to be used for the experiments in this thesis, a sinusoidal grating and a uniform random dot pattern (Fig. 3-4). Both, random dots and gratings, are known to elicit responses in areas 17 (e.g., [48, 14]) and PMLS (e.g., [73]).

In order to elicit maximal firing rates, both stimuli were optimized for areas 17 and PMLS with respect to their temporal and spatial frequencies [15, 73]. For area 17, the grating had a spatial frequency of 0.5 cycles/deg and moved with a velocity of 5 deg/s. The random dots had a diameter of 0.1 deg, also moving at 5 deg/s. The dot density for the stimulus was set to 1.3 dots/deg<sup>2</sup>. For area PMLS, the spatial frequency and velocity of the grating was 0.5 cycles/deg and 10 deg/s, respectively. Dots moved with 10 deg/s having a diameter of 0.2 deg. This led to an average luminance of 2 cd/m<sup>2</sup> for the random dot pattern.

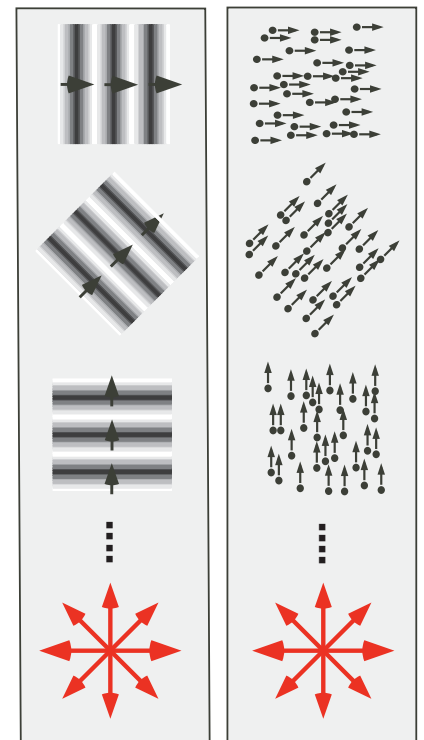


**Figure 3-3: Tuning curve stimulus**  
Identical stimuli moving in different directions are presented inside a quadratic aperture covering the receptive field of the cell. The direction of stimulus movement was varied in 8 steps of  $45^\circ$  each. During the experiments, stimuli were presented in random order to avoid habituation effects.

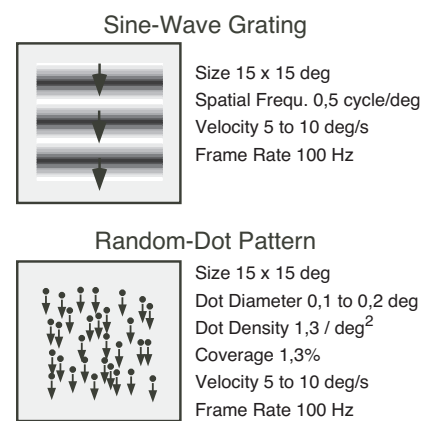


**Figure 3-4: Grating and RD stimulus**  
Gratings and random dots were optimized for areas 17 and PMLS with respect to their temporal and spatial frequencies as written in the figure above. The average luminance for the random dot pattern was 2 cd/m<sup>2</sup>.

### 3.3.2. Random Dot Stimulus with Changing Stimulus Coherence

Grating and random dot stimuli with a single direction of motion are coherent stimuli in the sense that the whole stimulus can be described by a single motion vector giving speed and direction of motion. For the random dot pattern, this coherence can easily be disturbed by moving a fraction of dots into another than the primary stimulus direction. In order to describe this stimulus, a single vector is not any more sufficient. This possibility to change the coherence of a stimulus can be used to study the influence of different levels of stimulus coherence on the processing of information and feature binding in the visual system. An example for this stimulus is shown in Fig. 3-5.

For the fully coherent stimulus, all dots moved with a constant velocity into the preferred direction of the cell. To decrease coherence, a certain percentage of randomly selected dots was hidden from the screen for the duration of one frame (10 ms). During this time, these dots were repositioned and reappeared at a new location. After another 10 ms dots were again hidden for the duration of one frame, repositioned and shown at a new position.

Alternatively, one could simply change the direction of motion for a given percentage of dots in order to disturb the coherence of the pattern. However, such kind of noise would add dots with a motion component pointing into the null-direction of the multiunit which could lead to an additional inhibition of the response. To avoid this inhibition, all motion directions  $89^\circ$  around the Null-direction would have to be excluded which in turn limits the degree of possible decoherence.

In this thesis, different levels of coherence were therefore achieved by randomly changing the position of 0%, 5%, 10%, 20%, 50% and 100% of the dots. These percentages were taken as the measure for the coherence of the stimulus. 0% corresponded to a fully coherent dot pattern and 100% to a pattern of incoherently moving

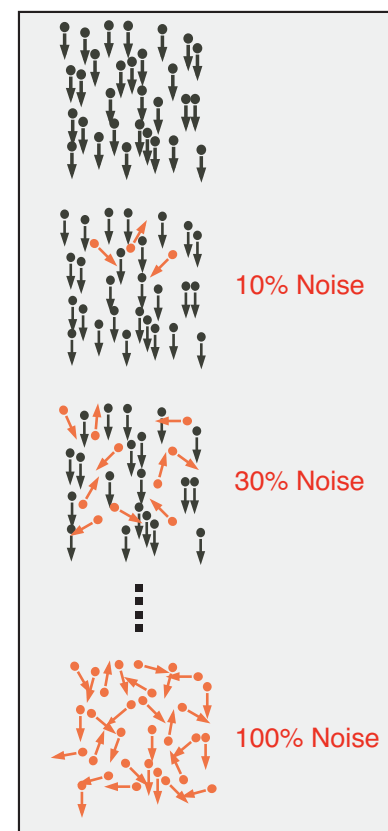


**Figure 3-5: The coherence stimulus**  
Different levels of coherence were achieved by randomly changing the position of 0%, 5%, 10%, 20%, 50% and 100% of the dots. These percentages were taken as the measure for the coherence of the stimulus. 0% corresponds to a fully coherent dot pattern and 100% to a pattern of incoherently moving dots containing a random mixture of directions and speeds in which all spatio-temporal combinations were equally probable and no motion direction existed.

dots containing a random mixture of directions and speeds in which all spatio-temporal combinations were equally probable and no motion direction existed.

The density of dots and the dot size were kept constant for all levels of coherence and were similar to the values used for the random dot pattern in the tuning curve experiment. The dots were of high contrast with respect to the background. Their low space-time density led to an average luminance of  $2 \text{ cd/m}^2$  for all levels of coherence. The stimulus was presented in a fixed quadratic aperture that covered the receptive fields of the cells. The main direction of movement was chosen such that it matched the preferred direction of a cell as calculated from the tuning curve measurement. A sinusoidal grating moving into the preferred direction of the cell was used as a control to ensure visually responsive cells. The parameters for the grating stimulus were the same used for the tuning curve experiment described above.

### **3.3.3. The Shape-From-Motion Stimulus**

In the second part of this thesis, a bar consisting of moving high luminance dots was used as a shape-from-motion (SFM) stimulus. The perceived shape of the bar was always moving into the preferred direction of the cell which was previously determined by the tuning curve experiment (3.3.1). For different stimulus conditions, dots defining the bar had different directions of movement relative to the shape. They were either moving into the same direction, into the opposite direction or perpendicular to the shape. The SFM bar itself was either shown on a black background or on a background pattern consisting of the same high-luminance dots that were used in the coherence experiment described in section 3.3.2. This background pattern either remained static or was moving into different directions relative to the direction of the shape of the bar. The different combinations of bar and background motion are shown in Figs. 3-6 to 3-11. Open circles depict the background dot pattern, black and gray bars represent solid moving bar stimuli, i.e., bars not built by random dot patterns but by a luminance defined rectangle. Black

and gray represent high and low luminance, respectively. Arrows give the direction of motion for the respective dots and bars. For better visibility, all figures show the stimuli with inverted luminance, i.e. light bars are shown as dark while a dark background is shown as a white square.

The whole stimulus set was divided into six subgroups. The first group (Fig 3-6) consisted of solid contrast bars and SFM bars on different backgrounds. These stimuli served as a reference and control for subsequent SFM stimuli. Panel A shows a high luminance bar moving over a black background. The onset and offset of the response elicited by this stimulus was used to define the time window during which the bar was moving over the receptive field. Firing rates elicited by the SFM bars were averaged over this time window for all 22 stimulus conditions. The stimuli shown in panel B and C measured the influence of different backgrounds on a contrast defined solid bar. The bar was either moving over a static random dot pattern (B) or over a dot pattern moving into the null direction of the cell (C). These results were compared to SFM bars moving over different dot backgrounds as shown below. The gray bars in Fig. 3-6 (D and E) represent contrast bars whose luminance was adjusted such that it matched the average luminance of  $2 \text{ cd/m}^2$  of the dot pattern. These stimuli were included to rule out the possibility that different firing rates elicited by a solid bar and a SFM stimulus were due to differences in luminance only. As for the high luminance contrast bar, the bar was shown on either a black background (D) or on a static dot pattern (E). The following two stimuli were SFM bars which were made up from dots moving into the same direction as the shape itself, thus moving into the preferred direction of the cell. To ensure that this type of random dot defined bars was able to elicit a neural response and in order to compare this response with those of the solid contrast bars, the SFM bar was shown moving over a black background (F) and over a static random dot background (G).

The second group (Fig. 3-7) consisted of SFM stimuli moving over non static backgrounds. Panel H shows the SFM bar moving over a non static random dot pattern. Because the background was

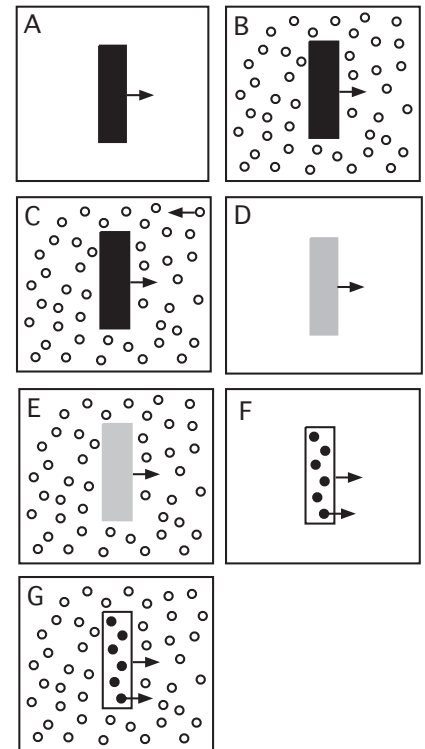


**Figure 3-6: SFM stimulus set I**  
Different stimulus bars moving over different backgrounds. Bars in all stimulus sets were moving into the preferred direction of the cell. **A** Contrast bar on a black background; **B** contrast bar on a static random dot background; **C** contrast bar on a background moving into the null direction; **D** luminance adjusted bar on a black background; **E** Luminance adjusted bar on a static random dot background. **F and G** The dots building the bar were moving into the preferred direction of the cells over a black background (F) and over a static random dot background (G). For better visibility, all figures show the stimuli with inverted luminance, i.e. light bars are shown as dark while a dark background is shown as a white square.

moving into the same direction and with the same velocity as the bar, it rendered the SFM stimulus invisible. No firing rate despite the activity elicited by the background motion was expected for this stimulus condition. For the stimulus shown in panel I, the direction of motion of the background pattern was rotated  $90^\circ$  so that it moved perpendicular to the preferred direction of the cell. This direction of motion should reduce the response of the cell to the background pattern and, in contrast to condition H, should lead to a response due to the movement of the SFM bar. An even stronger response was expected for the SFM bar shown in panel J. This stimulus represented the typical SFM constellation. The bar, defined by dots moving into the preferred direction of the cell, was shown on a dot background that was moving into the opposite direction relative to the dot movement of the bar. For the human observer, this stimulus gives the strongest perception of a shape moving over a moving background.

To further investigate the influence of the background on firing rates elicited by an SFM bar, stimuli K to N (Fig. 3-8) were designed to mask out the background motion in an area overlaying the receptive field [45]. Two different masking sizes were used. The smaller of the two masks was a square whose side length equals the width of the SFM bar, the larger mask had a side length equal to the length of the SFM bar. The masked area either matched the black background (K and L) or was filled with static random dots of the same size and density as the background dot pattern (H and I).

To determine the saliency of the SFM stimulus, visual flicker onset noise was introduced into the static random dot background (Fig. 3-9). This stimulus was used to investigate, if area PMLS is still able to perceive a SFM stimulus moving over a non-coherent dot pattern. The noise was of the same kind as described in section 3.3.2 except that here the dot pattern itself remained static. Only the fraction of dots that create the noise were hidden and repositioned as described above. Noise levels of 5% (Panel O), 10% (Panel P) and 20% (Panel Q) were used. For all three stimuli, dots defining the bar and the shape itself were moving into the preferred direction.

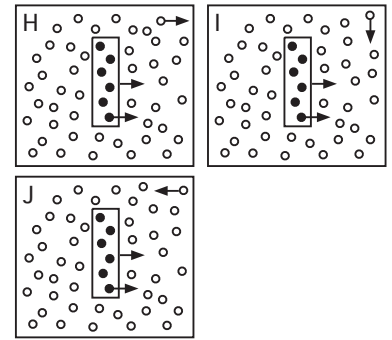


**Figure 3-7: SFM stimulus set II**

In this set, dots building the bar and the bar itself were moving into the preferred direction of the cells. **H** SFM bar on a random dot background moving into the preferred direction; **I** SFM bar on a random dot background moving  $270^\circ$  off the preferred direction; **J** SFM bar on random dot background moving into the null direction.

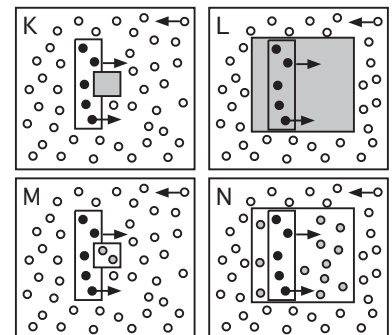


**Figure 3-8: SFM stimulus set III**

Dots building the bar and the bar itself were again moving into the preferred direction of the cells. **K to N** SFM bar moving over a random dot background moving into the null direction. This background was covered with a small black mask (K), a large black mask (L) and a small (M) and a large (N) mask filled with static random dots.

The fifth subgroup varied the relative direction of motion between the dots defining the bar and the shape itself (Fig 3-10). If cells in area PMLS are able to globally bind the dots in order to perceive the bar as one object, and if, in addition, the binding is signaled by a rate code, the relative motion of the dots with respect to the direction of motion of the virtual contour of the bar should not make a difference in the cell's response. If, however, this area is not capable of performing global binding but instead analyzes the component motion only, the response strength should also depend on the direction of the dots relative to the shape of the bar. Alternatively, if the rate code (see chapter 2.4) is not the underlying coding mechanism but a different binding mechanism, i.e., synchronization, is used to bind the dots in order to perceive the shape from motion bar, the cells' response should most likely also depend on the relative direction of dots and shape. Panel R shows a SFM bar whose dots were moving  $90^\circ$  off the direction of motion of the shape. The shape for all three stimuli in Fig. 3-10 was moving into the preferred direction of the cell. The superposition of dot and shape movement resulted in an effective dot movement of  $45^\circ$  relative to the preferred direction. Panel S corrected for the superposition of motion. In order to have a difference of  $90^\circ$  relative to the preferred direction, the dots were moving  $135^\circ$  off the direction of motion of the shape. Panel T shows the SFM bar with dots moving in the direction opposite to the direction of the shape itself. All three SFM bars were moving over a static dot background.

The last group of stimuli (Fig. 3-11) added a moving dot background to stimulus condition R and T. The background dots were moving perpendicular to the direction of motion of the shape but opposite to the direction of the dots defining it, i.e.,  $270^\circ$  off the preferred direction of the cell.

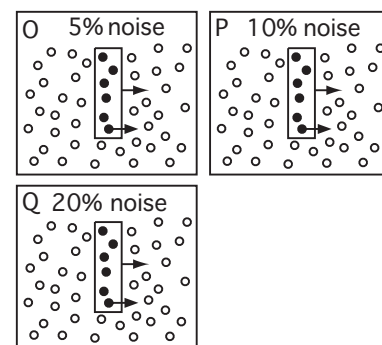


**Figure 3-9: SFM stimulus set IV**  
Dots building the bars and the shapes of the SFM bars were moving into the preferred direction of the cell. The static random dot background contains 5% (O), 10% (P) and 20% (Q) static flicker onset noise.

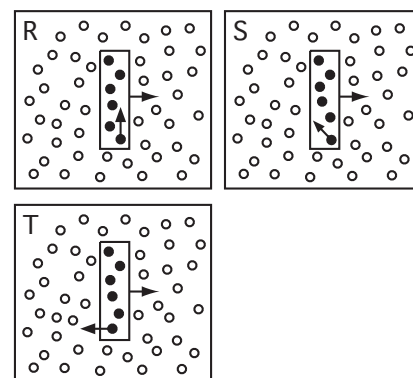


**Figure 3-10: SFM stimulus set V**  
All bars in this stimulus set were moving over a static random dot background into the preferred direction of the cell. **R** The dots building the bar were moving  $90^\circ$  off the preferred direction; **S** The dots building the bar were moving  $135^\circ$  off the preferred direction. **T** dots building the bar were moving into the null direction.

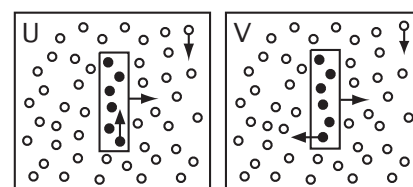


**Figure 3-11: SFM stimulus set VI**  
The SFM bar was again moving into the preferred direction of the cell. **U** same as R but with a background pattern that was moving  $270^\circ$  off the preferred direction of the cell; **V** same as T, but with a background moving  $270^\circ$  off the preferred direction of the cell.

### 3.4 Indices for Quantification of the Tuning curve

The characteristics of the tuning of a single cell or multiunit are important parameters for the analysis of mechanism dealing with the analysis of motion detection. Information about the preferred direction as well as the strength of directional selectivity of a cell are important if one tries to interpret firing rates and synchrony as a function of stimulus condition. This section will describe indices defined to quantify the preferred stimulus direction for a cell and the width of the tuning curve.

#### 3.4.1. Preferred Direction and Direction index

As described in more detail in section 3.3.1, one characteristic property of many cells in the visual system is their preference for stimulus movement into a direction that is characteristic for this cell [52]. Therefore, in order to compare responses from different cells it was important to know about their directional selectivity. A direction index was used to describe, how strongly the response of a cell depended on a certain direction of stimulus movement. It measures the difference between firing rates elicited by a stimulus moving into the preferred direction and the null direction of a cell.

To calculate the preferred direction of a cell and the so-called direction index, firing rates of a multi unit were measured for each of the eight stimulus directions of the tuning curve stimulus. The response elicited by each of the eight stimulus directions was represented by a response vector  $\vec{r}_i$ ,  $i = [1, \dots, 8]$ . Its length was given by the firing rate, its direction by the direction of motion of the particular tuning curve stimulus. The vector of the preferred direction  $\vec{R}$  was defined and calculated by taking the vector sum of these response vectors for each of the single directions

$$\vec{R} = \sum_{i=1}^8 \vec{r}_i . \quad \text{Equation 3-1}$$



The direction index (DI) was then given by the quotient of the absolute value of the vector of the preferred direction and the sum of the absolute values of the vectors of the single directions

$$DI = \frac{\left| \sum_{i=1}^8 \vec{r}_i \right|}{\sum_{i=1}^8 |\vec{r}_i|} = \frac{|\vec{R}|}{\sum_{i=1}^8 |\vec{r}_i|} . \quad \text{Equation 3-2}$$

The domain for this direction index lies between  $0 \leq DI \leq 1$ . A value of zero represents a completely directionally unspecific multi unit whereas a direction index of one stands for a perfectly tuned cell that responds in one direction of stimulus movement only. In the present thesis, visual inspection of the tuning of multiunits with a direction index of smaller than 0.1 showed a fairly round tuning curve with all direction eliciting approximately equal firing rates. These cells were therefore regarded as non directional selective. Tuning curves with an index of more than 0.3 showed a clear preferred direction and much smaller firing rates when stimulated in all other stimulus directions. Hence, this value was taken as a measure of a fairly well tuned multiunit.

Other methods used to determine the preferred direction of a cell are a least square fit of the tuning curve with a Gauss function [137]. It has been shown, however, that for tuning curves recorded in steps of  $45^\circ$ , as it is the case in the present experiments, the Gauss fit gives similarly accurate estimations of the preferred direction and as the vector average applied here [137]. Since the vector average is computational less time consuming and less error-prone it was used for the present analysis. A Fourier transform (FT) based algorithm can also be used to analyze the tuning curves [150]. In this algorithm, the direction preference was estimated by determining the phase angle of the first order term of the FT of a set of firing rates elicited by the different directions of the tuning curve stimulus. It has been shown, however, that this is equivalent to the vector averaging method which was therefore used in this thesis (for a detailed comparison of these methods see [137]).

### 3.4.2. Tuning Width Index

Not only the relative magnitude of firing rates in the preferred and the null-direction of a cell is an important measure for the tuning property but also the firing rate in directions adjacent to the preferred direction of the cell. The firing rate probability for stimulus movement into these directions close to the preferred direction of the cell determines the width of a tuning curve. The direction index introduced in section 3.4.1 was a good measure for the direction selectivity of a multi unit. It did, however, not provide satisfactory information about the width of the tuning curve. The direction index did not allow to distinguish, whether a low index value came from comparable firing rates in both the preferred and the null-direction, or from high firing rates elicited by stimulus movement in directions adjacent or orthogonal to the preferred direction of the cell. Therefore, in order to get a more reliable measure for the width of a tuning curve, a new index was necessary. Since no appropriate measure could be found in the literature, I developed the following new index during this thesis.

Again, eight response vectors  $\vec{r}_i$  were defined, one for each direction of movement that represent the firing rates elicited by the tuning curve stimulus. The length of each vector was again given by the firing rate elicited by the tuning curve stimulus and the direction by the direction of stimulus movement. The preferred direction  $\vec{R}$  was calculated using equation 3-1. To calculate the width index, vectors around the preferred direction from  $\vec{R} + 90^\circ$  to  $\vec{R} - 90^\circ$  were orthogonally projected onto the line perpendicular to the preferred direction of the cell. The index is given by the quotient of the sum of these projections  $\pi$  and the sum of the absolute values of all eight firing rate vectors:

$$WI = \frac{\sum_{i=1}^p \pi_i}{\sum_{i=1}^8 |\vec{r}_i|}, \quad p = \text{number of projections.} \quad \text{Equation 3-3}$$

The domain for this index is between  $0 \leq x < 1$ . Values close to zero represent a very narrow tuning curve. In order to get a value close to zero, cells must show very low firing rates in directions of  $\vec{R} \pm 90^\circ$  around the preferred direction of the cell. Values around one indicate broad tuning curves.

### 3.5 Analysis of Spike Signals

One of the basic signals measured in the electrophysiological experiments covered in this thesis was the spiking signal of a multi-unit. As described in section 2.2, in a first approximation a spike is an electrical impulse elicited by a cell when a certain threshold in the membrane potential has been reached. Measuring the arrival times  $t_1, t_2, \dots, t_N$  of spikes as a function of time gives the spike train  $\{t_i\}$ . Understanding the neural code would need a good understanding of the relationship between these spike trains and the events occurring in the outside world. A code most likely does include both the spike rate as well as the temporal organization of the spike trains. The simplest possible relationship between the outside world and the corresponding spike train would be that one particular time-dependent stimulus always triggers the same spike train that uniquely describes this stimulus. However, this is not the case. Many experiments have shown that repeated measurements always lead to different spike trains for the same stimulus. Therefore the only predictions that can be made are of probabilistic nature.

#### 3.5.1. Quantification of Firing Rates

A complete probabilistic description of a neural response given a time dependent stimulus  $s(t)$  is described by the conditional probability  $P[\{t_i\}|s(t)]$  which gives the relative likelihood to measure a spike train  $\{t_i\} = \{t_1, t_2, \dots, t_N\}$  given the stimulus  $s(t)$ . To get a sufficient estimate of this probability, one has to repeat the same stimulus many times and measure the spike train for each stimulus presentation. However, since it is impossible to determine the probability distribution  $P$  for all possible spike trains  $\{t_i\}$ , one measures the time dependent firing rate  $r(t)$ . This firing rate is defined as the

probability  $r(t)$  of detecting a spike at time  $t$  given a stimulus  $s(t)$ . In a real experiment, this probability can only be approximated for a finite time window of length  $\Delta\tau$ . The number of spikes occurring within this time window is then given by the relative frequency

$$p(t) = r(t)\Delta\tau. \quad \text{Equation 3-4}$$

The rate can thus be defined as the relative frequency per unit time that a spike will occur within a small time window around time  $t$ . This function of time is called the Peri-Stimulus-Time-Histogram (PSTH).

The graphical representation of the PSTH is a histogram that shows the action potentials of a cell or cell assembly as a function of time. Experimentally,  $p(t)$  is measured by counting the spikes occurring within a certain time window relative to the beginning of the stimulus. The results are averaged for many stimulus repetitions. The analysis of these firing rates gives general properties like tuning behavior or firing properties of a cell with respect to a given stimulus. For this thesis, the analysis of firing rates was used to investigate the effects of visual noise on the visual system (section 4.3) as well as to answer the question, if cells in area PMLS were able to detect the movement of shapes that are only defined by the movement of dots (see chapter 5).

As discussed in more detail in section 2.4, it is a question of ongoing debate, whether all information about a stimulus is contained within the firing rate of a cell or if, in addition, a temporal code is of importance to achieve certain abilities of the visual system (for recent reviews see [120, 44] and [124]). The techniques to investigate the temporal code are described in the following sections.

### 3.5.2. Cross Correlation Analysis

Precise timing between action potentials originating from different cells are known to play an important role in the processing of sensory information. To detect this synchrony of neural activity be-

tween two spike trains,  $g(t)$  and  $h(t)$ , the cross correlation function was approximated by the temporal mean of the product  $g(t)h(t)$  given by

$$CCF_{gh}(\tau) = \int_{-T}^T g(t)h(t + \tau)dt. \quad \text{Equation 3-5}$$

$\tau$  is the relative shift of the two spike trains  $g$  and  $h$ , a standardization factor was not considered. For the auto correlation function,  $g$  is set equal to  $h$ . The integral is calculated over one stimulus presentation or over a certain window within one trial. The analysis in this thesis was restricted to first order correlation analysis which is common for neurophysiological data (see for instance [32, 17, 43] or [117]).

As for the PSTH, the correlation analysis was carried out with a time discrete signal. The sampling interval was 1 ms. A longer time interval would have increased the probability for having more than one spike per time bin. A smaller window would have decreased the probability for coincidences such that a sufficient statistic under the experimental constraints would not have been possible. For the analysis of the discrete spike signals, the detected signal was converted into a binary representation based on the time resolution of the signal of one millisecond. A "1" represented an action potential, "0" represented no action potential in the given time bin. For the correlation analysis, the signals were shifted relative to each other and the CCF was computed by summing the binary multiplied shifted signals. The maximal shift was between 80 ms and 250 ms, based on the oscillatory structure of the resulting CCF. Hence, synchronization and oscillation could be detected in the alpha frequency range (5 Hz to 15 Hz) as well as in the gamma region (30 Hz to 70 Hz). The correlation function was graphically represented by a histogram showing the number coincidences against time shift, called the correlogram (Fig. 3-12).

Besides synchrony that is generated inside the brain (intrinsically generated synchronization), synchronized firing activity can also be due to a locking of the elicited firing rates to the external stimu-

lus. This so-called externally generated synchronization had to be removed from the cross-correlograms by subtracting the result of the so-called shift predictor which was calculated as follows: many experiments have shown that an internally generated synchronization pattern will never be exactly the same between two consecutive trials. In contrast, externally generated synchronization that is locked to an external stimulus will repeat itself for every stimulus presentation. Be  $g(t)$  and  $h(t)$  two spike trains from two electrodes elicited by a given stimulus  $s(t)$ . These spike trains were averaged for all stimulus presentations  $n$

$$G(t) = \frac{1}{n} \sum_{i=1}^n g_i(t)$$

$$H(t) = \frac{1}{n} \sum_{i=1}^n h_i(t) .$$

Equation 3-6

In order to remove the external synchronization between the two recording sites, a cross-correlation function was approximated by the temporal mean of the product of  $G(t)H(t)$

$$CCF_{GH}(\tau) = \int_{-T}^T G(t)H(t+\tau)dt .$$

Equation 3-7

This CCF is called the shift predictor and shows only synchronization events contained in all stimulus presentations.

A quantitative description of the correlograms was performed by fitting it with a mathematical function. The features of interest were the width and height of the center peak of the correlation function as well as the oscillatory behavior of the cell's response. One problem for the fitting procedure was a poor quality of the signal to noise ratio in the majority of the correlograms. This was due to the limited number of possible stimulus repetitions that was on the order of 10 to 20 trials in most experiments. In addition, fluctuations in signal quality between trials led to a further reduction in the signal to noise ratio. These fluctuations were due to fast changes in the arousal state of the animal. This was especially a problem in area

PMLS, where these changes happened far more often than in the primary visual area. Due to this low signal quality, the choice of a fitting function that was reliable with respect to the parameters in question became necessary. A first attempt to fit the data was performed according to the fitting procedure described by König et al. [60]. König used the sum of a generalized Gabor function and a Gauss function to fit the data. However, due to the Gabor function, fitting results of the present data were not satisfactory and the center peak of the correlation function was not reliably detected. Because visual inspection of all correlograms in area 17 revealed no oscillatory behavior for random dot stimuli with and without visual noise, the main parameters of interest were only the width and the height of the center peak of the correlation function. Therefore, the fitting function was reduced to a Gauss function with an additional linear and quadratic term. The equation was of the following form

$$f(x) = Ae^{\left(-\frac{1}{2} \frac{(x-\phi)^2}{a_2^2}\right)} + O + a_4x + a_5x^2. \quad \text{Equation 3-8}$$

$A$  gives the amplitude of the function which corresponds to the height of the center peak in the correlogram. The offset  $O$  is a measure of how many coincidences of action potentials occur by chance.  $a_4x$  and  $a_5x^2$  are the linear and the quadratic term, respectively, and are included in order to correct for very low frequency curvature in the correlogram due to fluctuations in the single spike trains.  $\phi$  is the shift of the maximum of the Gauss curve from zero and indicates a phase shift between the firing times of the two cells. A further important measure used to describe the correlogram was the half width of the center peak, which corresponds to the half width at the inflection point of the gauss curve which is given by  $a_2$ .

In addition to the height and width of the center peak, the relative modulation amplitude (RMA) was used for quantification of the correlation strength relative to the correlations occurring by chance. It is defined as the ratio between the amplitude of the central maximum (A) and the offset of the correlogram (O):

$$RMA = \frac{A}{O} . \quad \text{Equation 3-9}$$

In order to perform the fit, a new program based on the IDL programming language was developed (IDL, Interactive Data Language, Version 5.4, Research System Inc.).

Data in area PMLS showed an additional strong oscillation in the low frequency range. To quantify these data, a simple sine wave was fitted to the correlograms (IGOR professional, Version 3.16, WaveMetrics, Inc.). The equation for this sine wave was given by

$$y = K_0 + K_1 \sin(K_2 x + K_3) \quad \text{Equation 3-10}$$

$K_0$  gives the offset,  $K_1$  the amplitude,  $K_2$  the frequency and  $K_3$  the phase shift of the sine wave.

Fig. 3-12 gives a sketch of a typical correlogram containing the important parameters used for further analysis.

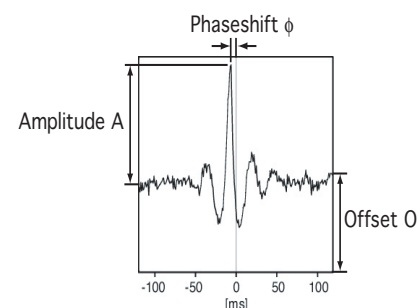


**Figure 3-12: Sample Correlogram**  
The figure shows a typical correlogram calculated from a multiunit in area 17 of the cat. Time in milliseconds is plotted against the number of coincidences. Phaseshift, amplitude and offset are explained in the text.

### 3.6 Analysis of the Local Field Potential

In contrast to spike signals, the LFP reflects changes in the dendritic signals. These changes are on a much slower time scale than the spiking activity. Furthermore, this signal does not consist of single time points representing the occurrence of one action potential but can be regarded as a continuous signal. The amplitude is sampled with a frequency of 1 kHz. Methods for analyzing this signal are described in the following paragraphs.



### 3.6.1. Power Spectrum of the LFP

Frequencies contained in the LFP are reflected in its power spectrum. Averaged over many stimulus repetitions, power spectra provide a very sensitive measure for changes in frequencies between different stimuli.

Be  $l(t)$  the LFP recorded from one electrode,  $L(f)$  the FT of  $l(t)$ . The power spectrum is then given by the square of the absolute value of the product of the FT and the complex conjugate of the FT:

$$P_l(f) = |L(f)L^*(f)|^2. \quad \text{Equation 3-11}$$

The asterisk indicates the complex conjugate. The power spectrum was normalized to one with the normalization condition  $\int P_l(f)df = 1$ . In order to compare the amount of power contained in different frequency bands across conditions, the power spectrum was summed over two different frequency ranges: the  $\alpha$ -band ranging from 6 to 18 Hz and the  $\gamma$ -band between 30 and 60 Hz. Strictly speaking, the FT has to be calculated over an infinite signal. This was, of course, impossible. For this thesis, a time window with a length between 2000 ms and 4000 ms was used. Taking the FFT of only a short part of a signal is equivalent to convoluting it with a box-car function

$$D(x) = \begin{cases} 1 & \text{for } a \leq x \leq a+M \\ 0 & \text{elsewhere} \end{cases} \quad \text{Equation 3-12}$$

with  $a$  being the beginning and  $M$  being the length of this part of the signal. The FT of this box-car function is the sinc function

$$\text{sinc} = \frac{\sin x}{x}. \quad \text{Equation 3-13}$$

According to the convolution theorem for the FT, the FT of a product of two functions equals the convolution of the FT of each of the functions. Therefore, multiplying the signal with a box-car function  $D(x)$  is equivalent to convoluting the FT of the signal with the FT of  $D(x)$ , the *sinc* function. The *sinc* function has the property of having large side maxima on both sides of the central maximum which contrib-

ute to frequencies sitting at these values. In order to avoid this error, the signal was multiplied with a windowing function which is equivalent to the convolution of the signal with the FT of this windowing function. The window function was chosen such that it showed smaller side lobes compared to the box-car function. However, this reduction in side lobes is accompanied by an increase in the width of the center peak. In this study, the Hamming window

$$H(x) = \begin{cases} 0,54 - 0,46 \cos\left(2\pi \frac{x}{M}\right) & \text{for } 0 \leq x \leq M \\ 0 & \text{elsewhere} \end{cases} \quad \text{Equation 3-14}$$

was used which shows a width at the central maximum of  $8\pi/M$  and a reduction of the side lobes relative to the height of the mean center peak of 41 dB.

### 3.6.2. Spike-Triggered Average

In addition to power spectra and the correlation between two spike channels, the correlation between a spike channel and a LFP was computed as follows: In a first approximation, the spike signal  $g(t) = \{t_i\}$  can be regarded as a sequence of delta functions:

$$g(t) = \sum_{i=0}^n \delta(t - t_i), \quad n = \text{number of spikes.} \quad \text{Equation 3-15}$$

Be  $l(t)$  the signal of the LFP. Using the property of the delta function

$$\int_{-\infty}^{\infty} \delta(x - x_0) F(x) dx = F(x_0) \quad \text{Equation 3-16}$$

and using equation 3-5, a correlation of  $l(t)$  with the spike signal  $g(t)$  leads to

$$STA_{gl}(\tau) = \sum_{i=0}^n l(t_i - \tau). \quad \text{Equation 3-17}$$

This function is called the spike-triggered average (STA) [41]. It gives a measure for the coupling between spikes and certain waveforms in the LFP. The algorithm for calculating the STA was as follows: For every time point  $t$  an action potential was detected at one electrode, a corresponding segment of the LFP was cut between  $t - x$  and  $t + x$ .  $x$  was between 80 ms and 250 ms in length. These LFP segments were averaged as shown in equation 3-17.

The resulting average waveform was different for the different stimulus presentations and provided a qualitative measure for the relation between spike and LFP signal. A quantitative measure was provided by the Spike-Field-Coherence described in the next section.

### 3.6.3. Spike-Field-Coherence

The STA as described in the previous section still depends on the power of the LFP. To get a measure independent of the LFP-power, the Spike-Field-Coherence (SFC) was introduced as an extension to the spike-triggered average. It was used to further quantify the coupling of spikes for certain frequencies in the LFP.

Be  $P_{STA_{gl}}(f)$  the power spectrum of the STA calculated according to equation 3-11

$$P_{STA_{gl}}(f) = |STA_{gl}(f)STA_{gl}^*(f)|^2. \quad \text{Equation 3-18}$$

Be  $l_i(t)$  a single LFP segment included into the STA and  $L_i(f)$  its FT. For the power of all LFP segments it follows with equation 3-11

$$P_L(f) = \sum_{i=1}^n |L_i(f)L_i^*(f)|^2. \quad \text{Equation 3-19}$$

For the calculation of the power spectrum of the STA (equation 3-18), summation was performed prior to calculating the power spectrum itself. The opposite holds for the calculation of the power of the sin-

gle LFPs (equation 3-19). Here the summation takes place after calculation of the power spectrum for the single LFP segments. The spike field coherence is then defined as

$$SFC(f) = \frac{P_{STA_{gl}}(f)}{P_L(f)} \quad \text{Equation 3-20}$$

For the calculation of the spike field coherence, LFP segments were cut around spike times as described for the STA in section 3.6.2. A STA was calculated by averaging over all of these segments of the LFP. In addition, a power spectrum of every single LFP was calculated. These power spectra were averaged (equation 3-19) and used to normalize the power spectrum of the STA (equation 3-18). Summing over the resulting spectrum gave the percentage of spikes that were coupled to a frequency within the range of the power spectrum. Integrating over only parts of the frequency range led to a measure of what percentage of spikes was coupled to a certain frequency range of the LFP power spectrum.

### 3.7 Statistical Analysis

The goal of most scientific experiments is to accept or reject a given hypothesis. In life sciences, it is often very difficult or even impossible to control experiments in order to avoid intrinsic errors in the measured data due to fluctuations in the experimental setup. Hence, statistical methods are used to reject or accept a given hypothesis by calculating the probability that the alternative hypothesis, the so-called Null hypothesis, is true.

The hypothesis about a variable of interest must be defined before the experiment, eg,  $x < 0$ . The Null hypothesis is then defined as the opposite to this hypothesis, in our example  $x \geq 0$ . The experiment measures a sample consisting of  $n$  single measurements (random variable) out of a population. In this thesis, the random variable would be for instance the firing rate of one multiunit given a stimulus  $s$ , the population would be all neurons of one area of the brain. For a first estimation of the value of the variable, the mean of the random variable is calculated. If this mean confirms the hypothesis, i.e.,  $x < 0$ , one has to prove that accepting the hypothesis is not only due to a coincidental choice of measurements from the population. The hypothesis can only be accepted, if the mean is significantly different from the mean predicted by the Null hypothesis. In statistical tests, this is done by calculating the probability that the result has been found although the Null hypothesis was true.

#### 3.7.1. Normal distribution

The mean of a random variable out of a population is defined by

$$\bar{x} = \frac{1}{n} \sum_{i=1}^n x_i, \quad \text{Equation 3-21}$$

where  $x_i$  are single measurements of a sample of size  $n$ . The standard deviation of the single measurement is then defined as

$$\sigma = \sqrt{\frac{\sum_{i=1}^n (x_i - \bar{x})^2}{(n-1)}}, \text{ with } n > 1. \quad \text{Equation 3-22}$$

Dividing  $\sigma$  by the square root of the number of measurements leads to the standard deviation of the mean or the standard error

$$\sigma_{\bar{x}} = \frac{\sigma}{\sqrt{n}}. \quad \text{Equation 3-23}$$

$\sigma_{\bar{x}}$  is a measure of how strongly the mean will differ when the measurement is repeated with a different sample out of the same population.

The central limit theorem states that the distribution of means of independent random variables of size  $n$  taken from the same population will approach a normal distribution when  $n$  increases [7]. This holds even when the distribution of single measurements is not a normal distribution. Hence, when  $n$  approaches infinity the distribution of means  $\bar{x}$  will approach a normal distribution given by

$$f(\bar{x}) = \frac{1}{\sqrt{2\pi\sigma_{\bar{x}}^2}} \exp\left(\frac{-(\bar{x} - \mu)^2}{2\sigma_{\bar{x}}^2}\right). \quad \text{Equation 3-24}$$

$\mu$  is the mean,  $\sigma$  the standard deviation of the distribution. It has been shown, that  $n \geq 16$  is sufficient to reach a normal distribution for the means [7, 139].

Be  $x_1$  the mean of a random variable. If the hypothesis states that the true value is larger than the value predicted by the Null hypothesis, the probability of mistakenly rejecting the Null hypothesis is given by

$$p = \int_{x_1}^{\infty} \frac{1}{\sqrt{2\pi\sigma_{\bar{x}}^2}} \exp\left(\frac{-(\bar{x} - \mu)^2}{2\sigma_{\bar{x}}^2}\right) d\bar{x} \quad \text{Equation 3-25}$$

with  $\mu$  being the value expected by the Null hypothesis. A probability of less than 0.05 is commonly used as an upper threshold for rejecting the Null-hypothesis and accepting the hypothesis. If  $p$  is less than 0.001 the result is called highly significant.

### 3.7.2. The t-Test

In this thesis, firing rates elicited by two different stimulus parameters are often to be compared. It has to be tested, if the means of the measured neural parameter (i.e., firing rate) for each recording site are significantly different for two different stimulus parameters. This comparison is done using a t-test for dependent sampling distributions.

For each pair of measurements  $x_1$  and  $x_2$  taken from the same recording site with two different stimulus conditions, the difference  $d$  is calculated by

$$d = x_1 - x_2. \quad \text{Equation 3-26}$$

The arithmetical mean for  $n$  differences  $d$  is given by

$$\bar{x}_d = \frac{\sum_{i=1}^n d_i}{n}. \quad \text{Equation 3-27}$$

A significant deviation of these mean difference from zero will reject the Null hypothesis that both distributions are equal. Be  $\sigma_{\bar{x}_d}$  the standard deviation of the mean differences defined by

$$\sigma_{\bar{x}_d} = \frac{\sigma_d}{\sqrt{n}} \quad \text{Equation 3-28}$$

with  $\sigma_d$  being the standard deviation of the single differences:

$$\sigma_d = \sqrt{\frac{\sum_{i=1}^n (d_i - \bar{x}_d)^2}{n-1}}. \quad \text{Equation 3-29}$$

If the number of measurements within one random variable is larger than 16, as it is always the case in this thesis when the t-test is applied, the probability that the Null-Hypothesis is true can be calculated from the normal distribution using equation 3-25 with  $\mu = 0$ .

### 3.7.3. Analysis of Variance (ANOVA)

For the comparison of more than two independent variables, eg, comparing more than two stimulus conditions, analysis of variance (ANOVA) was used to show that there is at least one significant difference between conditions. Applying multiple t-test, only, would increase the probability of getting a type I error, i.e., the Null hypothesis would be rejected although it was true [7]. ANOVA tests the Null hypothesis  $H_0$  that the means of all conditions are equal:  $H_0 : \mu_1 = \mu_2 = \mu_3 = \dots = \mu_n$ . In contrast, the hypothesis  $H_1$  states that at least two conditions have different means:  $H_1 : \mu_i \neq \mu_j, i \neq j$ .

Assume  $m \cdot b$  measurements, collected from  $b$  conditions and  $m$  measuring sites. One can define three types of variance. The total variance is given by

$$\sigma_T^2 = \frac{\sum_{i=1}^m \sum_{j=1}^b (x_{ji} - \bar{G})^2}{m \cdot b - 1} \quad \text{Equation 3-30}$$

where  $x_{ij}$  are all measurements for all conditions,  $\bar{G}$  is the arithmetic mean of all values and  $m \cdot b - 1$  are the degrees of freedom of the system.

In addition to the total variance  $\sigma_T^2$ , the fraction of variance due to the differences between conditions,  $\sigma_C^2$ , is calculated under the assumption that the only source of variance is between groups, i.e., all measurements within groups have the same value. The mean  $\bar{A}_j$  within one group is used as an estimate of this value. For this variance it follows

$$\sigma_C^2 = \frac{m \sum_{j=1}^b (\bar{A}_j - \bar{G})^2}{b - 1} \quad \text{Equation 3-31}$$



The third variance,  $\sigma_E^2$ , describes non controllable internal errors within groups. This variance is defined by

$$\sigma_E^2 = \frac{\sum_{i=1}^m \sum_{j=1}^b (x_{ji} - \bar{A}_j)^2}{b(m-1)} . \quad \text{Equation 3-32}$$

Assume that the  $H_0$  is valid. Consequently, all m samples have to be out of the same population and it follows that

$$\sigma_A^2 = \frac{\sigma^2}{m} . \quad \text{Equation 3-33}$$

where  $\sigma^2$  is the variance of the population and  $\sigma_A^2$  is the variance between groups given by

$$\sigma_A^2 = \frac{\sum_{j=1}^b (\bar{A}_j - \bar{G})^2}{(b-1)} . \quad \text{Equation 3-34}$$

Here,  $\bar{A}_j$  is again taken as an estimate for the mean values within conditions which fluctuates around the total mean  $\bar{G}$ . Using equation 3-31 it follows under the assumption that  $H_0$  is true:

$$\sigma_C^2 = \sigma^2 . \quad \text{Equation 3-35}$$

If  $H_0$  is true it also follows that  $\sigma^2$  corresponds only to the variance within one sample which is given by the internal error variance  $\sigma_E^2$ . Hence, it follow that

$$\sigma_C^2 = \sigma_E^2 . \quad \text{Equation 3-36}$$

If in contrast the  $H_1$  is to be accepted it follows that

$$\sigma_C^2 > \sigma_E^2 . \quad \text{Equation 3-37}$$

The significance of the difference between two variances is then calculated using the F-test (see for example [7]).

For the comparison of more than two independent variables and two different factors, A and B, the 2-way ANOVA is applied. It is calculated in an analog way. In addition to the total variance and the variance of non-controllable influences, the variance for factor A, variance for factor B and the variance for the interactions between the two factors have to be calculated. For a detailed description see for example 7.

#### 3.7.4. Fisher's Protected Least Significant Difference Test

After ensuring that there is a significant difference within the collected data by means of the ANOVA, Fisher's protected least significant difference test (Fisher's PLSD) was applied to test which of the conditions show the significant difference. Fisher's PLSD uses the results of the ANOVA to calculate a so-called critical difference (CD). This CD is defined as

$$CD = t(b(m-1), SF) \sqrt{\frac{2\sigma_E^2}{n}}. \quad \text{Equation 3-38}$$

Here,  $t(b(m-1), SF)$  is the t-value for  $b(m-1)$  degrees of freedom and a chosen significance level of  $SF$ .  $\sigma_E^2$  is the variance of the intrinsic error from the calculation of the ANOVA (equation 3-32). The CD is used as a bracket interval around each mean value. Intervals that overlap are not significantly different from each other.

## CHAPTER 4    **Incoherent Motion in Areas 17 and PMLS**

---

### **4.1 Introduction**

Motion arises when an object changes its position in space as a function of time [78]. These changes in the object's positions are detected by directionally selective neurons in the visual cortex and give rise to the perception of motion [83]. Many experiments trying to identify the underlying neural mechanism have been performed. The majority of these experiments were using visual stimuli that can be described by a single vector. This vector uniquely defines the direction and the speed of a moving object. Sinusoidal gratings [19, 38] or contrast bars [41, 29, 19] moving over the receptive field of a cell are two examples for this class of stimuli.

When two or more objects, moving into different directions, are superimposed, more than one vector is necessary to describe the motion of each of the components. The different motions can be independent, like two billiard balls rolling into different directions, or might be part of a global object, like a single goose in a swarm flying south. The visual system has to analyze these different vectors in or-

der to i) determine the local motion of each of the components and/or ii) to combine these vectors in order to extract a global percept of motion.

A random dot pattern is an example for a stimulus that cannot be described by one vector only. Instead, a single vector is necessary for every dot in the assembly to describe the stimulus in space and time. In the case of a coherent dot pattern, i.e., all dots are moving in the same direction, all these vectors will collapse into one vector describing this global motion. If, in contrast, some of the dots are moving into different directions, their vectors have to be processed separately by the visual system and a mechanism must exist that weights the different motion information and extracts the vector that reflects the global displacement of the remaining pattern.

Williams and Sekuler [149] used dynamic random dot patterns consisting of many localized motion vectors to examine the integration over space and time. They showed in psychophysical experiments that observers perceive the mean of all different directions distributed in the moving dot pattern. They also showed that the percept of global motion depends on the dot density, the size of displacement and the range of directions within the distribution. Later, Watamaniku [146] showed that the precision, with which an observer is able to discriminate the direction of motion, deteriorates for very short stimulus duration. This indicates that the minimum time needed to process the displacement of objects in order to form the perception of motion is very short. In addition, the discrimination precision decreases with the range of direction vectors present in the target. However, the discrimination performance does not depend on the randomness in direction of individual dot, as long as the number of dots moving into the global direction remains unchanged.

These psychophysical studies provided important information about spatial and temporal integration of local motion signals. However, little was known about the neural processes that were underlying this integration capabilities of the visual system. The question remained, how the excellent psychophysical performance of hu-

mans and animals in motion discrimination tasks was related to the individual cortical neuron. What was missing is the transformation between a sensory signal and its perceptual response.

In 1989, Newsome and coworkers [85, 12] recorded responses from area MT neurons in the monkey to dynamic random dot patterns that were similar to the stimulus used in this thesis. In addition, they performed psychophysical experiments in which the monkey had to discriminate the direction of global motion in random dot pattern with different stimulus coherence. They compared firing rates elicited by single neurons to the psychophysical performance recorded from the same animal and found that the sensitivity of single neurons to changes in stimulus coherence is similar to the discrimination performance in the psychophysical results. They concluded that area MT neurons are able to discriminate the direction of motion within a noisy random dot pattern on the basis of firing rates and that they can account for the low level of coherence at which the monkey is still able to detect the global motion within a noisy stimulus. Recently experiments with functional magnetic resonance imaging (fMRI) have shown that the blood-oxygenation-level-dependent (BOLD) signal does also depend on the coherence of a visual stimulus [101]. In this study, a decrease in the level of coherence in a natural stimulus led to a V-like change of the BOLD signal recorded from areas V1, V2, V3, V3A and V4 in an anesthetized monkey. Furthermore, Rees and coworkers [106] reported a linear decrease in the amplitude of the BOLD signal with decreasing coherence in a random dot texture pattern in human area V5.

When the visual system attempts to discriminate a weak motion signal within a noisy visual display based solely on changes in firing rates, the problem arises that, due to the variety of direction selective neurons, some of the signals available within the visual cortex will carry little or no information about the global motion of the particular stimulus but will only carry information about the noisy visual background. Hence, a mechanism must exist that, based on the particular task, distinguishes neurons that carry important from unimportant information. Furthermore, some of the

information might belong to two different objects and have to be separated and bound in space and time. Using the temporal structure within the firing activity of cells could solve this problem and extract the relevant from the vast amount of available information. This temporal coding scheme based on synchronized firing activity of cells has already been described in section 2.4.

Castelo Branco et al. [17] used two superimposed grating stimuli to show that synchronization is able to signal a global motion for a stimulus described by two independent vectors. Adelson and Movshon [1] showed that, with the right choice of stimulus parameters, these gratings are perceived as moving in two independent directions whereas different sets of stimulus parameters for the two gratings lead to a perception as one component plaid moving into a single direction. Castelo Branco et al. used this plaid stimulus to show that these differences in perception are reliably signaled by a change in the synchronization pattern between cells but not in a change in firing rates.

The present study focussed on a further link between perception of motion and the behavior of the underlying neural substrate in motion discrimination. The random dot stimulus used allowed to gradually titrate the motion signal within a visual stimulus from a strong motion perception to a completely random pattern. This stimulus is described in detail in section 3.3.2. It was investigated, how local incoherence is processed in the visual system of the cat and by which mechanism the brain extracts the direction of global motion from a noisy environment.

This stimulus has been used for psychophysical studies in humans [149, 98], for both psychophysical and electrophysiological studies in monkeys [85, 12] and cats [99, 10] as well as for fMRI studies in humans [106]. The psychophysical experiments with cats showed that the discrimination threshold to detect a motion vector within a noisy background is less than 5% stimulus coherence [98]. For the human observer, the same study reported a slightly better performance with a discrimination threshold of less than 1%.

The cell's response properties to texture stimuli have been extensively studied in both area 17 [48, 14, 15, 6, 125] and area PMLS [73] of the cat. These studies have shown that cells in both areas do respond to a moving coherent dot pattern. Casanova [14] reported that the amplitude of the response in area 17 depends on the size of the visual field stimulated by the dot pattern. Most cells are optimally activated when the texture pattern covers a field much bigger than the receptive field of the cell. Dot density, dot size and dot velocity are parameters that further affect firing rates [125]. In addition to experiments in the primary visual area of the cat, experiments in the monkey showed that single units in area V1 and MT can also be driven by the same type of random dot pattern [12, 128].

Besides experiments determining the response properties of multiunits in area 17 and PMLS to random dot texture patterns, there exists no study that investigated changes in synchronization due to a change in stimulus coherence in these two areas. Brecht et al. [10] examined such changes in synchronization in the superior colliculus of the awake cat. With decreasing stimulus coherence he found a broadening of the center peaks of the correlograms calculated between signals from two multi units, indicating a decrease in synchronization. No work has also been done on the influence of local incoherence on the LFP in areas 17 and PMLS.

The present study will therefore focus on the question how an incoherent random dot pattern will change the firing rates, the synchronization properties and the frequency distribution in the LFP. According to the binding hypothesis, the coherent random dot stimulus with all dots moving into a common direction should be able to synchronize the discharges of cells, as it has already been shown for the colliculus. Stimulus incoherence could then either lead to a broadening of the center peak of the correlograms due to a decrease in the precision of synchronization discharges or it could lead to a decrease in the RMA but leave the synchronization precision unaffected as long as a motion vector can be extracted from the stimulus. In addition, if stimulus noise leads to a broadening of the center peaks in the correlograms, power in the 40Hz region of the frequen-

cy spectrum of the LFP should decrease and a transition towards low frequencies would be expected. Furthermore, a decrease in the coupling between spikes and LFP in the high frequency region from 30 to 70 Hz would be likely.

In section 4.2, the effects of random dot patterns on the tuning properties of cells in areas 17 and PMLS will be studied to ensure that multiunits in both areas are directionally selective and have a sufficiently narrow tuning curve for both grating and random dot stimuli. In section 4.3 the question will be addressed, how firing rates change when the coherence of motion is destroyed. For a reliable motion detection, rates would be expected to change significantly near the detection threshold of 5% motion coherence. The temporal properties of the neural responses elicited by different levels of coherence will be described in section 4.4. to 4.6. Changes in synchronization patterns between different multiunit data will be investigate in section 4.4 whereas changes in the LFP and correlation between unit data and field potential will be studied in sections 4.5 and 4.6, respectively.



## 4.2 Tuning Behavior of Spatially Incoherent Stimuli

### 4.2.1. Introduction

Response selectivity to stimuli moving into the preferred direction of a cell is a well known and important feature of cells in area 17 and area PMLS of the cat [141, 90, 96]. Precise information about the directional preference of cells is therefore important for experiments investigating the processing of motion information in the visual system.

It has been reported that multiunits can show different preferred directions for different types of visual stimuli. Early studies by Hammond et al. [49] examined the response of cells in area 17 of the cat. They found differences in the preferred direction depending on whether cells are stimulated by a moving bar or by a random dot stimulus. This difference between the preferred direction of multiunits when stimulated with these two different types of stimuli can be as large as  $90^\circ$ . Later studies by the group of Bauer and Jordan [6] revealed that neurons in the upper cortical layers of area 17 have a stronger tendency to show different preferred directions when stimulated by gratings and random dots than cells in the lower layer of the primary visual cortex. Recent studies by the group of Casanova, however, showed that the difference between preferred directions for the majority of cells in area 17 and area PMLS is less than  $30^\circ$  regardless of whether they have been stimulated by a grating or a texture stimulus [14, 73]. In addition, Casanova et al. found that both drift velocity of the dots [15] as well as patch size of the stimulus [14] are important parameters that determine the responsiveness of cells in area 17. Consequently, in the present study stimulus size and random dot drift velocity were chosen according to these results in order to achieve the strongest neural response: The stimulus patch was bigger than the typical receptive field size and dots were moving at an optimal average speed.

In addition to differences in the preferred direction for different types of stimuli, texture stimuli can show so called bi- or multimodal tuning curve [6, 126]. These bi- or multimodal tuning curves

have two preferred directions, one within  $90^\circ$  on each side of the preferred direction found for bar stimuli. Such multimodal curves are usually found only for higher stimulus velocities [125].

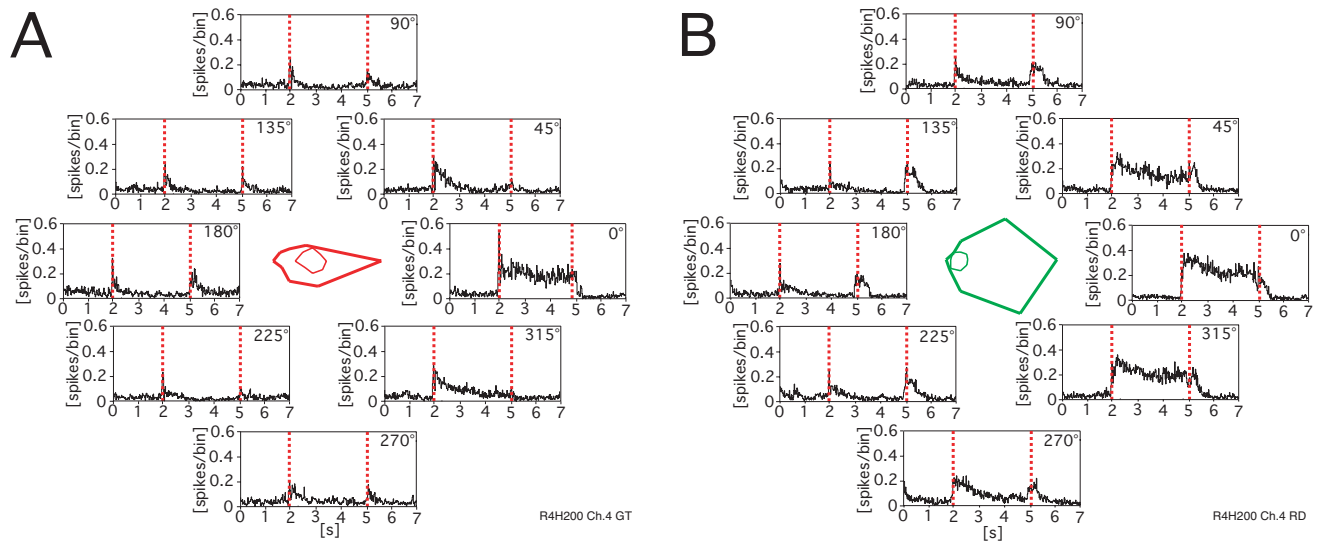
The experiments in the following section investigate, whether cells in areas 17 and PMLS show a comparable preferred direction when stimulated with drifting gratings and random dot patterns. To study the dependence of firing rates on stimulus direction, cats were presented with the tuning curve stimulus described in section 3.3.1. Preferred direction, direction index and tuning width index were calculated. The preferred direction and parameters of the tuning curve were important to determine stimulus properties in later experiments. Furthermore, it was important to ensure that the stimulus velocities were not already capable of leading to multimodal tuning curves. Finally, tuning width and directional selectivity between the two types of stimuli were to be compared between areas 17 and PMLS.

### 4.2.2. Results

#### *Area 17*

Figure 4-1 A shows an example for a neural response of area 17 multiunits stimulated with a grating tuning curve stimulus drifting in eight different directions. As described in detail in section 3.3.1, the tuning curve stimulus consisted of equal stimuli moving into eight different directions in steps of  $45^\circ$ . The  $0^\circ$  direction thereby corresponded to a rightward motion. Ten stimulus repetitions were averaged at each recording site. The figure shows PSTHs for all eight stimulus directions arranged counter-clockwise from  $0^\circ$  to  $315^\circ$  around a polar plot. Each point in the polar plot represents a vector corresponding to one stimulus direction. The length of each of these vectors is given by the average firing rate of the cell. The direction corresponds to the direction of motion of the stimulus.

In the example in Fig 4-1 Panel A, the strongest response was evoked by the sinusoidal grating stimulus moving into the  $0^\circ$  direction. For this direction of movement, the multiunit responds showed a sustained firing rate over the whole stimulus presenta-



tion. Movement in one of the other seven directions merely resulted in a strong ON- and OFF-response, induced by the initial appearance and disappearance of the stimulus, respectively. However, during the remaining time of the stimulation, firing rates were low.

Panel B in Figure 4-1 shows the same cell stimulated with a random dot tuning curve stimulus. As for the grating, the strongest response was elicited by a random dot pattern moving into the 0° direction. In contrast to the grating, however, the dot pattern also elicited a strong response to stimuli moving into adjacent directions, mainly 45° and 315°. Apart from the ON- and OFF-response, stimuli moving into the remaining directions did not evoke responses substantially above spontaneous activity.

Fig 4-2 shows superimposed the polar plots for the two tuning curve stimuli. The responses to the grating stimulus are given by the red line, the green line represents the responses to the random dot pattern. The straight lines indicate the preferred direction calculated as described in detail in section 3.4.1. The small polygons in the center of the graph represent the average firing rates during spontaneous activity recorded during the first 1000 ms of each trial. For the grating, the calculated preferred direction was 349°, the random dot tuning curve stimulus resulted in a preferred direction of 348°.

**Figure 4-1: Tuning curves for area 17**

Panel A and B show PSTHs recorded from area 17 for a grating and a random dot tuning curve stimulus, respectively. Red lines mark stimulus onset and offset, respectively. Numbers in the upper right corner indicate the direction of movement of the stimulus. Red and green polygons in the center of panel A and B show a polar plot representation of the grating and random dot response, respectively. The small polygons in the center represent spontaneous activity.

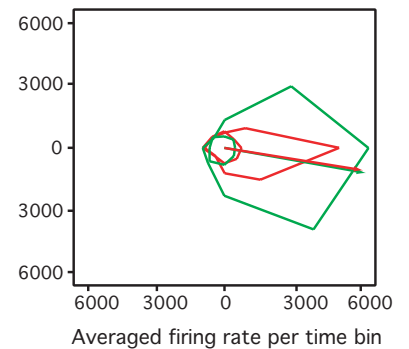


**Figure 4-2: Polar plot of a random dot and grating tuning curve**

The red polygon shows the polar plot for a grating tuning curve, the green line shows the tuning for the random dot stimulus. Spontaneous activity is displayed as the small polygon in the center. Red and green straight lines indicate the preferred directions for grating and random dots, respectively. Units on x- and y-axis are average firing rate per unit time bin.

The shape of the tuning curves for both stimuli were typical for direction selective cells (see 3.3.1). Only stimulus movement into the preferred direction led to a strong response whereas stimulus movement into the null direction did not evoke activity larger than during spontaneous activity. No multimodal tuning curves were found. To quantify this direction selective behavior, the direction index (DI) introduced in section 3.4.1 was used. Indices of more than 0.3 reflect a good directional selectivity of the cell, i.e., cells respond well in the preferred but poorly in the null direction. For the example in Fig. 4-1, the index was  $DI = 0,461$  for the grating and  $DI = 0,506$  for the random dot stimulus. Although the multiunit response showed a similar directional selectivity for both types of stimuli, higher firing rates at  $45^\circ$  and  $315^\circ$  for the random dot curve led to a considerably wider tuning curve. This was reflected in higher values for the width index (WI), which was introduced in section 3.4.2. The values were  $WI = 0,453$  for the grating and  $WI = 0,546$  for the random dot stimulus. The multiunits' responses were therefore much more restrictive to deviations from the preferred direction for the grating stimulus than for the random dot texture pattern.

The given example was typical for directional tuning of multiunits in area 17. Fig. 4-3 to 4-5 show the average data of all multiunits stimulated with the tuning curve stimulus. Data were recorded from 144 recording sites. Multiunits had to show a direction index for both the grating and the random dot tuning curve stimulus of at least 0.1 in order to be considered directional selective and included into the analysis (see section 3.4.1 for details). 96 multiunits (66%) fulfilled the criterion for the grating, 88 multiunits (61%) for both the grating and the random dot tuning curve stimulus. These 88 multiunits were included into further analysis.

The preferred direction for the grating and random dot pattern were within  $20^\circ$  for the majority of the recording sites. In the histogram in Fig. 4-3 the absolute value of the difference between the two preferred directions is plotted against the number of occurrences. An arrow marks the mean of the distribution. For further analysis, four data points with values higher than the mean plus two times

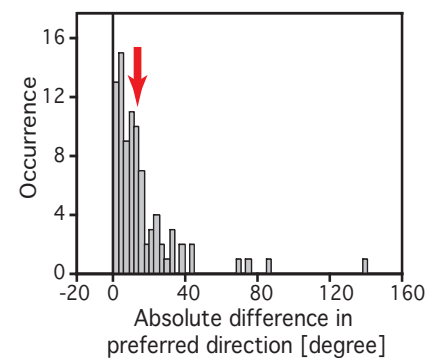


**Figure 4-3: Differences in preferred direction in area 17**

Histogram of the absolute difference between preferred directions for a multiunit stimulated with a grating and a random dot tuning curve stimulus. The arrow marks the mean of the distribution at  $12.43^\circ$ .

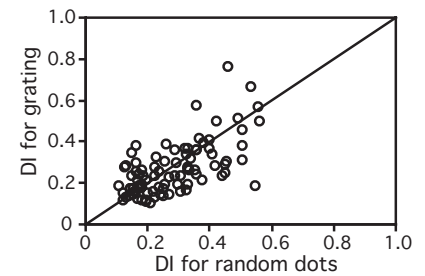
the standard deviation were excluded from the data set. The resulting mean difference was  $12^\circ \pm 1.3$ . A one-sample t-test gave a highly significant difference between the two distributions ( $t(84) = 10.1$ ;  $p < 0.001$ ).

Multiunits in area 17 did not have different directional selectivity when stimulated with a grating and a random dot pattern. The scatter plot in Fig. 4-4 shows the direction indices for the random dot tuning curve plotted against those for the grating stimulus. All values are distributed around the diagonal with a coefficient of correlation of  $r=0.65$ . The mean difference between the two indices is  $\bar{\Delta DI} = -0,013$ . A paired t-test revealed no statistically significant differences ( $t(84) = -1.13$ ;  $p = 0.27$ ).

However, the width of the tuning curve for grating and random dot stimuli were different. The scatter plot in Fig. 4-5 plots the width index for the random dot stimulus against the value for the grating tuning curve. As discussed in section 3.4.2, small values of the width index reflect narrow tuning whereas high values signal a broader tuning curve. Stimulation with the random dot stimulus always led to a broad tuning curve which was reflected in the resulting means for the two distributions. Whereas the grating showed a mean width index of  $0.437 \pm 0.117$ , the random dot tuning curves had an average width index of  $0.57 \pm 0.040$ . The resulting mean difference in tuning width was  $\bar{\Delta WI} = -0,133 \pm 0,0119$  and a paired t-test revealed a significant difference ( $t(84) = 10.8$ ;  $p < 0.0001$ ) between the two distributions.

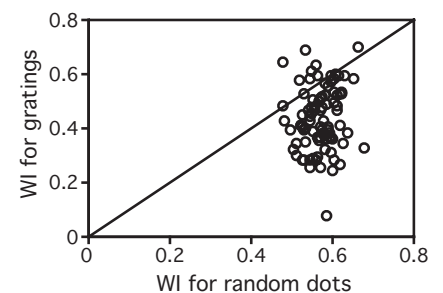
#### Area PMLS

Fig. 4-6 shows a tuning curve example of a multiunit in area PMLS for a grating stimulus (Panel A) and a random dot stimulus (Panel B). The layout is the same as in Fig. 4-1. The response of the multiunit to a grating stimulus moving into the  $0^\circ$  direction showed the strongest response. The ON-response was followed by a constant level for the remaining time of the stimulus presentation. This ON-response was more pronounced than in the multiunit example for area 17 (Fig. 4-1). A much weaker response was found for stim-



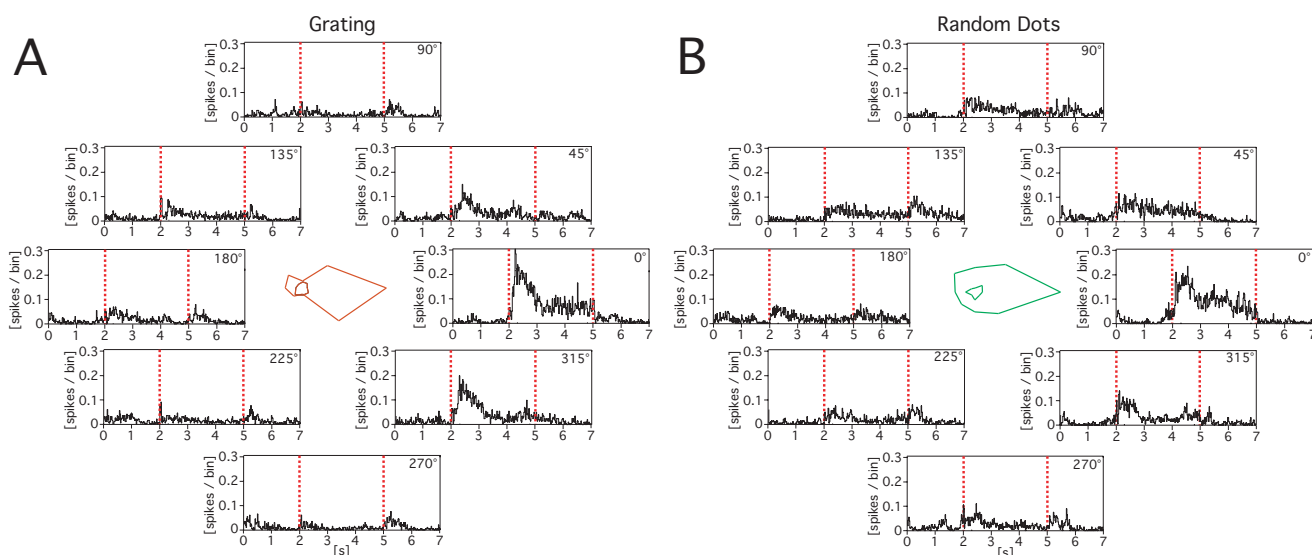
**Figure 4-4: Direction indices in area 17**

The scatter plot shows the direction indices for random dots against the indices for gratings. Only multiunits with direction indices of larger 0.1 for both types of stimuli were included into the figure. The solid line gives the diagonal.



**Figure 4-5: Width indices for area 17**

Width indices for random dots are plotted against those for the grating stimulus. Multiunits had to show a direction index of larger 0.1 in order to be included. The solid line gives the diagonal.



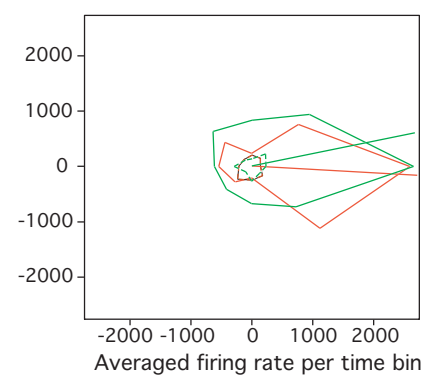
ulation in directions adjacent to the preferred direction, i.e., at  $45^\circ$  and  $315^\circ$ . Almost no response above the level of spontaneous activity was elicited when the grating stimulus moved in a direction perpendicular or opposite to the preferred direction. This reduction in firing rates for movements in other than the preferred direction was less pronounced for the random dot tuning curve (Fig. 4-1, Panel B). The strongest response was again found for stimulation in the  $0^\circ$  direction, but neural responses above spontaneous activity were elicited when stimulated in any of the eight directions.

Fig. 4-7 shows the superimposed polar plots for the grating and random dot tuning curve examples. The layout of this figure is as in Fig. 4-2. The shape of the polar plot was again typical for a directional selective cell. Stimulation into directions other than the preferred direction led to a reduction in firing rates. This reduction was less pronounced for the random dot stimulus leading to a broader tuning curve for the texture pattern compared to the grating. The calculated preferred direction for this multiunit was  $357^\circ$  for the grating and  $12^\circ$  for the random dot tuning curve stimulus.

Responses to grating and random dot stimuli were recorded from 156 multiunits. 95 of these multiunits (61%) showed a direction index of more than 0.1 for the grating stimulus and 88 multiunits (56%) showed a direction index of more than 0.1 for both grating and random dot tuning curve stimuli (see also 3.4.1). As for area 17, only these multiunits were included into further analysis. None of

**Figure 4-6: Tuning curve for area PMLS**

Panel A and B show PSTHs for a grating and a random dot tuning curve stimulus recorded from area PMLS, respectively. The figure has the same layout as figure 4-1.



**Figure 4-7: Polar plot for a cell in PMLS**

The figure shows the superimposed polar plots for the grating and random dot tuning curves. The layout of this figure is as in Fig. 4-2.

the multiunits showed bimodal tuning curves when stimulated with the random dot pattern. Figs. 4-8 to 4-10 show the average results for the directional tuning properties.

For the majority of the multiunits, the difference in preferred direction between the two stimuli was smaller than  $20^\circ$ . In the histogram in Fig. 4-8, the distribution of absolute differences between the preferred directions is plotted against the number of multiunits. An arrow marks the mean at  $11.5^\circ \pm 1.15$ . A one-sample t-test revealed a highly significant difference between the two distributions of preferred directions ( $t(87) = 9.98$ ;  $p < 0.0001$ ).

The direction indices (DI) for area PMLS are plotted into a scatter plot in Fig 4-9. Direction index for the random dot stimulus is shown against the index for the grating tuning curve. In contrast to area 17, direction indices for the grating tuning curve were shifted towards lower values but the indices for the two stimuli were better correlated with a coefficient of correlation of  $r = 0.820$ . The mean difference in the direction index between the two stimuli was  $-0.06 \pm 0.01$ . A paired t-test revealed a highly significant difference ( $t(87) = -0.64$ ;  $p < 0.0001$ ).

The tuning width index revealed a further difference in tuning properties between the two stimuli. This index is plotted for the random dot pattern against those for the grating stimulus in Fig. 4-10. The distribution was shifted towards higher values for the random dot tuning curve stimulus. The mean width index for the grating tuning curve stimulus was at  $WI = 0.490 \pm 0.01$ , the mean value for the random dot stimulus at  $WI = 0.568 \pm 0.006$ . The resulting mean difference between the stimuli was  $\bar{\Delta} WI = -0,08 \pm 0,01$ . A paired t-test showed a highly significant difference ( $t(87) = -7.45$ ;  $p < 0.0001$ ).

#### 4.2.3. Discussion

The results in this section showed that both sine wave gratings and random dot texture stimuli were able to elicit neuronal responses in areas 17 and PMLS of the cat. The response strength of the majority of cells varied as a function of stimulus direction and cells were direction selective for both types of stimuli in the striate and

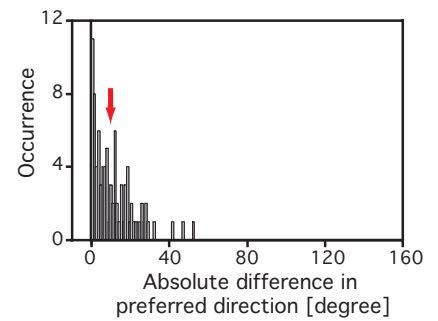


**Figure 4-8: Differences in preferred direction in area PMLS**

The distribution of absolute differences between the preferred directions for the grating and the random dot tuning curve plotted against the number of multiunits. An arrow marks the mean of the distribution.

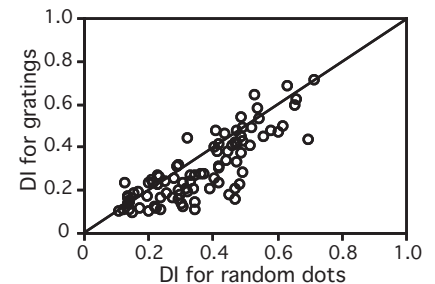


**Figure 4-9: Differences in direction indices for area PMLS**

The direction indices for area PMLS are plotted into a scatter plot. Direction index for the random dot stimulus is shown against the index for the grating tuning curve. The black line marks the diagonal.

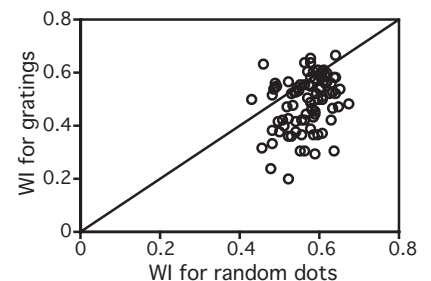


**Figure 4-10: Width indices for PMLS**

The tuning width indices for the random dot tuning curve is plotted against those of the grating tuning curve. The black line marks the diagonal.

extrastriate area. In area 17, directional selectivity for grating and random dot stimuli was similar. In contrast, area PMLS showed a better directional selectivity for the random dot pattern than for the grating stimulus. The difference in preferred direction for the two stimuli was found to be less than  $20^\circ$  for the majority of the cells in both areas. Within our range of stimulus parameters, no bimodal tuning curves were found upon stimulation with the random dot pattern.

Multiunits in the primary visual area that responded to the motion of random dots did not show significant differences in the directional selectivity compared to the grating stimulus. Cells that were highly direction selective for gratings were also highly selective to the motion of random dot texture patterns. This was in agreement with a study by Casanova et al. [15] who also reported a comparable selectivity for the two stimuli. In addition to similar direction selectivity, most of the multiunits in area 17 recorded in this study showed a similar preferred direction for grating and random dots with a difference of less than  $20^\circ$  for 79% of cells. Casanova [15] and Skottun [126] reported similar results. The present findings therefore contradict results reported by Bauer et al. [6] and Hammond [48] who found a strong anisotropy for the preferred direction of gratings and random dots. Hence, the present results are more in favor of Skottun et al. [126] who proposed a similar directional mechanism for grating and random dot stimuli and cannot confirm two different mechanisms proposed by Bauer and Hammond.

Although the direction indices were not different, differences between tuning curves obtained from gratings and random dot patterns were found for the width index. Cells in area 17 showed a broader tuning to random dot patterns than for the grating stimuli. Similar findings have been reported by Casanova et al. [15]. The difference in width can be explained by examining the two stimuli in the frequency domain. Whereas the random dot pattern on average contained equal fourier power for all orientations (see also [126]), the grating exhibited one orientational and directional frequency only. Consequently, even when dots were moving slightly off the



preferred direction, some spatial frequencies were still within the preferred direction of the cell and might have resulted in the considerably broader directional tuning for the random dot stimulus.

As for area 17, the preferred directions of multiunits in area PMLS were also similar. More than half (54%) of the cells showed a difference of less than  $10^\circ$  and 82% showed a difference of less than  $20^\circ$  for the two types of stimuli. These results were in general agreement with a study by Merabet et al [73]. However, this group found larger differences between preferred directions for the two stimuli with 31% of all cells showing a difference of more than  $30^\circ$ . Consequently, they suggested that the mechanisms underlying the directional tuning for grating and random dot stimuli are not necessarily the same for all cells in this area. The smaller differences in the preferred direction found in the present study were most likely due to different methods used to compute the preferred direction of cells. Merabet et al. used stimulus directions in steps of  $30^\circ$  for their tuning curve experiments. They then took the stimulus direction that elicited the highest firing rate as the preferred direction of the cell which could only be one out of eleven directions in steps of  $30^\circ$ . This procedure resulted in less accurate estimations of the preferred direction than the vectorial summation method described in section 3.4.1., which gave continuous values. Consequently, the more accurate algorithm for computing the preferred direction did not confirm the hypothesis that different mechanisms might underlie the directional tuning for gratings and random dots in area PMLS. Instead, a common mechanism seems to exist for the two stimuli, as already proposed for area 17 by Skottun et al. [126].

As for area 17, the analysis revealed that the majority of recorded multiunits in area PMLS were directional selective. However, in contrast to area 17, cells in area PMLS showed a better directional selectivity for the random dot stimuli than for the sine wave gratings. Similar differences have been previously reported [73]. The better selectivity for the random dot stimulus is in favor of the hypothesis that area PMLS serves as the motion area in the visual system of the cat [21] whereas area 17 mainly is thought to be responsible for the

detection of basic forms and objects [76]. Motion detection relies on a good mechanism for direction discrimination whereas an area predominantly concerned with form and object recognition needs more reliable information about the orientation of objects than about their directions of motion. The random dot stimulus might therefore be less salient for area 17 than for area PMLS and the strong motion component is more accurately analyzed in area PMLS. Nevertheless, despite the difference in directional selectivity, the higher coefficient of correlation found between the direction index for gratings and random dots in area PMLS speaks in favor of a similar directional mechanism for the two types of stimuli.

Similar to area 17, differences in tuning width between grating and random dot tuning curves were also found for area PMLS. As for the primary visual cortex, the difference in frequency space is most likely responsible for this difference in tuning width.

It has been suggested that significant processing of direction of motion is performed already in the early areas in the cat visual pathway [121] and that directional selectivity in higher visual areas is more a result from afferent inputs than from intrinsic computations. These inputs might emerge rather from cortical than from subcortical regions. Spear and Bauman [130] reported a decrease in directional selectivity in area PMLS upon removal of areas 17 and 18. For the strongest effect on area PMLS, both areas had to be removed. Further evidence for motion and direction selectivity at early cortical stages in the visual system comes from a study by Smith and Spear [127]. Here they removed the superior colliculus and thus blocked the tecto-thalamic pathway to area PMLS. They did not find any change in the directional selectivity as they found upon removal of area 17 and 18. Lesion of the lateral suprasylvian area itself had only little or no effect on the detection of moving gratings. Cats correctly reported the direction of motion at threshold level [97]. However, the animals were unable to detect differences in speed or flickering rate, especially at high temporal and spatial frequencies. Studies in area MT of the monkey [84] showed that lesions in this area led to a strong elevation in the noise threshold for motion de-

tection in a random dot pattern similar to the one used in the present experiments. However, motion detection was still possible up to a noise level of 40% to 90%, depending on the speed of the dots.

These studies together with the results from this section strengthen the idea that the basic directional mechanism is a cortical process already at early stages of the visual system and that this mechanism is the same for grating and random dot stimuli.

## 4.3 Effects of Visual Noise on Firing Rates in Areas 17 and PMLS

### 4.3.1. Introduction

In the preceding chapter, tuning properties of cells in areas 17 and PMLS for grating and random dot stimuli were investigated. In the present chapter, the dependence of firing rates on different levels of visual noise in a dynamic random dot pattern moving into the preferred direction of a cell was studied. Firing rates have long been thought of as the only and most important information coding element in the brain and numerous studies looked at changes in rates due to different visual stimuli. Much less work has been done on investigating the influence of stimulus coherence on the visual system [85,12,10]. Only a few groups looked at changes in firing rates due to changes in coherence by introducing visual noise into a random dot pattern.

Cats are able to detect a global motion direction from a dot pattern containing 95% of incoherently moving dots [98]. In order to extract the motion signal from the noisy random dot stimulus, integration over a rather large space is required. Because of their larger receptive fields compared to area 17 [96, 141], cells in area PMLS seem to be best suited for this type of analysis. In psychophysical studies changes in perception upon removal of this area [97, 110] were investigated and it was found that animals without this area show permanent performance deficits in speed discrimination and in the integration of local motion signals. In contrast, no deficits in discriminating opposite directions of motion of a sinusoidal grating were found [97]. This led to the conclusion that lateral suprasylvian cortex plays an important role in the processing of stimuli requiring integration of motion information.

In addition to these studies in the cat, physiological experiments have indicated that the middle temporal visual area (MT) in the monkey, which is thought to be the equivalent to area PMLS in the cat, is important for the detection of motion. It has been shown that deletion of this area leads to an elevation of the psychophysical de-

tection threshold for motion discrimination within a dynamic random dot pattern with increasing levels of stimulus noise whereas contrast sensitivity stays the same [84]. The group of Newsome [85, 12] investigated the influence of noise in random dot patterns on direction discrimination and firing rates in area MT of the monkey. They showed that the performance of a monkey undergoing a direction discrimination task correlates well with firing rates of single area MT neurons. They found that the sensitivity of most MT neurons was very similar to the psychophysical sensitivity and could account for the absolute psychophysical discrimination threshold.

This section of my thesis was intended to investigate, whether changes in the coherence of the common motion in a dot pattern is signaled by a change in firing rates of multiunits in the two visual areas 17 and PMLS of the cat as it was reported for single units in monkey area MT. As already described in the introduction to the preceding section, cells in both areas 17 and PMLS are known to respond to random dot motion. However, in the cat, little is known about the influence of visual noise on firing rates. Although cats can discriminate very weak direction signals, the neural mechanism underlying this direction discrimination is largely unknown. The stimuli used for this experiment are described in detail in section 3.3.2.

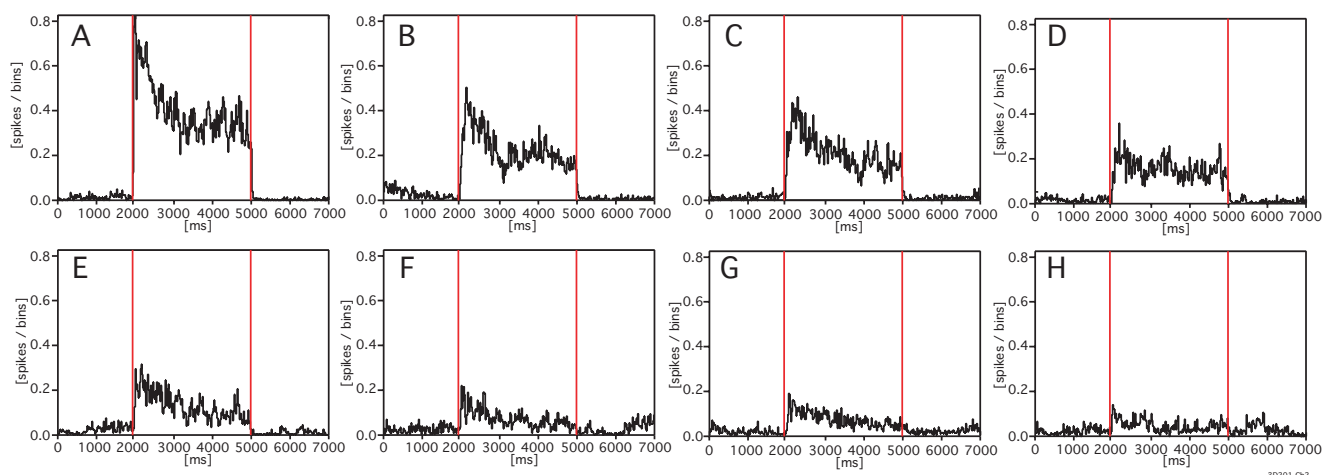
#### **4.3.2. Results**

In order to determine how neural responses in areas 17 and PMLS depend on stimulus coherence, cats were presented with different random dot stimuli with decreasing levels of coherence. Dot patterns with seven different noise levels of 0%, 5%, 10%, 20%, 30%, 50% and 100% were used. Gratings are a very effective stimulus for eliciting responses in area 17 [47, 14]. Hence, a sinusoidal, oriented grating moving in a direction orthogonal to its orientation was included as a control to ensure visually responsive multiunits. The stimuli are described in detail in section 3.3.2. The direction of motion for the stimuli corresponded to the preferred direction of the multiunits which was determined by the tuning curve experiment

described in section 3.3.1. Firing rates were measured as a function of stimulus coherence. At each recording site, 10 to 20 stimulus presentations were averaged. Spontaneous activity was determined by computing the average spikes per second from 0 ms to 1900 ms of each trial. The stimuli were presented 2000 ms after the onset of the trial and stimulus activity was averaged from 2200 ms to 4800 ms, excluding the strong initial response due to stimulus onset (ON-response). If not mentioned otherwise, all significance tests were done with Fisher's protected least significant difference (PLSD) test.

### Area 17

Cells in the primary visual cortex of the cat responded to gratings and the random dot pattern with different levels of stimulus noise. Figure 4-11 shows an example for a response to a grating stimulus (Panel A) and to random dot patterns with 0%, 5%, 10%, 20%, 30%, 50% and 100% of noise (B to H, respectively) recorded from one multiunit. The firing probability per millisecond averaged over ten stimulus presentations is plotted against time in a PSTH. Red lines at 2000 ms and 5000 ms depict stimulus onset and offset, respectively.



After an initial strong response, the firing rate for the grating (A) gradually decreased during the first 1000 ms and stayed constant for the remaining time of stimulus presentation. After the end of the stimulus, firing rates sharply dropped to the level of spontaneous activity. A random dot pattern without noise significantly decreased the firing probability for the cell compared to the grating

**Figure 4-11: Firing rates as a function of decreasing coherence in area 17**

The figure shows PSTHs for a grating stimulus (A) and for random dot stimuli with decreasing stimulus coherence (B to H). Time in milliseconds is plotted against average spikes per time bin. Vertical bars at 2000 ms and 5000 ms show the beginning and the end of the stimulus, respectively.

stimulus (4-11, Panel B). However, cells showed the same strong initial response and rates reached a plateau after approximately 1000 ms. Increasing levels of noise in the random dot pattern led to a gradual decrease in firing rates as shown in panels C to H of figure 4-11. At 100% noise, the response was only 11% of the response elicited by the grating but still 2.4 times above the level of spontaneous activity. In addition, the intensity of the initial transient response decreased as the noise level increased and a tonic response started right after stimulus onset for 50% and 100% of stimulus noise.

Data were recorded from 110 multiunits in area 17. In order to be included into the quantitative analysis, cells had to fulfill the following criteria: 1) Stimulus-induced firing rates for the grating had to increase by at least 50% percent from spontaneous activity. This criterion excluded recording sites that were not responsive to visual stimulation. Data from 88 sites (80%) fulfilled this criterion. 2) The difference between the preferred direction of the multiunit and the direction of stimulus motion had to be less than 30 degree. In total, 32 recording sites (36% of cells) fulfilled both criteria described above. Average firing rates for these multiunits are shown in Fig. 4-12 for all eight stimulus conditions and were plotted against stimulus conditions. Firing rates are given relative to the noise free random dot pattern. Error bars represent one standard error of the mean.

Analysis of variance showed highly significant differences in relative firing rates between the different stimulus conditions (ANOVA,  $F(7, 304) = 11.14$ ,  $p < 0.0001$ ). The grating stimulus evoked the strongest response of all eight stimulus conditions. The mean relative firing rate was  $1.48 \pm 0.15$  being about 50% higher than the rate for the noise free random dot stimulus (Critical Difference (CD) = 0.22,  $p < 0.0001$ ). An increase in visual noise and therefore a decrease in stimulus coherence did not lead to changes in firing rate for noise levels between 5% and 20% (CD below 0.22 and all  $p > 0.75$ ). When the level of stimulus decoherence was increased to more than 20%, firing rates decreased. For 30% visual noise, rates dropped by approximately 11% to a mean relative rate of  $0.89 \pm 0.89$ . However,

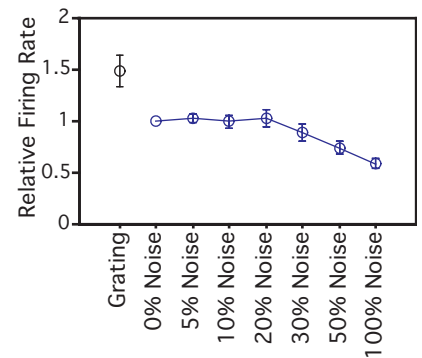


**Figure 4-12: Firing rates as a function of coherence in area 17**

The figure shows average relative firing rates as a function of stimulus coherence in area 17. The preferred direction of the cells always was within  $\pm 30^\circ$  of stimulus direction. Error bars show one standard error of the mean. Firing rates are shown relative to the random dot stimulus which was set to one.

this decrease was not statistically significant ( $p = 0.18$ ). The first significant differences in firing rates compared to the noise free dot pattern was at 50% decoherence ( $CD = 0.21$ ,  $p = 0.02$ ). The completely incoherent stimulus with 100% noise showed the lowest relative firing rate. The mean was  $0.59 \pm 0.05$  leading to a reduction relative to the noise free dot pattern of approximately 47% ( $CD = 0.22$ ,  $p < 0.0001$ ). In addition, the difference between firing rates elicited by a stimulus with 30% and 100% noise was also significant ( $CD = 0.21$ ,  $p = 0.0047$ ).

In order to compare the dependence of firing rates on stimulus coherence between areas 17 and PMLS, data were fitted with a linear, an exponential and a power law equation, respectively. Since the mean firing rates did not change for noise level of 0%, 5% and 10% and 20%, only values for noise levels of 20% and more were included into the fit (see also discussion). Best results based on the coefficient of determination ( $R^2$ ) were obtained for the power law with  $R^2 = 0.996$ . The result is shown in Fig. 4-13. The equation from the resulting fit was

$$y = 2,875x^{-(0,345)}$$

Goodness of fit for the other two models was  $R^2 = 0.90$  and  $R^2 = 0.94$  for the linear and the exponential model, respectively.

It was further investigated, whether the decrease in firing rates was a function of the tuning properties of the multiunits. Changes in firing rates were tested as a function of the direction and width index. Both indices were calculated from the measurement of the random dot tuning curve (see section 4.2 for details). Fig. 4-14 shows the decrease of firing rate with respect to the direction index for seven levels of stimulus noise. The blue trace shows firing rates for multiunits with a direction index of  $DI < 0.2$ . Green and red traces represent multiunits with a direction index of  $0.2 < DI < 0.4$  and  $DI > 0.4$ , respectively. A 3-way ANOVA („Firing rates“ x „direction index“ x „noise level“) was used to determine significant differences in the dependence of firing rates on noise levels for the three different ranges of the direction index. Significant differences were only found within each single range as a function of stimulus coherence

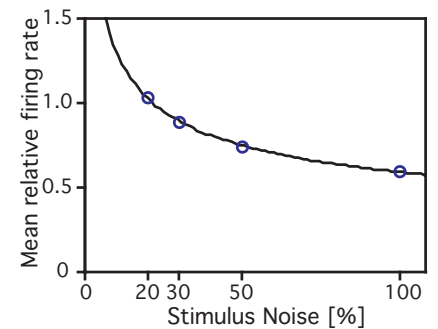


**Figure 4-13: Fit of firing rates from A17**

Average firing rates from area 17 as a function of stimulus noise fitted with a power law equation. Since the mean firing rates did not change for noise level of 0%, 5%, 10% and 20%, only values for noise level of 20% and more were included into the fit.

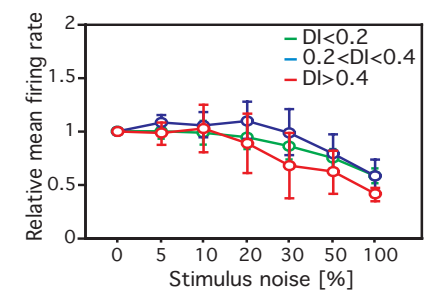


**Figure 4-14: Firing rates for different direction indices in area 17**

The figure shows the decrease of firing rate with respect to the direction index for seven levels of stimulus noise. The blue trace shows firing rates for multiunits with a direction index of  $DI < 0.2$ . Green and red traces represent multiunits with a direction index of  $0.2 < DI < 0.4$  and  $DI > 0.4$ , respectively. Firing rates are given relative to the noise free random dot pattern.



(ANOVA,  $F(6, 217)=4.5$ ,  $p=0.0003$ ) but not between the ranges as a function of the direction index (ANOVA,  $F(2, 217) = 1.3$ ,  $p = 0.28$ ). Thus, the decrease in firing rates was a very stable finding with respect to different direction indices.

Similar results were found for the width index (Fig. 4-15). The blue trace shows multiunits with a width index of  $WI > 0.55$  which corresponds to a fairly broad tuning curve. The red trace shows average relative firing rates for narrow tuning curves with width indices of  $WI < 0.55$ . There was no effect of tuning width on firing rates as all the differences between groups were not statistically significant (3-way ANOVA,  $F(6, 224) = 4.13$ ,  $p = 0.0006$  within group;  $F(1, 224) = 0.57$ ,  $p = 0.45$  between groups).

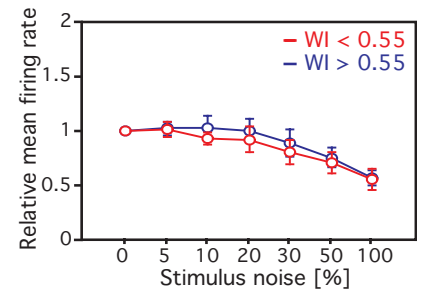
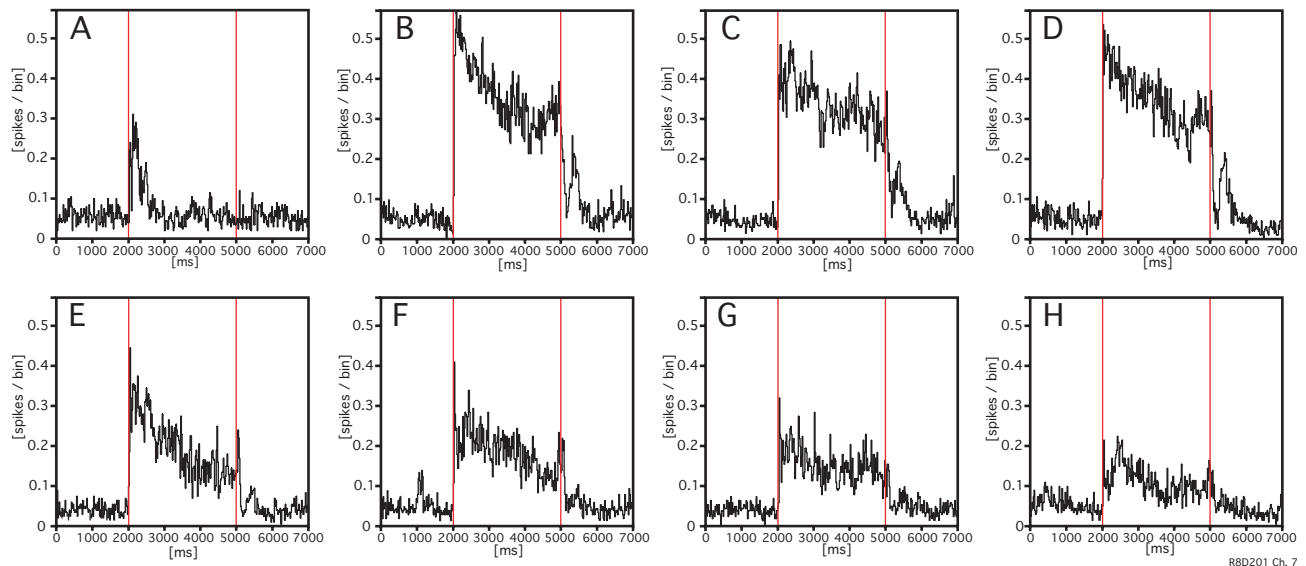


**Figure 4-15: Firing rates for different width indices in area 17**

The figure shows the decrease of firing rate with respect to the width index for seven levels of stimulus noise. The blue trace shows multiunits with a width index of  $WI > 0.55$  which corresponds to a fairly broad tuning curve. The red trace shows firing rates for narrow tuning curves with width indices of  $WI < 0.55$ . Firing rates are given relative to the noise free random dot pattern.

### Area PMLS

Figure 4-16 shows an example collected from one multiunit recording site in area PMLS with 10 stimulus repetitions averaged. The notation is the same as in figure 4-11. In contrast to area 17, the random dot pattern without noise was the most salient stimulus in



this area. The grating stimulus elicited a weaker response (Fig. 4-16, Panel A) and showed a strong ON-response that decreased almost to spontaneous activity within 1000 ms after stimulus onset. For the noise free dot pattern, firing rates were higher compared to all other stimulus conditions and did not drop to spontaneous activity but remained at a high rate. For the following five noise levels, an increase

**Figure 4-16: Firing rates as a function of decreasing coherence in area PMLS**

The figure shows PSTHs for a grating stimulus (A) and for random dot stimuli with decreasing stimulus coherence (B to H). Time in milliseconds is plotted against average spikes per time bin. Vertical bars at 2000 ms and 5000 ms show the beginning and the end of the stimulus, respectively

in incoherence from 5% to 100% led to a decrease in average firing rate. At 100% decoherence, firing rate remained almost constant during stimulus presentation.

The quantitative analysis for area PMLS is shown in Fig. 4-17. The axes were as in Fig. 4-12 and the same inclusion criteria for the multiunits were applied. Data were collected from 195 multiunits. 162 of these multiunits (83%) showed a grating response of more than 50% above spontaneous activity. Out of these, 40% had a preferred direction within 30° of the direction of stimulus movement. In addition, the relative firing rate had to be within two standard errors of the mean for each stimulus condition (63 out of 65 multiunits). These 63 multiunits were included into the further analysis.

A 2-way ANOVA (rates x DI) revealed a highly significant effect of stimulus conditions for area PMLS ( $F(7, 504) = 35.66, p < 0.0001$ ). Paired comparison showed that, in contrast to area 17, multiunits showed their strongest response to a random dot stimulus with no noise. The response to the grating with a mean relative firing rate of  $0.78 \pm 0.04$  was on the order of 20% smaller than for the noise free random dot pattern ( $CD = 0.1, p < 0.0001$ ). In addition, rates were stronger affected by stimulus incoherence in area PMLS than in area 17. Already a noise level of 5% led to a significant reduction in firing rates as the average rates dropped to  $0.75 \pm 0.03$  relative to the noise free dot pattern ( $CD = 0.09, p < 0.0001$ ). A noise level of 10% did not led to a further decrease compared to 5% noise (mean value  $0.75 \pm 0.04, p = 0.84$ ). Relative to 10% decoherence, all higher levels of noise showed a significant decrease in the neural response rate (difference between 10% and 20%:  $CD = 0.1, p = 0.004$ ). At 100% decoherence, firing rates were 1/3 of the rates for the noise free dot pattern (mean  $0.37 \pm 0.04$ ). Differences to noise levels of 30% and lower were statistically significant ( $CD = 0.1, p = 0.0009$ ). The rates changed less with a further increase in noise as 50% decoherence showed no significant difference in firing rates compared to 100% noise ( $p = 0.08$ ).

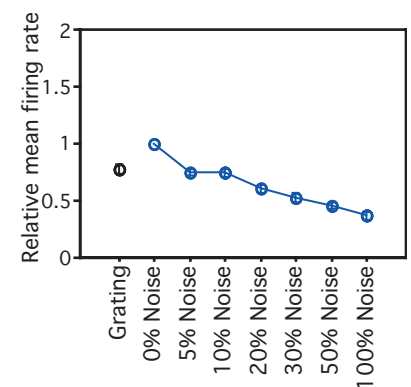


**Figure 4-17: Firing rates as a function of coherence in area PMLS**

The figure shows average relative firing rates as a function of stimulus coherence in area PMLS. The preferred direction of the multiunits always was within  $\pm 30^\circ$  of stimulus direction. Error bars show one standard error of the mean. Firing rates are shown relative to the random dot stimulus which was set to one.

In order to compare the dependence of firing rates on stimulus coherence to area 17, data were fitted with a linear, an exponential and a power law function. The power law resulted in the best fit based on the  $R^2$  value. Fig. 4-18 shows this fit of the mean relative firing rates for noise levels of more than 5%. The fit equation was

$$y = 1,44x^{-(0,273)}$$

leading to an  $R^2$ -value of 0.99. The goodness of fit values for the other two models was  $R^2=0.85$  for the linear and  $R^2=0.92$  for the exponential fit.

In addition to the decrease in firing rates with stimulus coherence it was investigated, how this decrease depended on the direction index and the tuning width index of the multiunits. Fig. 4-19 shows relative firing rates against stimulus coherence for different ranges of the direction index (DI). Values for multiunits with a low directional tuning of  $DI < 0.2$  (green), for direction indices of  $0.2 < DI < 0.3$  (red) and for strong direction selective cells with a direction index of more than 0.3 (blue) were all within one standard error of the mean. 3-way ANOVA (Firing rates x direction index x noise level) showed no significant differences between ( $F(2, 430) = 1.60, p = 0.2$ ) but only within groups ( $F(6, 430)=27.98, p<0.0001$ ). Fig. 4-20 shows firing rates as a function of stimulus coherence for different width indices. Cells with a narrow tuning of  $WI < 0.55$  are shown in red, cells with a broader tuning of  $WI > 0.55$  are shown in blue. The decrease in firing rates did not depend on the width of the tuning curve and no statistical differences were found between the two groups (3-way ANOVA („Firing rates“ x „width index“ x „noise“),  $F(6, 437)=39.15, p<0.0001$  for the effect of stimulus noise,  $F(2, 437) = 0.49, p = 0.49$  for the effect of width index).

*Stimulation in the null direction*

Changes in firing rates were investigated when the stimulus was moving in the null direction of the multiunits. The null direction was defined as the direction opposite to the preferred direction which was obtained from the tuning curve described in section 3.3.1. Figure 4-21 shows these averaged data. All data are again given rel-

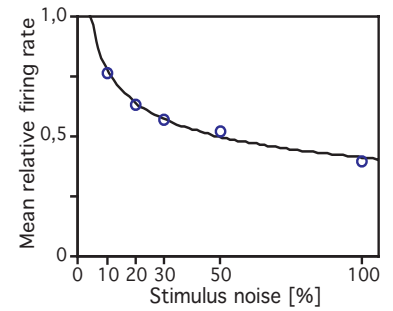


**Figure 4-18: Fit of firing rates in PMLS**

Average firing rates from area PMLS as a function of stimulus noise fitted with a power law equation. Since the mean firing rates did not change for noise level of 0%, 5% and 10%, only values for noise level of 10% and more were included into the fit

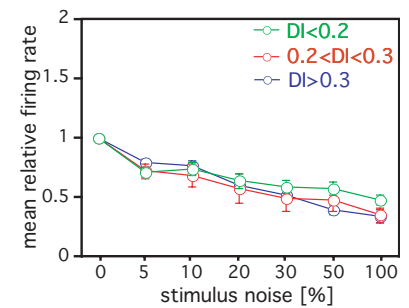


**Figure 4-19: Firing rates for different direction indices in area PMLS**

Decrease of firing rate with respect to the direction index is plotted for seven levels of stimulus noise. The green trace shows firing rates for multiunits with a direction index of  $DI < 0.2$ . Red and blue traces represent multiunits with a direction index of  $0.2 < DI < 0.3$  and  $DI > 0.3$ , respectively. Firing rates are given relative to the noise free random dot pattern.

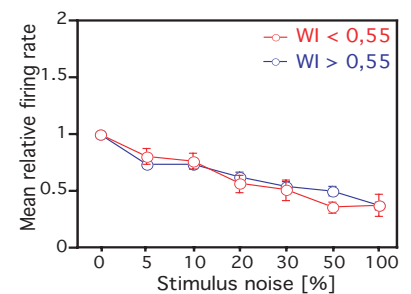


**Figure 4-20: Firing rates for different width indices in area 17**

Decrease of firing rate with respect to the width index is plotted for seven levels of stimulus noise. The blue trace shows multiunits with a width index of  $WI > 0.55$ . The red trace shows firing rates for narrow tuning curves with width indices of  $WI < 0.55$ . Firing rates are given relative to the noise free random dot pattern

ative to the noise free random dot pattern. To be included into the analysis, firing rates for one multiunit had to be at least 50% above spontaneous activity and the difference between stimulus direction and the null direction of the cell had to be less than 30°. In figure 4-21, red crosses and blue circles indicate results for area 17 and area PMLS, respectively.

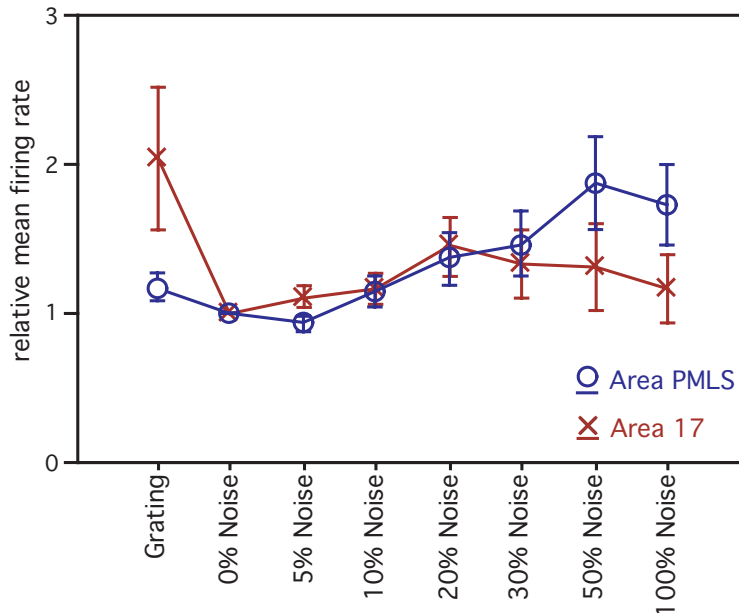


**Figure 4-21: Firing rates as a function of coherence for areas 17 and PMLS: Stimulation in the Null direction**

Analysis of firing rates elicited by stimulation in the null direction of a multiunit for both area 17 (red) and area PMLS (blue). The figure shows average relative firing rates as a function of stimulus coherence. The preferred direction of the multiunits had to be within  $\pm 30^\circ$  of the null direction. Error bars show one standard error of the mean. Firing rates are shown relative to the noise free random dot stimulus which was set to one.

For area 17 none of the differences between different stimulus conditions were significant (2-way ANOVA,  $F(7, 98) = 1.7$ ,  $p = 0.12$ ). For area PMLS, firing rates dropped for noise level of up to 5% and increased for higher noise level to reach their maximum at 50% de-coherence (ANOVA,  $F(7, 183) = 3.32$ ,  $p = 0.002$ ). Significant differences were found between 5% and 30% noise ( $CD = 0.52$ ,  $p = 0.045$ ). In addition, noise levels of 50% and 100% showed significant changes in firing rates when compared to firing rates elicited by the grating stimulus, ( $CD = 0.52$ ,  $p < 0.04$ ), by the noise free random dot pattern ( $CD = 0.52$ ,  $p < 0.006$ ) and by noise level of 5% and 10% ( $CD = 0.52$ ,  $p$  always less than 0.03).

### 4.3.3. Discussion

This section showed that firing rates of the majority of multiunits vary as a function of stimulus coherence in both areas 17 and PMLS. When decreasing the coherence of the stimulus by introducing visual noise into the random dot pattern, both areas showed a

decrease in firing rates with increasing level of noise. However, the minimal noise level leading to a first reduction in response rate was different for the two areas. Neurons in area 17 were found to be less sensitive to changes in stimulus coherence. Noise levels of less than 20% did not change their response and higher noise levels were necessary to see a monotonic decrease in firing rates. The lowest response was obtained with a fully incoherent stimulus at 100% visual noise. In contrast, area PMLS was more sensitive to stimulus coherence. Cells in this area showed a reduction in response already at a very low noise level of 5%. Higher noise levels led to a monotonic decrease in firing rates. As for area 17, the lowest neural response was found at a decoherence level of 100%.

A possible explanation for the different behavior of the two areas might be the differences in receptive field size. The probability of having incoherent dots within the area covered by a receptive field increases with the size of the field. In the present experiments, the dot density in area 17 and PMLS was 1.3 dots per  $\text{deg}^2$ . At a noise level of 5%, an area of  $26 \text{ deg}^2$  was necessary to reach a probability of  $p=1$  of finding at least one randomly replaced dot within the receptive field. Consequently, with an average field size of 1.6 to  $6.3 \text{ deg}^2$  in area 17, the probability of having one non-coherent dot inside the receptive field was  $p\approx 0.25$ . In contrast, the average receptive field size in area PMLS was between 14 to  $40 \text{ deg}^2$ . Hence, already at 5% noise the probability of having at least one non-coherent dot within this area is  $p\approx 1$ . At 20% noise, however, one randomly replaced dot was already found in an area of  $5.2 \text{ deg}^2$ . Therefore, at this noise level the probability of having one non-coherent dot within a receptive field of area 17 increases to  $p\approx 1$ .

These differences in receptive field size might explain, why area 17 was less sensitive to small changes in the coherence of motion compared to area PMLS. Taking the difference in receptive field size into account, both areas show comparable dependences of firing rates on visual noise. This provides further evidence that area PMLS, because of its larger receptive field size, is more responsible

for the detection of global patterns whereas area 17 seems to be more involved in the analysis of local features. The mechanism underlying the computation in the two areas, however, might be similar.

Further evidence for a similar mechanism in the processing of texture motion in the two areas came from the fit of the mean firing rates for different levels of stimulus coherence in area 17 and PMLS. Data in area PMLS were fitted for noise level of more than 5%, whereas area 17 data were fitted for noise level of 20% and higher. For both areas this corresponded to the noise level that, based on the difference in receptive field size, led to a probability of  $p \approx 1$  for having a non-coherent dot inside the receptive field. Best results for both areas were found for a fit with a power law with an exponent of  $-0,345$  for area 17 and  $-0,273$  for area PMLS. These results indicate that the rates in the two areas decrease with approximately the same rate taken into account the different receptive field sizes. No significant dependence of firing rates on tuning width and direction index was also found for both areas indicating that the mechanism leading to a decrease in firing rate is independent of the mechanism underlying the tuning properties of cells in both areas.

When cells were stimulated into the null direction, no statistically significant changes in firing rates with decreasing levels of stimulus coherence in area 17 were found. Only in area PMLS, firing rates elicited by the grating and random dot pattern with noise levels of up to 10% were found to be significantly different from those elicited by noise level of 50% and 100%. Since the randomly replaced dots did not carry motion information, it might be that the large number of replaced dots at 50% and 100% stimulus noise lead to a weak apparent motion that is recognized by area PMLS. In addition, cells in area PMLS might be more sensitive to the increasing flicker signal introduced by the flicker-onset noise which could also lead to an increase in firing rates upon stimulation in the null direction. Furthermore, multiunits in area PMLS showed a higher response to the grating than to the random dot pattern, when the stimulus was moving in the null direction of the cell. This was most likely due to the fact that the directional selectivity in area PMLS is stronger for

the random dot than for the grating stimulus (see section 4.2.2 for details). Therefore, compared to a stimulation with random dots, the cells' response to the grating stimulus was stronger when stimulated in the null direction.

The results from area PMLS were similar to earlier studies by the groups of Newsome et al. in monkey area MT [85, 12]. Using a similar visual stimulus this group found a monotonic decrease of firing rates in single neurons with a decrease of stimulus coherence in the awake, behaving animal. However, they reported that the decrease in firing rates was highly correlated with the monkey's ability to correctly discriminate the direction of motion in a psychophysical discrimination task. Averaged over many experiments they already found clear differences in firing rates for noise levels of 87.2% and 99.2%. In contrast, the present results did not show any significant differences in firing rates for noise levels of 30% and more. Therefore, based on these data and for the anesthetized cat, a reliable direction discrimination in a noisy random dot pattern based solely on firing rates seems not very likely.

A reason for these discrepancy in findings might lie in the fact that the present experiments were using anesthetized as opposed to awake animals. The discrimination of direction near the physiological detection threshold however might require an attentive mechanism. This issue is discussed in more detail in the discussion at the end of this chapter.

## 4.4 Synchrony in Incoherent Stimuli

### 4.4.1. Introduction

A rate code based on the firing activity of cells or cell assemblies might not be the only possible coding mechanism of the brain. Studies by Sejnowski [118] and others pointed out that an information processing strategy that is solely based on the analysis of firing rates, imposes serious limitations on the processing capacity of the brain (see chapter 2.4 for more details). Influenced by the assembly theory proposed by Donald Hebb [51], another mechanism for information coding was proposed: Stimulus-dependent synchronization and oscillation of neuronal responses in the millisecond range could serve to define functional relations among distributed neurons [122, 31, 124]. This use of temporal structure inherent in the firing pattern of cells circumvents many problems of a pure rate coding theory. Since it was first proposed, strong experimental evidence has been found in different areas of the brain [28, 10, 4, 116] that supports this hypothesis.

The role of synchrony and oscillation in the coding of motion coherence will be investigated in this section. It has been shown that bar and grating stimuli are capable of inducing synchronized oscillatory activity on a millisecond time scale between cells and cell assemblies in both areas 17 and PMLS [41, 24, 27]. In addition, long-range synchronization between different brain areas [28], between the two hemispheres [29] as well as corticotectal interactions [9] have been reported.

Only very few studies investigated the effect of coherently moving random dot patterns on synchrony. Brecht et al. [10] showed that response synchronization and oscillatory modulation of synchronized responses upon stimulation with a random dot pattern occurs frequently in the superior colliculus of awake cats.

So far, no study has investigated the influence of random dot pattern and stimulus coherence on synchrony in the primary and the motion area of the cat, areas 17 and PMLS. In this section I try to answer the question, whether synchrony is a more reliable measure



for the coherence of stimulus motion than firing rates. The binding hypothesis predicts that both, sinusoidal grating and coherent dot pattern, should lead to synchronous firing activity (see chapter 2.4 for more details). Adding noise to the dot pattern should gradually decrease the amount and the precision of synchrony as the coherence of motion and consequently the binding cue decreases. On the other hand, precise synchronization might remain as long as the cortex can discriminate a global motion within the random dot pattern and will break down as soon as the noise level will exceed a certain discrimination threshold.

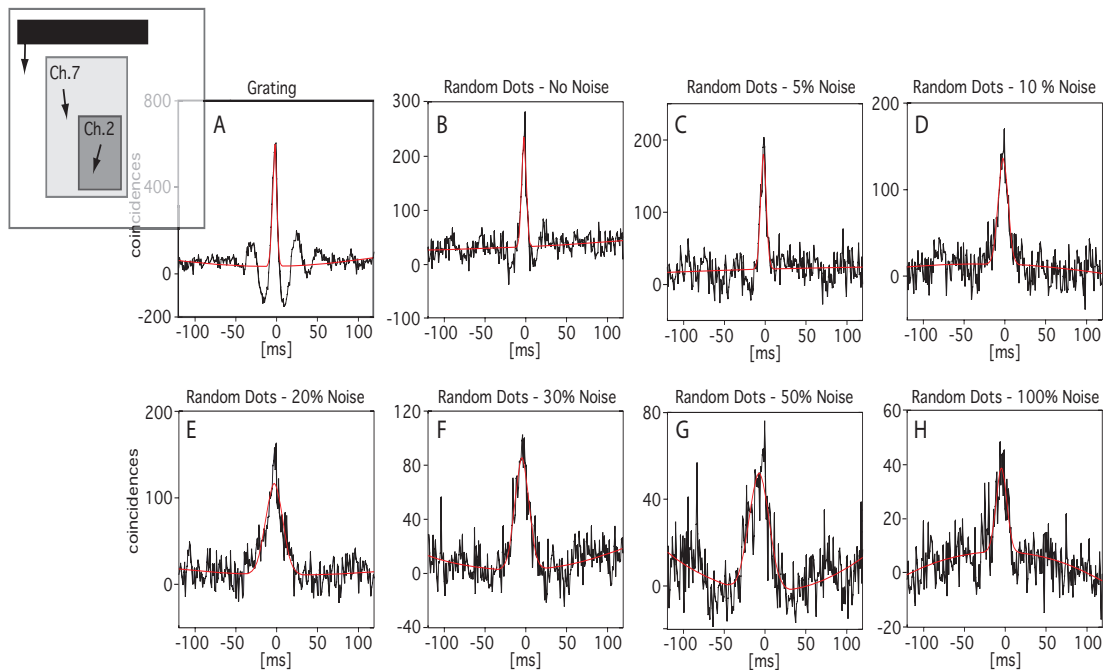
The stimulus used in this section is described in section 3.3.2 and was identical to the one used in the previous chapters. Multi-unit activity was recorded for seven seconds and the stimulus appeared from 1000 ms to 4000 ms after start of the trial. Data were recorded with a time resolution of 1 ms and 10 to 20 stimulus repetitions were averaged.

#### 4.4.2. Results

##### *Area 17*

Fig 4-22 shows an example for correlation analysis for two multiunits recorded from area 17. The panels show cross correlograms for a grating (A), a random dot stimulus without noise (B) and for random dot stimuli with increasing noise levels from 5% to 100% (C to H). Ten trials were recorded and the correlograms for each were averaged. Time shift from zero is plotted against the summed number of coincidences per bin. The shift-predictor was subtracted from the correlograms to correct for stimulus locked synchronization. A Gauss curve fitted to the data as described in section 3.5.2 is shown in red for each of the correlograms. This fit was chosen such that it gave best results for the center peak but was not intended to fit the whole correlogram.

The cross correlogram for the grating stimulus (Fig. 4-22, A) showed a strong correlation peak centered around zero indicating synchronization between the firing activity of the two multiunits. The half width at the inflection point as determined by the Gauss fit



was 2.7 ms. In addition, side lobes were found on both sides of the central maximum leading to an oscillatory firing pattern with an oscillation frequency of 35 Hz. The RMA, i.e., the ratio between the height of the center peak and the offset of the correlogram, was 1.04. The pure random dot pattern (Fig. 4-22, B) also showed a narrow center peak. With 2.8 ms, the half width of this peak was slightly broader than the center peak found for the grating stimulus. However, side lobes almost vanished. In addition, the RMA dropped from 1.04 for the grating to 0.58 for the coherent random dot stimulus. As expected from the decrease in firing rates with increasing level of noise (section 4.3), the number of entries in the correlogram, i.e., the number of coincidences, decreased. Consequently, the signal to noise ratio was lower for the random dot compared to the grating stimulus. When adding visual noise to the random dot pattern, the center peak remained in the correlograms but the width broadened. At 5% decoherence, half width at the inflection point was 3.5 ms and increased to 12.3 ms for more than 50% visual noise. Side lobes and oscillations did not appear for random dot pattern containing visual noise. Whereas increasing stimulus decoherence led to an increase in the width of the center peak, it had little effect on the RMA. Values for the RMA stayed between 0.4 and 0.5 for all levels of coherence.

**Figure 4-22: Correlograms for different level of coherence in area 17**

The figure shows an example for cross-correlograms for eight different stimuli. Time shift from zero is plotted against the summed number of coincidences. A red line shows a gaussian fit to quantify the center peak. The correlograms were calculated with a maximal shift of 120 ms. The relative position of the receptive fields (light gray and gray rectangle), the preferred direction of the two multi units (arrows within the rectangles) and the direction of motion of the stimulus (black bar) are sketch in the upper left corner.

Data averaged over all recording sites confirmed the results from the example shown above. Fig. 4-23 to 4-24 give the averages for the correlation analysis of pairs of area 17 multiunits. Fig. 4-23 shows the mean center peak half width at the inflection points as a function of stimulus coherence. Error bars represent one standard error of the mean. Only pairs of cells that showed optimal synchronization conditions were included into the analysis: The difference in preferred direction of the two multiunits had to be less than  $90^\circ$ . Furthermore, the difference between the vector average of the two preferred directions and the direction of motion of the stimulus had not to exceed  $45^\circ$ . This constellation is sketched in the little inset in the upper left corner of the figure. The two white rectangles give the receptive fields of the multiunits where the preferred direction is perpendicular to the line drawn in the center of each RF. The gray bar represents the stimulus with a direction of movement perpendicular to its orientation axis. If not otherwise stated, all statistical tests were performed with Fischer's PLSD.

Decreasing stimulus coherence led to a statistically significant broadening of the central maximum in the cross correlograms (ANOVA,  $F(7, 520) = 23.46$ ,  $p < 0.0001$ ). The grating stimulus showed the narrowest center peak half width with a mean of  $2.18 \pm 0.05$  ms. When presenting a random dot pattern without stimulus noise, this peak broadened significantly by more than a factor of two to a mean value of  $5.3 \pm 0.5$  ms ( $CD = 1.65$ ,  $p < 0.0001$ ). Introducing noise further increased the center peak width. At 5% noise, the mean reached  $7.3 \pm 0.9$  ms and was significantly different from the noise free dot pattern ( $CD = 1.72$ ,  $p = 0.009$ ). Increasing the noise to 10% (mean  $8.6 \pm 0.7$ ) and 20% (mean  $8.3 \pm 0.5$ ) led to a further not significant increase in the half width of the center peak ( $p$  always larger than 0.29). The difference between 20% and 30% noise was again statistically significant ( $CD = 1.76$ ,  $p = 0.045$ ). The mean value increased to  $10.08 \pm 0.05$ . The widest value for the center peak (mean  $10.9 \pm 0.7$ ) was found for 50% decoherence. This mean value was significantly different from the value at a noise level of 20% and below ( $CD = 1.8$ ,

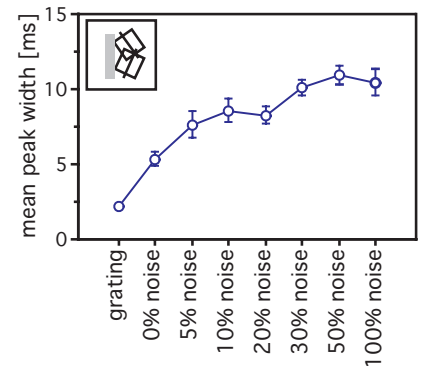


**Figure 4-23: Center peak width area 17**

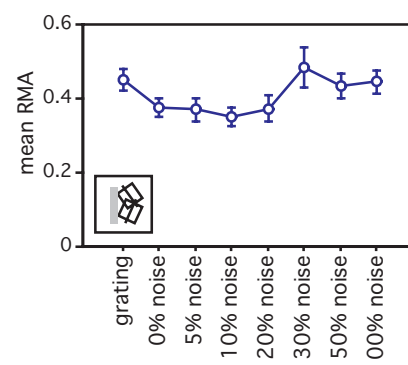
The figure shows the mean center peak width for correlograms in area 17. Only multiunits stimulated under optimal synchronization conditions were included. The difference in the preferred direction of the multiunits had to be within  $90^\circ$  and the stimulus direction had to be within  $45^\circ$  of the average multiunit direction. The inset shows a sketch of the relative position of RFs and stimulus direction. Error bars indicate one standard error of the mean.

$p = 0.004$ ) but not from the width at 30% noise ( $p = 0.35$ ). The fully decoherent random dot stimulus led again to a non-significant decrease in the mean value of the center peak to  $10.5 \pm 0.9$ .

Fig. 4-24 shows changes in the RMA as a function of stimulus coherence for area 17. The same inclusion criteria as for the analysis of the center peak width in Fig. 4-23 were applied. Hence, the RMA was calculated under optimal synchronization conditions. ANOVA revealed small significant changes between the mean values for the different stimulus conditions ( $F(7, 526) = 2.13, p=0.04$ ). The correlograms for the grating stimulus showed a mean value for the RMA of  $0.45 \pm 0.03$ . This value decreased to  $0.38 \pm 0.02$  for the random dot pattern without noise which was not statistically significant ( $CD = 0.09, p = 0.09$ ). Further increase in noise up to 20% did not lead to changes in the RMA between adjacent noise levels. Differences between these values were less than one standard error of the mean and were not significant. The first significant difference was found between RMA values of the grating stimulus and the random dot pattern containing 10% visual noise ( $CD = 0.09, p = 0.03$ ). Increasing incoherence to 30% led to a strong increase in the RMA value to a mean of  $0.49 \pm 0.05$ . The differences between this RMA value and those for all other noise levels was highly significant ( $CD$  between 0.09 and 0.1,  $p$  always less than 0.02). Higher levels of incoherence led again to a decrease in the RMA. The mean value reached  $0.43 \pm 0.03$  for 50% and  $0.45 \pm 0.03$  for 100% noise. None of these changes were significant.

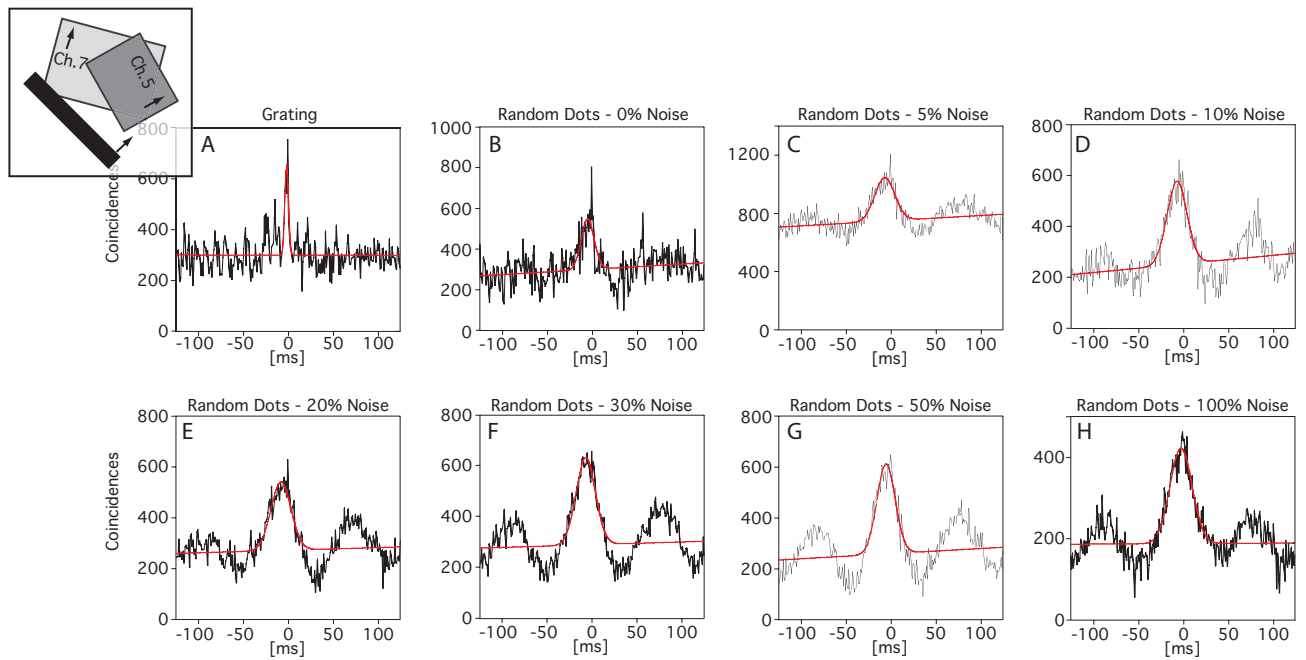
#### Area PMLS

Fig 4-25 gives an example for the correlation analysis for two multiunits in area PMLS. The layout is the same as for Fig 4-22. The width of the center peaks was again quantified by fitting a Gauss curve to the data. This fit was chosen to best fit the center peak of the correlogram and did not pick up the oscillatory behavior. The figure illustrates one of the rare examples of multiunits in area PMLS that show a narrow synchronization peak when stimulated with a grating stimulus. The width for the center peak as given by the inflection point of the Gauss curve was 2 ms. The behavior for the seven ran-



**Figure 4-24: RMA as a function of coherence**

The figure gives the RMA as a function of stimulus coherence. Error bars show  $\pm$  one standard error of the mean. Inclusion criteria and layout are as described in Fig. 4-23.



dom dot pattern, however, was typical for pairs of multiunits in area PMLS. The center peak of the correlogram broadened significantly from the grating to the random dot stimulus without noise. No side lobes and oscillations on a short time scale were found. Adding noise to the stimulus led to a further broadening of the center peak of the correlogram. In addition, a low frequency oscillation in the alpha frequency range from 5 and 15 Hz built up and increased with increasing levels of noise. At 30% noise, this oscillation reached almost half the amplitude of the central maximum. It stayed as a prominent feature up to a fully incoherent stimulus with 100% visual noise.

Pairs of multiunits recorded from area PMLS fell in two separate groups regarding their synchronization behavior for the grating stimulus. The distribution of the width of the center peak of the cross-correlograms is given in the scatter plot in Fig. 4-26. Only cross-correlograms that complied with the criteria of a good fit were included into this plot. Within this data set, 17 out of 56 pairs showed a center peak half width between 1 and 4 ms, the remaining 39 pairs showed half width values of more than 8 ms. Therefore, for the analysis of the synchronization behavior, data were split into two separate groups. One group included all pairs that showed a half width of the central maximum of less than 5 ms. The remaining

**Figure 4-25: Synchronization as a function of coherence in area PMLS**

The figure shows cross-correlograms as a function of stimulus coherence for area PMLS. The layout of the figure is the same as in figure 4-22: The red line shows a Gaussian fit, the inset gives the relative position of the receptive fields. **A** grating; **B** a noise free random dot pattern; **C** to **H** random dot patterns with 0% to 100% of stimulus noise.

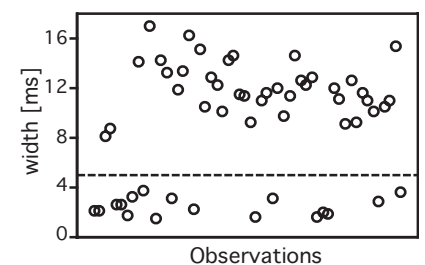


**Figure 4-26: Width distribution for the grating stimulus in area PMLS**

The figure shows the center peak width of the cross-correlograms for the grating stimulus in milliseconds. The black horizontal line marks a width of 5 ms.

pairs were put into a different data set. For comparison, all pairs in area 17 showed a center peak width for the grating stimulus between 1 and 3.5 ms.

Fig. 4-27 and 4-28 show the average results for the correlation analysis of area PMLS multiunits that exhibit a narrow correlation peak for the grating stimulus. The same inclusion criteria as for area 17 were applied. Within this subgroup, significant differences in synchronization width were found (ANOVA,  $F(7, 92) = 4.85$ ,  $p < 0.0001$ ). The mean width for the noise free random dot pattern showed non-significant increases from  $2.4 \pm 0.2$  ms for the grating to  $5.2 \pm 1.2$  ms (CD = 4.31,  $p = 0.2$ ). Adding noise to the texture elements led to a monotonic increase in the center peak width up to noise levels of 50%. This 50% noise stimulus showed the broadest center peak with a mean value of  $11.5 \pm 2.0$  ms. Relative to the grating stimulus, all these increases in center peak width were statistically significant (CD between 4.08 and 3.66,  $p$  always less than 0.01). However, within the group of random dot stimuli, only the difference between values of 0% noise and noise levels of more than 30% (all CD between 4.22 and 3.91,  $p = 0.02$  for 30%,  $p = 0.002$  for 50% and  $p = 0.01$  for 100%) and between 5% and 50% noise (CD = 3.67,  $p = 0.04$ ) were significant. A fully incoherent stimulus led to a small non-significant decrease of the center peak width relative to the 50% noise value (CD = 3.35,  $p = 0.57$ ).

The monotonic increase of the width of the center peak was not found for the RMA. The mean values with error bars indicating one standard error of the mean are given in Fig. 4-28. Mean RMA values for all stimulus conditions lie between 0.22 for the noise free random dot pattern and 0.35 for 50% stimulus noise. None of the differences between the stimuli was statistically significant (ANOVA,  $F(7, 92) = 0.57$ ,  $p = 0.78$ ).

The second subgroup of data consisted of pairs of multiunits with a broad synchronization peak for the grating stimulus of more than 5 ms. The averaged data for this set are shown in Fig. 4-29 and 4-30. In contrast to multiunits that showed a narrow synchronization for the grating stimulus, these data showed only little changes

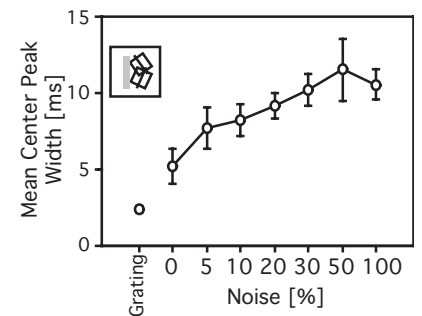


**Figure 4-27: Center peak width for narrow grating synchronization**

Mean center peak width is plotted against stimulus conditions. Only multiunits showing a precise synchronization for the grating were included. All pairs were stimulated under optimal synchronization conditions as sketched in the inset (see text). Error bars indicate  $\pm$  one standard error of the mean.

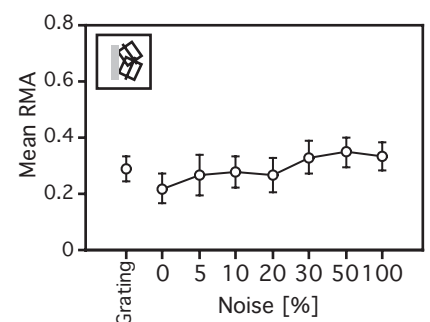


**Figure 4-28: RMA as a function of coherence**

The figure plots RMA against stimulus conditions. Inclusion criteria are the same as in figure 4-27. Error bars show  $\pm$  one standard error of the mean.

in center peak width due to noise. Fig. 4-29 shows the average half width at the inflection point as a function of stimulus coherence (ANOVA,  $F(7, 110)=3.58$ ,  $p = 0.002$ ). Surprisingly, the grating stimulus showed the broadest synchronization with a mean value of  $13.54 \pm 1.16$ . The average width value dropped significantly to  $9.54 \pm 0.44$  when going to a random dot pattern without stimulus noise (CD = 1.9,  $p < 0.0001$ ). Adding noise to the dot pattern led to an increase in the width of the center peak. However, except for the difference between the noise free random dot pattern and the 100% noise stimulus (CD = 1.8,  $p = 0.047$ ) there were no statistically significant changes between the different noise levels.

The average RMA for this subset is shown in Fig. 4-30. None of the differences between values were statistically significant (ANOVA,  $F(7, 110) = 1.69$ ,  $p = 0.12$ ). The highest value for the RMA was found for the grating stimulus that decreased for the noise free random dot stimulus and showed a monotonic increase with increasing level of stimulus noise.

In addition to synchronization on a short time scale, many multi-units in area PMLS showed a low frequency oscillation. To quantify this oscillatory behavior, cross-correlograms were fitted with a sine wave function (see chapter 3.5.2 for details). Fig. 4-31 gives the mean values for the oscillation frequency. In order to be included into the analysis, cells had to match the following criteria: 1) Cells had to show a center peak in the correlogram for the grating stimulus that was detected and quantified by the Gauss-fit procedure. 2) The difference between the preferred direction of the two multiunits had to be less than  $90^\circ$ . 3) The vector average of these two preferred directions and the stimulus direction must not differ more than  $45^\circ$ . The figure shows mean oscillation frequencies for stimuli with 5% to 100% noise with error bars indicating one standard error of the mean. For the grating and the 0% noise stimuli, low frequency oscillation has not been found. All oscillations were in a frequency band between 12 and 15 Hz (alpha-band). The increase in stimulus noise led to a non-significant decrease in oscillation frequency (ANOVA,  $F(5, 78) = 1.53$ ,  $p = 0.19$ ). In particular, the 5% noise stim-

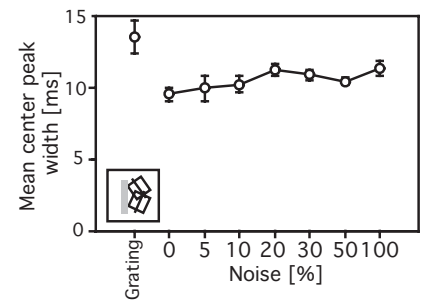


**Figure 4-29: Center peak width for broad grating synchronization**

The figure plots average center peak width as a function of stimulus coherence for pairs of multiunits that show a broad synchronization for the grating stimulus. Only pairs stimulated under optimal synchronization conditions were included as sketched in the little inset in the lower left corner. Error bars give  $\pm$  one standard error of the mean.

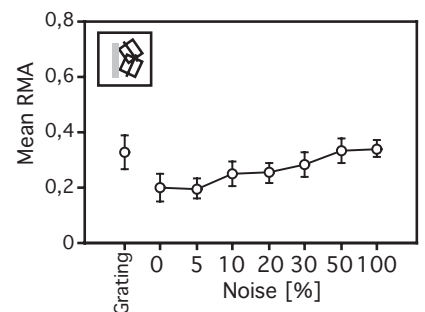


**Figure 4-30: RMA for broad grating synchronization**

The RMA for multiunits exhibiting a broad grating synchronization is plotted against stimulus conditions. The layout is the same as for figure 4-29.

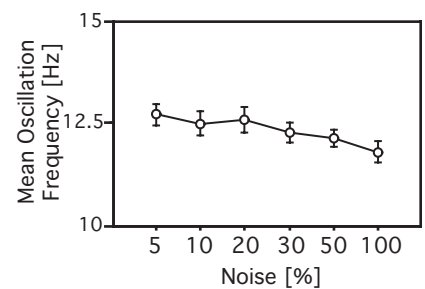


**Figure 4-31: Frequency as a function of coherence for alpha oscillations**

The figure shows the average oscillation frequencies for low frequency components in the cross-correlograms as a function of stimulus noise. Error bars show  $\pm$  one standard error of the mean. The same inclusion criteria as for the fit of the center peak applied. In addition, the correlogram had to show a center peak that was detected and quantified by the Gauss-fit procedure. Grating and noise free RD pattern were excluded because they showed no low frequency oscillations.

ulus showed the highest oscillation frequency with a mean value of  $12.7 \pm 0.3$  Hz. With increasing levels of noise this value decreased monotonically to reach a value of  $11.8 \pm 0.3$  Hz for a fully incoherent stimulus.

In addition to the oscillation frequency, the amplitude of the first oscillation peak relative to the height of the correlogram's center peak was calculated. Fig 4-32 plots these relative amplitudes as a function of stimulus coherence. These values were distributed around a mean value of 0.75. 2-way ANOVA showed no significant difference ( $F(5, 78) = 0.94, p = 0.46$ ).

#### 4.4.3. Discussion

The results showed that grating stimuli and random dot texture pattern were able to frequently elicit synchronized responses in area 17 and area PMLS of the anesthetized cat. However, the properties of synchronization with respect to probability, synchronization strength and temporal precision found for the two areas and stimuli were different.

For area 17, synchronization patterns for the grating stimulus resembled those previously described [42, 28, 31, 124]. Synchronization strength as determined by the RMA and temporal precision as determined by the half width at half height of the center peak in the cross-correlograms were comparable to earlier studies. Most of the cells showing synchronization for a grating stimulus also showed synchronization for the random dot pattern without stimulus noise. No significant differences were found for the synchronization strength between the two stimuli. In contrast, the temporal precision of synchronous discharge for the dot pattern decreased leading to broader synchronization peaks in the correlograms. Oscillations in the gamma frequency range that have been frequently reported for gratings [42, 28] were not found. In addition to coherent random dot pattern, non-coherent texture stimuli were also able to elicit synchronized responses for a variety of noise levels. As a result of the decoherence, the precision of the synchronization further decreased

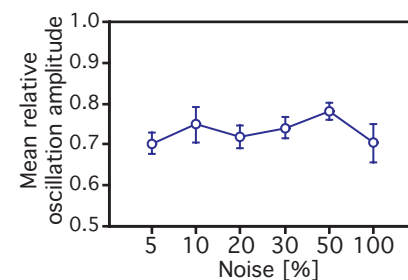


**Figure 4-32: Relative Amplitude of the alpha oscillation**

The amplitude of the low frequency oscillations relative to the height of the center peak of the correlogram is plotted against stimulus noise. Error bars show  $\pm$  one standard error of the mean. The same inclusion criteria as for figure 4-31 applied.



and oscillations on a fast time scale were not found. The synchronization strength, however, was comparable for all random dot protocols with noise levels of up to 20%. Increasing the noise level further led to a significant increase in the RMA value.

For area PMLS, only a subset of multiunits showed narrow synchronization of less than 5ms center peak width with respect to the grating stimulus that resembled those found in previous experiments [28]. For this subset, synchronization strength as well as temporal precision for the grating were in agreement with this earlier study. Synchronization elicited by coherent and non-coherent random dot pattern, however, showed a different signature. The precision of synchronization as well as synchronization strength were markedly reduced compared to the grating stimulus. In addition, visual noise led to a further increase in the width of the synchronization peak whereas RMA values were not affected.

As shown previously, temporal correlation in area 17 [42, 31, 124, 44] and PMLS [28] depends on whether the cells are responding to the same or to different objects. Synchrony is observed only between cells stimulated by the same object whereas stimulation with different objects leads to a strong reduction in synchronized firing activity. The same synchronization behavior has been found in many other visual areas in the cat and monkey (for review see [122, 31, 124]). The loss of gamma oscillation with random dot patterns and a decrease in the precision of synchrony with decreasing stimulus coherence found in the present study demonstrates a similar dependence of cortical synchrony on motion coherence. Only dots exhibiting the same direction of motion and thus forming an assembly that should be bound according to the Gestalt criterion of common fate ([148], see also chapter 1) seem to be able to synchronize the firing activity of cells in both areas 17 and PMLS. In contrast, dots with different directions of motion reduce the probability of synchronous firing depending on the level of visual noise introduced into the random dot pattern. Similar results have been reported previously for synchronization in the superior colliculus [10] where the precision of synchrony gradually decreased with incoher-

ent motion stimuli. The gradual increase in synchronization width found in the present data rules out the possibility that the precision of synchronization acts as a biological switch that stays more or less constant as long as a global direction of motion is detectable and vanishes as soon as the visual system is not able to discriminate a global motion.

Broad synchronization peaks like those found in the data from this study could also be attributed to stimulus locked rate fluctuations and thus reflect externally driven changes in firing rates rather than internally generated synchronization pattern. However, the fact that the shift predictor was flat demonstrated that the correlation pattern found in this study was not stimulus locked but most likely resulted from internal neuronal interactions.

Broad synchronization peaks in the visual cortex have previously been reported by other authors [81, 88]. These broad peaks were attributed to shared common input from the retina or lateral geniculate nucleus [81]. Several arguments suggest that the correlations observed in the present study are due to internal neuronal dynamics rather than common input. First, area PMLS does not depend on monosynaptic direct retinal input but gets its input mainly from area 18, the superior colliculus and several nuclei of the thalamus (see section 2.3). This makes it unlikely that broad correlation peaks in area PMLS were due only to shared retinal input. In addition, stimulus induced retinal oscillation found in previous studies [82] were of much higher frequency than the oscillations found in the present study [16].

Broad synchronization peaks have also been attributed to burst firing of cells on a time scale of 50 ms [26]. The influence of bursts as the source of broad synchronization peaks seems unlikely in the present case since jittering the data of only a few milliseconds abolished the synchronization peak in the correlogram. Correlation peaks due to burst, however, should be relatively unaffected by a jitter on this time scale and shifts of several tens of milliseconds should be necessary in order to destroy this kind of correlation.

Broad synchronization peaks have also been reported for inter-hemispheric connection [88]. In that study, the width of the center peaks in cross correlograms depended on the degree of overlap of the receptive fields of the two cells and on the difference in the preferred directions of the recorded multiunits. Since electrode positions in the present study were chosen such that the receptive field overlap and the preferred directions matched optimal synchronization conditions, broad synchronization peaks due to a mismatch in these parameters is also unlikely.

In addition to broad synchronization peaks, stimulus noise led to strong low frequency oscillations around 12 Hz in area PMLS. This oscillation frequency was largely independent of the amount of noise in the random dot pattern. In addition, the strength of the oscillation relative to the center peak in the correlogram did not change significantly.

Oscillation in neural responses in cats have been previously described [24, 41]. These oscillations between 30 and 70 Hz were stimulus related and depended on the movement of the stimulus over the receptive field. The precise frequency varied between trials even when the same stimulus was shown [24, 27, 41]. Oscillations have also been found in the retina and the geniculate nucleus but with a higher frequency of 70 to 100 Hz [82,16]. In contrast, during background activity, oscillations between 1 and 30 Hz were found [24, 41]. The origin for these cortical oscillations is still a question of debate. Cells exhibiting a rhythmic firing pattern might serve as a pacemaker for oscillatory behavior of cortical neurons [69]. Alternatively, massive backcoupling in the network of cortical cells could lead to oscillatory firing patterns as observed in many experiments [69]. On the functional level, these oscillations may mediate the formation of assemblies of neurons that represent a given stimulus pattern. This was first suggested for the olfactory system where local EEG and single cell recordings showed oscillations between 40 to 80 Hz in a stimulus dependent way [40, 20]. Later, the formation of

cell assemblies was also proposed for the visual cortex [42, 24, 28] where they may form coherent domains of activity that represent essential features of sensory stimuli.

In the low frequency region, two types of alpha oscillations are distinguished in the literature. i) Alpha-spindles oscillate with 7 to 14 Hz with a duration of 1.5 to 2 s and repeat every 5 - 10 s. They are associated with a synaptic blockade throughout the thalamus [69] and occur during sleep as well as during barbiturate anaesthesia. The frequency of these alpha-spindles depends on the states of the brain and is the lower the deeper the sleep or state of anaesthesia [131]. ii) Alpha oscillations occur frequently in a state of relaxed wakefulness and particularly at eyes closed [69]. They are generated by cortical neurons forming a dipole layer in cortical layers IV/V. These cortical alpha rhythm seems to be generated in small cortical areas and spreads in different directions by means of cortico-cortical connections.

It cannot be ruled out that in this thesis the low frequency oscillations have to be attributed to the effect of anesthetics. A study by Brecht et al [10] is in favor of this hypothesis. They looked at responses to random dot patterns in the superior colliculus of awake cats and found a dependence between the appearance of low frequency oscillations and the arousal state of the animal. Furthermore, oscillation frequencies were higher in the awake than in the anesthetized animal. However, in the present study, visual inspection of the data did not show strong frequency fluctuations for the alpha oscillation. This would have been expected if they were solely due to anaesthetics effects, given that the animals went through slight fluctuations in the state of anaesthesia. In addition, precise synchronization has been found for the grating stimulus in area PMLS. This might be explained by the fact that a grating, consisting of a continuous repetition of low and high luminance, is a more salient stimulus to the visual system than is the random dot pattern. Therefore, this stimulus might be able to lead to synchronized responses in area PMLS despite the attenuating effects of anaesthetics. On the other hand, if no precise synchronization was found for the grating

stimulus, the synchronization pattern for the random dot stimulus did not change with stimulus noise and a very broad synchronization remained regardless of the level of coherence. This different behavior of multiunits also speaks against a broadening of synchronization peaks due to anesthetic effects only.

The low frequency oscillations especially in motion area PMLS might reflect the response of the cortex to random dot stimuli. It has been proposed that oscillations in the alpha frequency range might mediate connections over larger distances in the cortex [132]. The sine wave grating, however, is a highly salient repetitive stimulus whose motion information can be analyzed locally, i.e., no integration over a wider space of the visual field is necessary to extract the information necessary for the visual system to detect and analyze the direction of motion. In contrast, for the random dot pattern, the cortex needs to search for information over a wider visual space in order to extract the global motion of the stimulus. This integration space has to be even larger when the stimulus coherence is reduced by visual noise. Therefore, a local analysis of the stimulus is not sufficient to detect the properties of a random dot pattern. The transition from gamma to alpha frequencies in area PMLS might reflect this search and integration of information over a wider visual space because low frequencies can be synchronized over a larger cortical distance [13, 55]. This might be a further indication that area PMLS plays an important role in the processing of stimuli requiring integration of motion information [110] and that oscillatory behavior may play a crucial role in performing this task.

Further evidence supporting this idea comes from a recent study by Cantreas et al. in the Guinea pig [18]. They showed that in a slice preparation the spatiotemporal activation pattern upon electrical stimulation depends on the application frequency. Whereas 40 Hz oscillation leads to a rapid restraining of excitation to a small area directly above the stimulation electrode, 10 Hz oscillation does not lead to a localization of the excitation area but leads to a lateral spread within a few milliseconds.

Recently, several authors reported the occurrence of alpha frequencies during a visomotor Go/No-Go task in awake, behaving cats depending on the mental state of the animal. In these studies, strong alpha components were reported when the animal was expecting a certain stimulus [32] or when presented with a behaviorally relevant stimulus [132]. In contrast, a decrease in alpha and an increase in gamma frequencies was found for novel, unexpected stimuli. An EEG study on humans by Mima et al. [74] reported an increase in EEG coherence for the alpha band when the subject was recognizing a meaningful visual object spanning the visual midline. This increase did not occur for passive viewing or for meaningless objects. Von Stein et al. [133] concluded that low frequency oscillations are therefore involved in top-down processing depending on the mental and expectational state of the animal. Closed eyes, a situation where alpha oscillations are often found, were regarded as the extreme form of this top-down processing where no new stimulus is entering the visual system and, consequently, no bottom up is possible. They further propose that the high frequency oscillation in the gamma frequency range occur over smaller distances between different electrodes and are involved in the analysis of newly, unexpected stimuli in a feed forward fashion.

Another study by Fries et al. [37] on awake, behaving macaque monkeys reported that attention also modulates the occurrence of alpha frequencies. They recorded from neurons in cortical area V4 while the monkeys were attending to behaviorally relevant stimuli and ignored distracters. Attention during a delay period led to a decrease in alpha frequencies compared to the non-attended situation. If, in addition, a stimulus was presented the decrease in alpha was maintained and an increase in gamma frequencies was found.

Thus, the transition between alpha and gamma frequencies can serve two purposes: i) On the subconscious level, the transition to alpha frequencies could lead to an increase in the integration space used to search and gather necessary information about a stimulus ii)

On the level of attention, the transition from alpha to gamma frequencies could restrict the focus of attention from a global search state to a local focus to the area of interest.

## 4.5 Power Spectra of the Local Field Potential

### 4.5.1. Introduction

After the preceding sections were concerned with the analysis of spiking activity of multiunits, experiments in the following two sections will analyze the LFP and its correlation to the multiunit spike signal. In contrast to the multiunit signal which reflects the extracellular action potentials of cells, the LFP reflects changes in the postsynaptic potential. It reflects the sum of membrane currents and subthreshold synaptic activity in a certain volume of cortical tissue [27]. The half decay distance of the LFP around its origin within the brain has been found to be between 100 and 200  $\mu\text{m}$  [27, 43]. Thus, the LFP is recruited essentially from a single orientation column [27]. Consequently, it is integrated over a much larger region compared to the multiunit spike signal and is therefore even more an assembly signal. In addition, it has been shown recently that the LFP correlates well with the BOLD signal from fMRI studies [68], which represents changes in the oxygenation level of hemoglobin for a given task.

Previous studies have shown that oscillation and synchronization in the gamma frequency range in the neural spike response of cats are leading to peaks in the power spectrum of the LFP [24, 41]. These oscillations are stimulus related leading to spectral components between 30 and 70 Hz while the stimulus is moving through the receptive fields of the cells. In contrast, background activity shows peaks in a frequency region between 1 and 30 Hz [24, 41]. The precise frequencies often vary between trials even when exactly the same stimulus is shown [24, 41, 27].

The previous section showed that a decrease in coherence leads to an increase in the center peak width of the correlograms for area 17 and to a peak broadening and strong alpha oscillations in area PMLS. In addition, it has been shown that the BOLD signal depends on the coherence of a given stimulus in both monkeys [101] and humans [106]. In the present section I will investigate, if the increase in center peak width in the two areas is accompanied by a transition



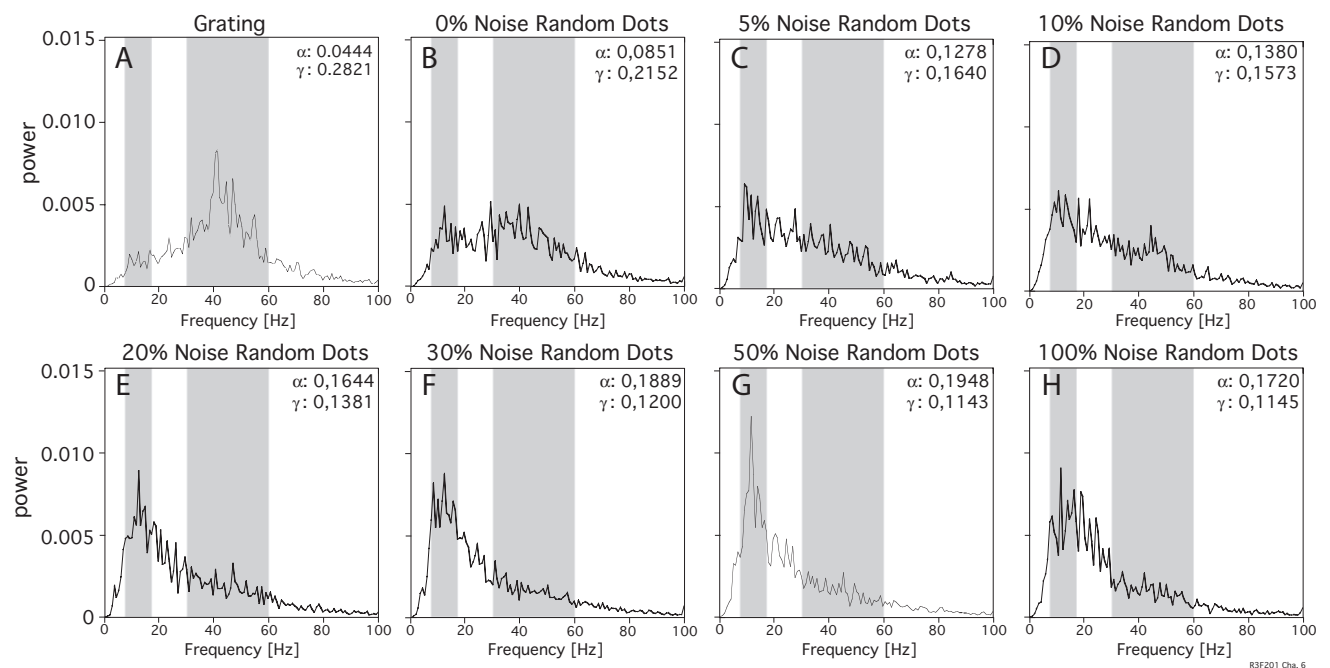
from high to low frequency components in the LFP. It will be further investigated, if these shifts within the power spectrum of the LFP were identical for areas 17 and PMLS or if the two areas would show a different response to decreasing stimulus coherence.

The LFP was recorded in parallel with the spike signals analyzed in the previous sections. The same stimuli were used. Data were recorded for seven seconds, including two seconds of spontaneous activity before and after the stimulus. Data were filtered between 1 Hz and 100 Hz and were sampled with 1 kHz. Power spectra were computed and the power was summed over the alpha (6 Hz to 18 Hz) and the gamma (30 Hz to 60 Hz) frequency band.

#### 4.5.2. Results

##### *Area 17*

Figure 4-33 shows an example for a power spectrum of the LFP recorded from one multiunit in area 17. The figure shows the normalized power spectrum  $P(f)$  of the measured LFP vs. frequency in Hertz. The normalization condition was  $\int P(f)df = 1$ . Data were recorded with a time resolution of 1 ms and the power spectrum was calculated for data measured between 2300 ms and 4800 ms after start of the experiment. Since the LFP data were filtered from 1 Hz to 100 Hz (see chapter 3.2) the sampling frequency of 1 ms was sufficient to unambiguously sample the signal (Nyquist criterion). The LFP was convoluted with a Hamming window prior to performing the fourier transform to avoid side lobes due to the convolution of the signal with a box-car function. This was described in detail in section 3.6.1. The gray shaded areas in Fig. 4-33 mark the frequency ranges for the  $\alpha$ -band from 6 Hz to 18 Hz and for the  $\gamma$ -band from 30 Hz to 60 Hz. Power summed over these frequency bands are given as values for  $\alpha$  and  $\gamma$  in the upper right corner of each graph. The data point at 50 Hz was excluded from the summation, since contamination of the data with the line signal could not be completely avoided.



In area 17, a decrease in stimulus coherence led to a shift in signal power from high frequencies in the range of 30 Hz to 60 Hz towards low frequencies ranging from 6 Hz to 18 Hz. In particular, panel A shows the power spectrum of the signal elicited by a multi-unit stimulated with a sine wave grating. The low frequency range contained only a small amount of power ( $\alpha = 0.04$ ). In contrast, a high amount of power ( $\gamma = 0.28$ ) was found in the high frequency region above 30 Hz. A pronounced peak was visible slightly above 40 Hz. This peak vanished when a coherent random dot stimulus was shown (Fig. 4-33, panel B). What remained was a broad shoulder of frequencies ranging from 10 to 45 Hz. This decrease in the gamma band was accompanied by slightly higher signal power contained in the low frequency region ( $\alpha = 0.09$ ). Adding noise to the stimulus led to a further transition from high to low frequencies in the spectrum: power above 30 Hz decreased and got shifted towards low frequencies. At 20% noise, a strong peak around 16 Hz grew in. This peak increased and shifted to even lower frequencies when increasing the noise level to 50%. At this level of coherence, the amount of power contained in the gamma frequency band dropped more than two-fold to  $\gamma = 0.11$  compared to the grating stimulus with  $\gamma = 0.28$ . In contrast, the amount of power within the alpha band increased by a factor of 4.4 from  $\alpha = 0.04$  for the grating stimulus to  $\alpha = 0.2$  for the

**Figure 4-33: LFP power spectra for different level of coherence in area 17**

The figure shows LFP power spectra for the 8 different stimulus conditions in area 17. The power spectrum is plotted against frequency in Hertz, with the overall power normalized to one. Alpha and gamma frequency bands are shaded in gray. The numbers in the upper right corner indicate the power summed over the respective frequency region.

50% noise dot pattern. In this example, a further increase in incoherence, i.e., raising the noise level to 100%, led to a slight decrease in alpha power ( $\alpha=0.17$ ).

Figure 4-34 shows the LFP data averaged over all multiunits. Average normalized power summed over the alpha band (6 to 18 Hz, blue) and the gamma band (30 to 60 Hz, red) is plotted against the different stimulus conditions. Only cells with a difference between preferred direction and stimulus direction of less than  $30^\circ$  were included into the analysis. It has been shown that the LFP signal exhibits orientational and directional preference similar to those found for multiunit activity [24, 41, 27]. Therefore, the preferred direction of the cells was determined by the tuning curve experiment described in section 4.2. Out of 123 recording sites, 47 (38%) fulfilled this criterion. All statistical test in the following results were done with Fisher's PLSD.

The pooled LFP data resembled the dependence between stimulus coherence and signal power found in the example shown above. The differences in alpha and gamma power for the different noise levels were highly statistically significant (ANOVA,  $F(7, 358)=73.45$ ,  $p < 0.0001$  for the gamma band and  $F(7, 358)=27.93$ ,  $p < 0.0001$  for the alpha band). In the gamma frequency band, the grating stimulus elicited the highest average power with a mean of  $0.23 \pm 0.007$ . This power reduced for stimulation with the random dot pattern. The mean for the noise free texture stimulus decreased to  $0.18 \pm 0.007$  resulting in a highly significant difference between the two stimuli ( $CD = 0.01$ ,  $p < 0.0001$ ). Adding noise to the random dot pattern further reduced the power in the high frequency region. Noise levels of 5%, 10% and 20% showed significant decreases in this frequency region compared to the lower noise level ( $CD$  always 0.01,  $p < 0.0001$  for 5%,  $p = 0.047$  for 10% and  $p = 0.03$  for 20% noise). Increasing stimulus incoherence of 30%, 50%, or 100%, however, did not lead to pairwise significant differences in power that was contained in the high frequency band ( $CD$  always 0.01, 20% to 30%  $p = 0.13$ , 30% to 50%  $p = 0.53$ , 50% to 100%  $p = 0.75$ ).

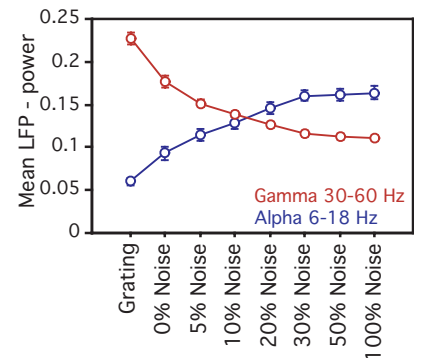


**Figure 4-34: Alpha and gamma power in area 17 as a function of coherence**

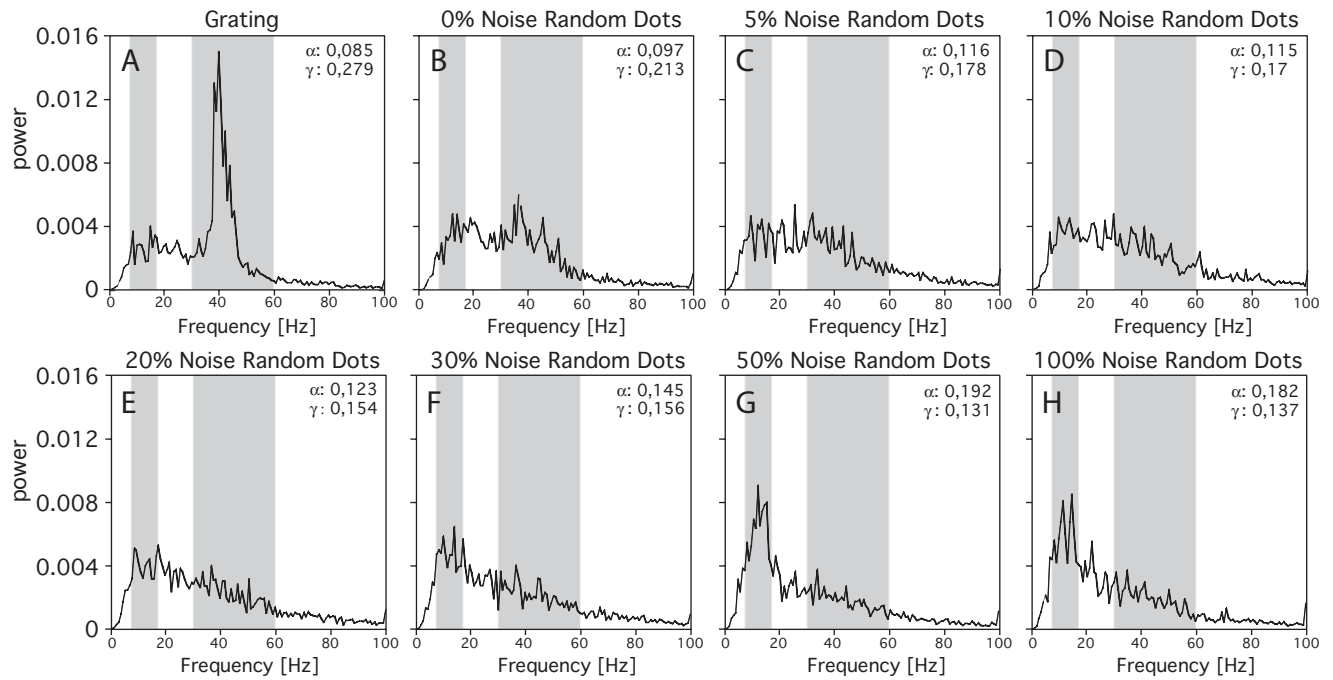
Normalized LFP power averaged over all multiunits and summed over the alpha band (blue) and the gamma band (red) are plotted against the different stimulus conditions. Only cells with a difference between preferred direction and stimulus direction of less than  $30^\circ$  were included into the analysis

The alpha frequency band ranging from 6 Hz to 18 Hz showed the opposite dependence on stimulus coherence (blue trace in Fig. 4-34). The power spectrum of the response to the grating stimulus showed the lowest power with a mean of  $0.06 \pm 0.004$ . Stimulation with the random dot pattern increased this value. The mean changed to  $0.09 \pm 0.008$  showing highly significant differences between the two stimuli (CD= 0.02,  $p = 0.001$ ). Adding noise led to a monotonic increase up to an incoherence level of 30%. However, significant paired differences between two adjacent noise levels were only found between 0% and 5% stimulus noise (CD=0.02,  $p = 0.03$ ). For higher noise levels, only larger differences in stimulus noise showed significant changes (5% and 20%,  $p = 0.0009$ , 10% and 30%,  $p = 0.0008$  and 20% and 100%,  $p = 0.04$ , CD always 0.02). No significant differences were found for noise levels of 30%, 50% and 100%, showing mean alpha power of  $0.16 \pm 0.006$ ,  $0.16 \pm 0.007$  and  $0.17 \pm 0.007$ , respectively ( $p = 0.13$ ,  $p = 0.8$  and  $p = 0.77$  for pairwise significance with the preceding noise level, CD always 0.02).

#### *Area PMLS*

Fig. 4-35 shows an example for a power spectrum of the LFP for one multiunit recorded from area PMLS. The normalized power spectrum is shown vs. frequency in Hertz (see also area 17, see Fig. 4-33). Sampling condition and inclusion criteria were identical to Fig. 4-33.

The global changes in the power spectrum of the LFP in area PMLS resembled those described for area 17. High frequency components decreased with increasing levels of noise whereas low frequency power increased. In particular, the power spectrum of the response evoked by the grating stimulus (Panel A) showed a high amount of power in the gamma region between 30 Hz and 60 Hz ( $\gamma = 0.28$ ). In addition, a strong peak appeared around 40Hz. In contrast, only little power was found in the alpha frequency band ( $\alpha = 0.09$ ). When stimulating with a random dot pattern, the strong gamma component disappeared.



Only a small peak remained around 40 Hz ( $\gamma = 0.21$ ). The power spectrum for low frequency values increased slightly ( $\alpha = 0.1$ ). Adding noise to the dot stimulus led to a further disappearance of the gamma peak and an increase in the alpha band (Panel C to H). At five percent stimulus noise, the low frequency contribution increased to  $\alpha = 0.12$  and the gamma components decreased to  $\gamma = 0.18$ . At higher noise levels, the low frequency contribution further grew in and reached a maximum at 50% noise ( $\alpha = 0.19$ ). At the same time, the gamma band region of the power spectrum decreased with decreasing coherence of the stimulus and reached a value of  $\gamma = 0.13$  at 50% noise. Power contained in the alpha band increased again for the fully incoherent stimulus from  $\alpha = 0.19$  at 50% noise to  $\alpha = 0.18$  at 100% noise and a slight increase was found in the gamma frequency region ( $\gamma = 0.14$  as opposed to  $\gamma = 0.13$  at 50% noise).

Fig. 4-36 shows the averaged power of the LFP in area PMLS for the eight stimulus conditions for high (red trace) and low (blue trace) frequencies. Bands were defined as for area 17 (see above). To be included into the analysis, the preferred direction of the multiunit, which was determined by the tuning curve experiment described in section 4.2., had to be within  $\pm 30^\circ$  of the stimulus direction. 201 out of 276 cells (72%) fulfilled this criterion and were

**Figure 4-35: Analog Power Spectrum in Area PMLS**

The figure shows an example for LFP power spectra calculated from the eight different stimulus conditions in area PMLS. The layout is as in Fig. 4-33., the overall power is normalized to one. The numbers in the upper right corner indicate the power summed over the respective frequency region.

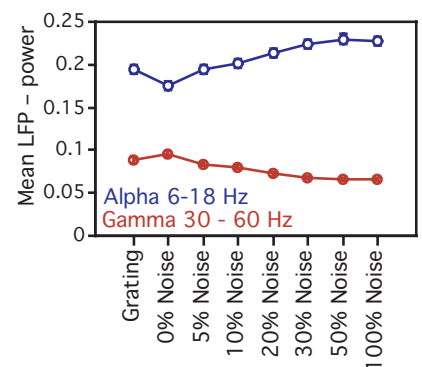


**Figure 4-36: LFP Power in Area PMLS**

Normalized LFP power averaged over all multiunits and summed over the alpha band (blue) and the gamma band (red) are plotted against the different stimulus conditions. Only cells with a difference between preferred direction and stimulus direction of less than  $30^\circ$  were included into the analysis.

included into the analysis. For both frequency bands, analysis of variance gave highly significant differences between different stimulus conditions (ANOVA,  $F(7, 1597)=19.35$ ,  $p < 0.0001$  for the gamma band and  $F(7,1597)=13.59$ ,  $p < 0.0001$  for the alpha band).

The random dot pattern without noise contained the highest amount of average gamma power in the eight stimulus conditions. The mean power elicited by this type of stimulus was  $0.096 \pm 0.003$ . The grating stimulus did show a significantly lower mean of  $0.088 \pm 0.003$  (Fisher's PLSD,  $CD = 0.007$ ,  $p = 0.023$ ). The gamma power decreased monotonically when visual noise was introduced into the dot pattern. At noise level of five percent, the LFP signal contained a mean gamma power of  $0.085 \pm 0.003$  which was significantly different from the noise free dot pattern (Fisher's PLSD,  $CD = 0.007$ ,  $p = 0.002$ ). Another significant change in gamma power was found between 10% and 20% stimulus noise (Fisher's PLSD,  $CD = 0.007$ ,  $p = 0.029$ ). The difference between 5% and 10%, however, did not become significant (Fisher's PLSD,  $CD = 0.007$ ,  $p = 0.296$ ). Noise levels of more than 20% also did not lead to significant reductions in the amount of power contained in the gamma frequency band.

The opposite dependence on stimulus coherence was found for the alpha band in the LFP power spectrum. In this frequency range, the coherent random dot pattern showed the smallest amount of low frequency components with a mean of  $0.18 \pm 0.005$ . The value for the grating was significantly higher, showing an average power of  $0.2 \pm 0.005$  (Fisher's PLSD,  $CD = 0.02$ ,  $p = 0.01$ ). Introducing noise to the random dot stimulus led to a monotonic increase in alpha power. However, only the difference between the noise free dot pattern and the five percent noise level was significant (Fisher's PLSD,  $CD = 0.01$ ,  $p = 0.008$ ). All other pairwise differences between mean alpha power for adjacent noise levels were not significantly different. However, in contrast to the gamma frequency band, significant changes could be found for differences between non-adjacent noise levels of more than 20%. The differences in alpha power between 20% and 50% visual noise and between 20% and 100% were statisti-

cally significant (Fisher's PLSD,  $CD = 0.01$ ,  $p = 0.02$  and  $p = 0.04$ , respectively). No statistical significant difference in alpha power were found between noise levels of more than 30%.

### 4.5.3. Discussion

The data in this section showed that low- and high frequency components in the power spectrum of the LFP depend on the coherence of random dot stimuli for both areas 17 and PMLS. High frequency components were reduced and low frequency components increased with increasing levels of visual noise. The absolute values for alpha power were higher in area PMLS than in area 17 for all stimuli whereas higher values for gamma power were found in area 17.

For area 17, a high amount of power in the gamma band was found for the grating stimulus and little power was found for frequencies below 30 Hz. These high frequency peaks reflect the appearance of gamma synchronization found in the correlation analysis of spike signals in the preceding section. It is in agreement with earlier studies which also reported high amounts of gamma power in the LFP for the grating stimulus whereas the low frequency components were suppressed [24, 41]. For random dot stimuli with different levels of stimulus noise, power in the gamma frequency range between 30 Hz and 70 Hz showed a monotonic decrease with decreasing stimulus coherence. In contrast, power contained in the low frequency bands of the LFP between 6 and 18 Hz (alpha band) showed a monotonic increase. This shift in frequency for the random dot pattern also reflects nicely the findings of the synchronization analysis in the previous section. The broadening of the synchronization peak in the unit data was accompanied by a decrease of the high frequency components and an increase of the low frequency components in the LFP.

For area PMLS peaks in the power spectrum in the gamma frequency range for the grating stimulus were found. However, in contrast to area 17, the grating did not, on average, elicit the strongest response in the gamma band. The highest amount was found for the

noise free random dot pattern. The grating stimulus further did not show the lowest values for the alpha frequency range which was again found for the noise free random dot pattern. These findings were different from the result found in the preceding section. The correlation analysis revealed an increase in the center peak width when going from a grating to a random dot pattern. Consequently, one would expect a decrease in high frequency components for the LFP. It has been shown, however, that not every frequency component found in a power spectrum of the LFP is reflected by a change in oscillation frequencies or center peak width in the unit data [27]. This might explain the difference between the two results.

When increasing the level of stimulus noise, power in the gamma frequency band decreased with decreasing coherence. In addition, power in the alpha band increased with the level of stimulus noise. As for area 17, the frequency distribution of the LFP in area PMLS confirmed the unit data from the preceding section. The broadening of the center peak was reflected by a decrease and increase of high and low frequency components, respectively. In addition, the strong alpha oscillations found in the correlograms in area PMLS were also reflected in the LFP as a strong increase in the alpha frequency band.

For the primary visual area it has been proposed that low and high frequencies in the LFP might serve different functions [36]. They might engage different couplings within the networks which could support different coding tasks [36]. Strong bands compared to the remaining frequencies in the power spectrum were either found for high frequencies from 35 Hz to 70 Hz or in the low frequency regions between 8 Hz and 16 Hz. No distinct bands were found in the intermediate frequency region between 16 Hz and 35 Hz. From this finding it might be speculated that the cortex processes coherent and incoherent visual stimuli in two different modes. The high frequency oscillations could be dealing with the local processing of coherent stimuli, e.g., gratings that can be analyzed by processing information from a small area of the visual field. As described in the discussion of the preceding section, this high frequency oscillation



might also be involved in mediating attention and to analyze new, surprising inputs. Whereas, especially for area 17, the locally defined grating was dominated by this high frequency oscillation, decoherence was leading to an involvement of more and more neurons which imposes the need to reduce the frequency in order to integrate the information over a larger cortical space. The integration of a larger ensemble of neurons might be mediated by using low frequency oscillations in the alpha frequencies range as found in the present study. This might support the idea described in the discussion to the preceding section that low frequency oscillations are a mechanism to integrate information over a larger spatial scale. This low frequency oscillations might be more involved in the analysis of spatially distributed information as well as top-down processing.

Further evidence for this idea comes from studies by Eckhorn et al. This group reported that the oscillation frequency in the monkey visual cortex in the range between 30 and 90 Hz depends on the size of the stimulus [25]. A larger stimulus patch leads to lower frequencies whereas a smaller patch leads to an increase in the oscillation frequency. Accordingly, Schanze et al. [115] proposed that the oscillation might serve as a gating function. The frequency of the oscillation should be adjusted according to the properties of the object and the performed task.

However, these studies have been performed with coherent stimuli. It seems reasonable to speculate that a non-coherent stimulus, like a random dot pattern that needs to be analyzed over a much wider visual space in order to extract the global motion, will lead to even lower oscillation frequencies as the number of involved neurons increases. While fast oscillations might support feature binding on a small spatial scale, slow oscillations can occur synchronized across larger cortical regions and might support binding for more widely spread feature representations [13, 55].

It can, of course, not be ruled out that the strong alpha components were due to anaesthetic effects. However, the fact that a monotonic increase with decreasing stimulus coherence for this frequencies was found made it unlikely that the anesthetics were the

## Chapter 4

only reason for this transition. In addition, gamma frequencies have been found in the data and showed a monotonic change with the applied stimulus. Hence, the change in coherence has most likely some influence on the appearance of low frequency components in the LFP.

## 4.6 Spike Field Coherence

### 4.6.1. Introduction

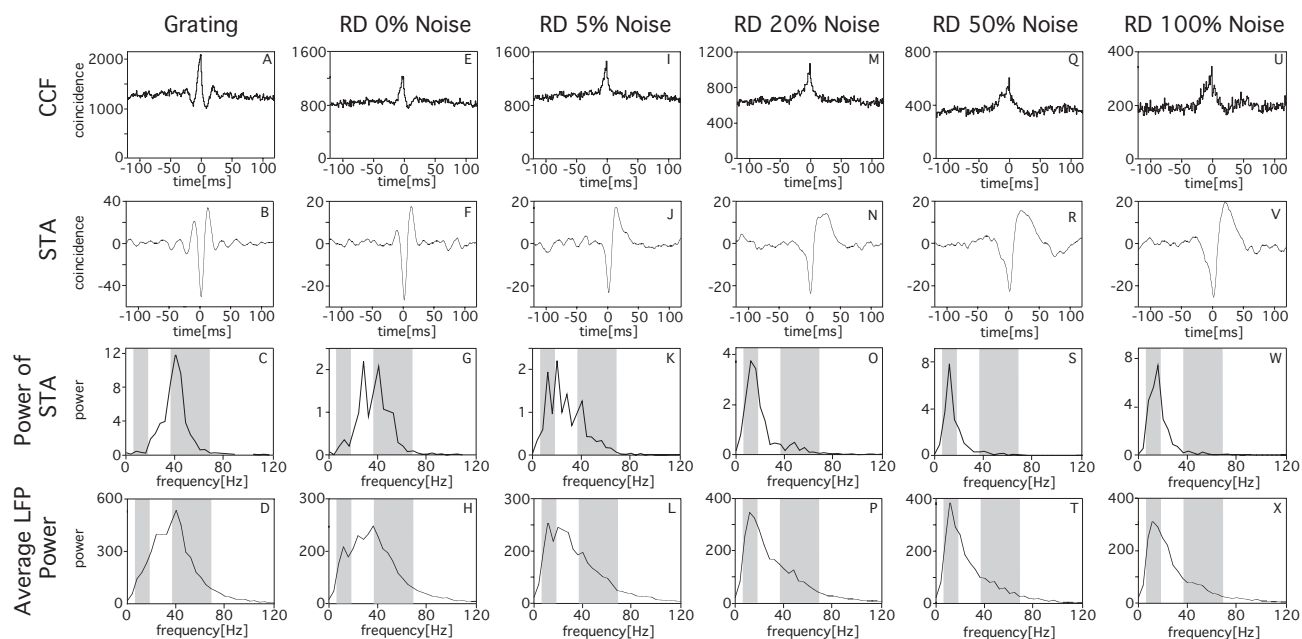
Experiments in the previous two sections have shown that a decrease in the coherence of motion within a random dot texture pattern led to a shift from high to low frequency components in both the spike data and the LFP. The experiment in this chapter now investigates the correlation between these two types of signals for high and low frequencies. The spike-field-coherence is hereby used as a correlation measure. It has been used before to correlate these two signals [39]. Details on calculating the spike-field-coherence can be found in section 3.6.3.

For the following section, unit data and LFP were recorded for the random dot stimuli. The recording conditions have been described in the preceding sections (see 4.3.1 and 4.5.1 for details).

### 4.6.2. Results

#### *Area 17*

Fig. 4-37 shows one example data set used to calculate the Spike-Field-Coherence (SFC). Data were taken from one multiunit in area 17. Both, spike signal and LFP, were recorded from the same electrode. Each column shows, from top to bottom, the cross correlogram (CCF), the spike triggered average (STA) of the LFP, the power spectrum of the spike triggered average and the averaged power spectrum of all LFP segments used to calculate the spike triggered average (for details on this calculation see section 3.6.3). The columns show from left to right results for the grating stimulus, the random dot pattern without visual noise and for random dot patterns with noise levels of 5%, 20%, 50% and 100%, respectively. In this example, the shift predictor is not subtracted from the cross-correlogram.



The CCF computed for the grating stimulus showed a distinct center peak of 2.7 ms half width at the inflection point with side lobes on both sides of the central maximum. A narrow center peak was also found in the spike triggered average together with a 40 Hz oscillation. Consequently, a peak at 40 Hz in the power spectrum of the STA reflected this high amount of power in the  $\gamma$ -frequency band between 30 and 60 Hz, whereas almost no power was contained in the low frequency region ranging from 6 to 18 Hz. The averaged power of the LFP also showed high values above 16 Hz and only little power in the low frequencies. The value for the spike field coherence was calculated by dividing the power spectrum of the STA by the averaged power of the LFP and summing over the frequency band of interest. For this example, the resulting SFC values for the gamma and alpha frequency bands were 0.056 and 0.006, respectively.

The pure random dot stimulus without visual noise also showed a strong center peak in the cross-correlogram but side lobes vanished. The same was found in the STA. The center peak remained but no oscillations were visible. The power spectrum of the STA and the averaged LFP both showed a strong decrease in the 40 Hz region compared to the grating stimulus. In addition, power in the low and medium frequency range between 6 Hz and 18 Hz and

**Figure 4-37: Dataset for the SFC analysis in area 17**

The data set used to calculate the Spike-Field-Coherence (SFC) is illustrated. Both, spike signal and LFP, were recorded from the same electrode. Each column shows, from top to bottom, the cross correlogram (CCF), the STA of the LFP, the power spectrum of the STA and the averaged power spectrum of all LFP segments used to calculate the STA. The columns show from left to right results for the grating stimulus and for random dot patterns with noise levels of 0%, 5%, 20%, 50% and 100%, respectively. In this example, the shift predictor is not subtracted from the cross-correlogram. The value for the SFC was calculated by dividing the power spectrum of the STA by the averaged power of the LFP and summing over the frequency band in question.

between 20 Hz and 38 Hz increased. The corresponding SFC values decreased to 0.014 for the gamma band and stayed approximately constant at 0.006 for the alpha frequency band. A reduction of stimulus coherence with stimuli containing 5%, 20% and 50% noise led to a further broadening of the center peaks and a complete reduction of side lobes in the CCF as well as in the STA. At 50% noise, the center peak in the CCF broadened to 12.3 ms. Consequently, high frequencies in the power spectrum of the STA above 40 Hz got attenuated and low frequencies got amplified. A sharp peak at 10 Hz became the predominant feature in the spectrum. The same held for the average power spectrum of the LFP. Frequencies over 40 Hz got attenuated and the power shifted down to frequencies below 30 Hz. The SFC values changed to 0.004 for the gamma and 0.028 for the alpha band.

The decrease in coupling between spikes and high LFP-frequencies and the increase in coupling between spikes and low frequency components with increasing level of visual noise were reflected in the average data. These data are shown in Fig. 4-38 and 4-39. To be included into the analysis, the difference in preferred direction of the LFP channel, the spike channel and the direction of stimulus movement had to be less than 30°. All statistics was performed using Fisher's PLSD. Fig. 4-38 shows only auto-SFC values, i.e., LFPs and spike times were recorded from the same electrode. Spike field coherence values are plotted as a function of stimulus coherence. The coupling to low frequencies between 6 Hz and 18 Hz are represented by the blue, the coupling to high frequencies between 30 and 60 Hz are illustrated by the red trace.

2-way ANOVA showed highly significant differences in coupling of spikes to gamma frequencies for different levels of stimulus coherence ( $F(7, 461) = 20.14, p < 0.0001$ ). Highest SFC values were found for the grating stimulus with a mean of  $0.03 \pm 0.003$ . This coupling decreased significantly by almost 40 percent to a mean of  $0.02 \pm 0.002$  when the multiunit was stimulated with a random dot pattern without stimulus noise ( $CD = 0.005, p < 0.0001$ ). Decreasing stimulus coherence led to a further decrease in coupling strength.

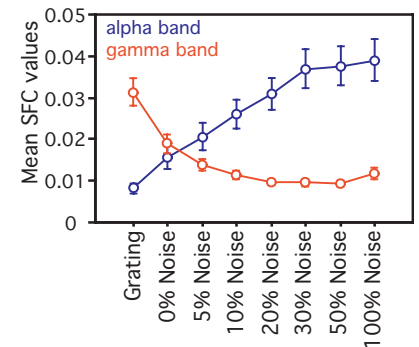


**Figure 4-38: Auto-SFC values in area 17**

The figure shows mean SFC values for area 17 as a function of stimulus condition. The blue line represent the results for the alpha band, the red one shows data obtained for the gamma frequencies. Error bars denote  $\pm$  one standard error. Both, LFP and spike signals came from the same electrode.

However, only differences between 0% and 5% (CD = 0.004,  $p = 0.02$ ) and between 5% and 50% noise (CD = 0.004,  $p = 0.045$ ) were significant. All other pairwise differences were not statistically distinguishable. The fully incoherent stimulus led again to an increase of spike field coherence values relative to the 50% noise level. However, this increase of 33% to a mean of  $0.012 \pm 0.001$  was also not significant (CD = 0.004,  $p = 0.275$ ).

The coupling of spikes to alpha frequencies between 6 Hz and 18 Hz showed the opposite dependence on stimulus coherence. ANOVA revealed a significant decrease in the SFC values for increasing levels of stimulus noise ( $F(7, 461) = 8.23$ ,  $p < 0.0001$ ). These data are shown in blue in Fig. 4-38. Again, LFP and spike signals were recorded from the same electrode. The smallest SFC values were found for the grating stimulus (mean  $0.008 \pm 0.001$ ). Stimulation with random dot patterns with increasing levels of noise led to a monotonic increase in coupling between low frequencies and spike signals. However, none of the differences between subsequent noise levels were statistically significant (CD always 0.01,  $p$  always more than 0.26). In contrast, all but the 0% noise stimuli showed statistically significant changes relative to the grating (CD always 0.01,  $p$  always less than 0.03). Further significant differences were found between the noise free random dot pattern and stimuli with more than 20% incoherence (CD = 0.01,  $p < 0.005$ ). In addition, coherence levels of more than 30% show significant differences when tested against 5% and 10% noise level (CD always 0.01,  $p = 0.003$  and  $p = 0.04$ , respectively). The highest SFC value was reached for the completely incoherent stimulus with a mean value of  $0.04 \pm 0.003$ .

So far, the analysis was restricted to SFC values calculated from LFP and spike signal that came from the same electrode. SFC values based on LFP and spikes originating from different electrodes (cross-SFC) are shown in Fig. 4-39. The same inclusion criterion as for the auto-SFC was applied. Although average coupling between LFP and spike data was weaker than for the auto-SFC, a similar significant relationship between noise levels and spike field coherence was found (ANOVA,  $F(7, 1486) = 43.14$ ,  $p < 0.0001$  for gamma,  $F(7,$

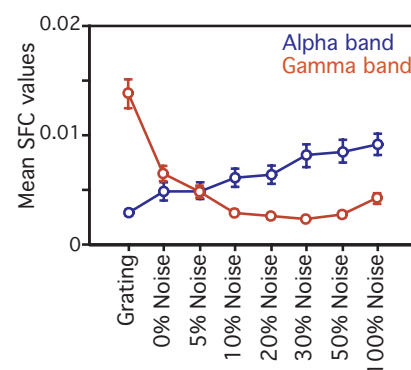


**Figure 4-39: Cross-SFC values in area 17**  
Mean SFC values are plotted for area 17, where LFP and spike signals came from two different electrodes. The layout is as in Fig. 4-38.

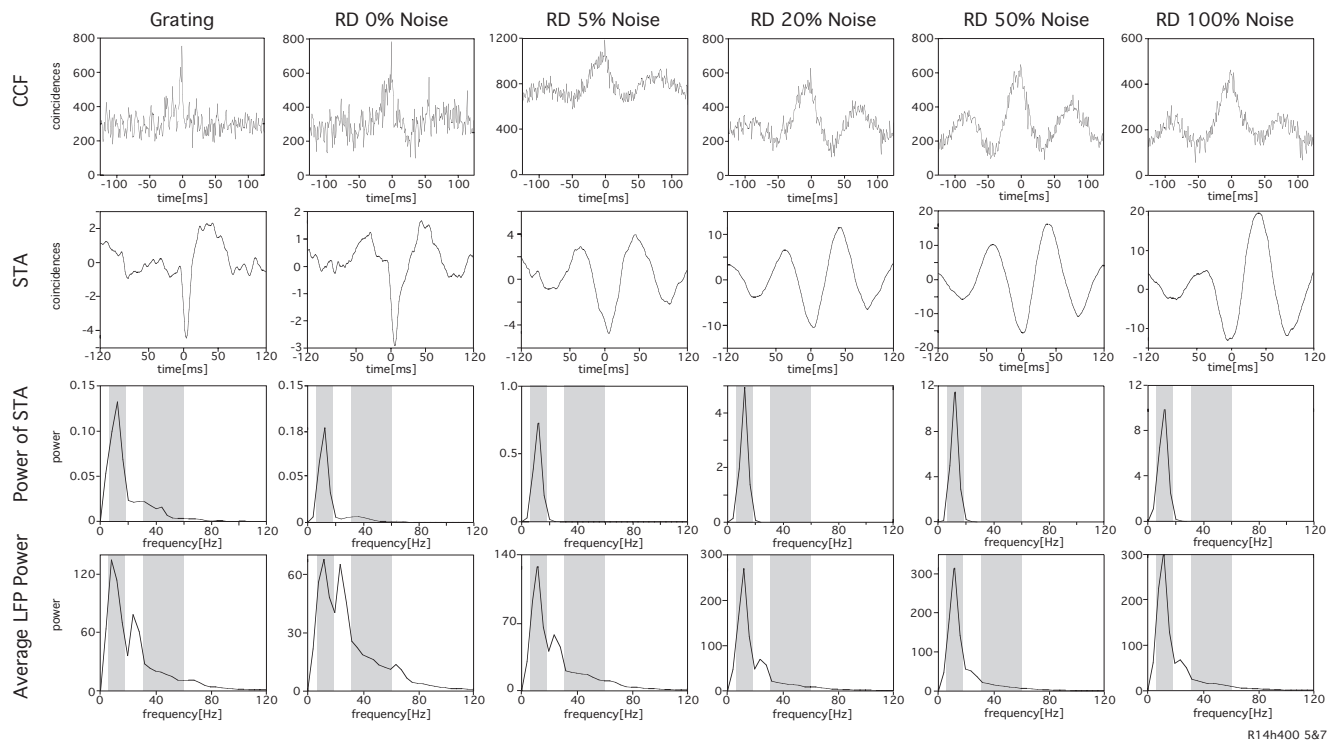
1486) = 5.58,  $p < 0.0001$  for alpha). In particular, for the gamma frequency range, the grating showed the strongest coupling with a mean SFC value of  $0.017 \pm 0.002$ . The random dot pattern without noise showed a strong and highly significant reduction leading to a mean of  $0.008 \pm 0.001$  (CD = 0.002,  $p < 0.0001$ ). Introducing noise further reduced the coupling. 5% incoherence led to a mean value of  $0.005 \pm 0.001$  which was a significant reduction relative to the noise free random dot pattern (CD = 0.001,  $p = 0.023$ ). For higher levels of stimulus noise, only changes relative to the 5% level were significant (CD = 0.001,  $p = 0.003$  between 5% and 20% and  $p = 0.001$  between 5% and 30%). The fully incoherent stimulus showed a mean spike field coherence of  $0.004 \pm 0.001$ . Significant differences were found between this noise level and 30% and 50% decoherence, respectively. (CD = 0.001,  $p = 0.01$  and  $p = 0.05$ , respectively).

In contrast, SFC values for the alpha frequency range increased monotonically from the grating stimulus to the fully incoherent stimulus with 100% visual noise. However, none of the adjacent noise levels led to paired significant differences in coupling strength. The grating showed the lowest SFC value (mean  $0.003 \pm 0.0003$ ). Although the coupling increases already for the noise free random dot pattern, only noise levels of 10% and more showed a significant increase relative to the grating stimulus (CD = 0.002,  $p = 0.018$  at 10% noise). Further significant increases were found between the noise free random dot pattern and noise levels of more than 30% (CD = 0.002,  $p$  always less than 0.008), between 5% noise and noise levels of more than 30% (CD = 0.002,  $p$  always less than 0.008), between 10% noise and noise level of more than 50% (CD = 0.002,  $p$  always less than 0.046) as well as between 20% and 100% noise (CD = 0.002,  $p = 0.022$ ).

#### *Area PMLS*

An example data set for the calculation of the SFC with results recorded from one multiunit in area PMLS is shown in Fig. 4-40. The layout is the same as in Fig. 4-37. Columns from top to bottom show the cross correlogram, the spike triggered average (STA), the power of LFP and the average power spectra of all single LFP segments, re-

spectively. Rows from left to right show data for the grating stimulus, the random dot pattern without noise and for random dot patterns with 5%, 20%, 50% and 100% noise, respectively.



The cross-correlogram for the grating stimulus (Fig. 4-40, panel A) showed a narrow center peak with a half width at the inflection point of 2.04. No oscillations were found. A narrow center peak was also seen in the spike triggered average resulting in a broad shoulder around 40 Hz in the power spectrum of the STA. The same was found in the average power spectrum of the LFP. In contrast to area 17, however, the low frequency region below 20 Hz contained most of the power. The resulting SFC values for the gamma and the alpha band were 0.0005 and 0.0009, respectively. The random dot stimulus (Fig. 4-40, panel B) led to a broadening of the center peak in both the correlogram and the STA. As a consequence, the shoulder around 40 Hz in the power spectra of STA and LFP, found for the grating stimulus was also reduced. This shoulder vanished completely, when noise was added to the random dot pattern (Fig. 4-40, panel C to F). In addition, the peak at 15 Hz found in the averaged power spectrum of the LFPs got shifted to lower frequencies. The same attenuation of high frequency components was found in the correlograms

**Figure 4-40: Dataset for the SFC analysis in area PMLS**

The layout for this figure is the same as for Fig. 4-37. The SFC value was calculated by dividing the power spectrum of the STA by the averaged power of the LFP.



and the STA. Only a broad center peak remained. At 100% noise (Fig. 4-40, panel F), all high frequency components vanished and only low frequency oscillations remained in the correlogram and the STA. The SFC values change to 0.028 for the alpha and 0.0002 for the gamma frequency range.

For a quantitative analysis data were averaged over all recording sites (Fig. 4-41 and 4-42). The figures give SFC values as a function of stimulus condition. SFC values integrated over the gamma frequency band (30 Hz to 70 Hz) are shown in red, data for the alpha band are shown in blue (6 Hz to 18 Hz). In order to be included into the analysis, the difference in preferred direction of the multiunits for the LFP signal and for the spike signal had to be less than  $30^\circ$ . The preferred directions were determined by the tuning curve experiment described in section 4.2. Please note the different scales for the gamma and alpha frequency range in Fig. 4-41.

ANOVA revealed significant changes in the spike-field coherence values for the gamma band plotted in Fig. 4-41 ( $F(7, 641) = 9.77, p < 0.0001$ ). The spike data and the LFP were recorded from the same electrode (auto-SFC). Responses elicited by the grating stimulus showed the strongest coupling. When stimulating with a noise free random dot pattern, this mean value of  $0.01 \pm 0.002$  was significantly reduced to  $0.007 \pm 0.001$  ( $CD = 0.002, p < 0.0001$ ). The introduction of noise to the stimulus led to a monotonic decrease in the SFC between spikes and LFP in the gamma frequency band. However, the SFC values for all random dot patterns remain in the range of  $0.006 \pm 0.001$  regardless of their noise level. Consequently, none of these changes turned out to be statistically significant ( $CD$  always 0.002,  $p$  always above 0.25).

In contrast to the weak coupling between spikes and high frequency components of the LFP, the coupling turned out to be much stronger for alpha frequencies (ANOVA,  $F(7,641)=5.26, p < 0.0001$ ). The lowest SFC was found for the noise free random dot pattern. The mean value for this stimulus was  $0.012 \pm 0.002$ , a non significant difference to the grating stimulus with a mean of  $0.018 \pm 0.0005$  ( $CD = 0.007, p = 0.121$ ). Introducing noise led to a monotonic increase in

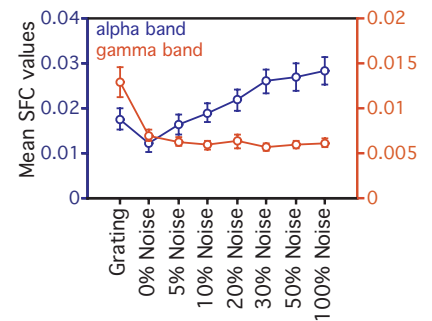


**Figure 4-41: Auto-SFC values in PMLS**

The figure gives SFC values as a function of stimulus condition. LFP and spike signals were obtained from the same electrode. SFC values for the gamma frequency band are shown in red, data for the alpha band are shown in blue. Please note the different scales for the gamma and alpha frequency range. Error bars denote  $\pm$  one standard error of the mean.

the coupling. However, a noise level of 20% was necessary to get statistically significant differences in SFC values relative to the noise free random dot pattern (mean  $0.022 \pm 0.002$ ,  $CD = 0.007$ ,  $p = 0.006$ ). Further significant differences were found between 5% and more than 30% noise ( $CD$  always 0.002,  $p$  always less than 0.007) and between 10% and noise levels of 30% and more ( $CD$  always 0.002,  $p$  always less than 0.049). Pairwise differences in SFC values between stimuli with more than 30% noise were not statistically distinguishable.

Fig 4-42 shows spike field coherence data, where LFP and spike signals were recorded from different electrodes (cross-SFC) (ANOVA,  $F(7, 810)=5.72$  for gamma frequencies,  $F(7, 810)=6.63$  for alpha frequencies, both  $p < 0.0001$ ). SFC values are given as a function of stimulus coherence. The same inclusion criteria as for the auto-SCF data applied. For the high frequency band, the coupling between LFP and spikes decreases from  $0.004 \pm 0.001$  for the grating to  $0.002 \pm 0.0003$  for the random dot stimulus. This reduction is statistically significant ( $CD = 0.001$ ,  $p < 0.0001$ ). However, the introduction of visual noise to the random dot pattern did not lead to further significant changes in SFC values. The means remain at  $0.002 \pm 0.0002$  for all levels of decoherence (Fisher's PLSD,  $CD = 0.001$ ,  $p$  always above 0.12).

For the alpha frequency range, lowest coupling between spikes and LFP was found for the random dot pattern. The mean value of  $0.007 \pm 0.001$  was significantly different from the value for the grating stimulus (mean  $0.012 \pm 0.001$ ,  $CD = 0.001$ ,  $p = 0.012$ ). An increase in decoherence led to a significant increase in SFC values from  $0.007 \pm 0.001$  for the noise free dot pattern to  $0.012 \pm 0.0001$  for the 10% noise level ( $CD = 0.001$ ,  $p = 0.004$ ). Whereas doubling noise to 20% does not change the SFC values, 30% noise led again to a non significant increase in the coupling to  $0.016 \pm 0.0002$  ( $CD = 0.001$ ,  $p = 0.076$ ). Significant differences were found only between 20% and 50% noise ( $CD = 0.001$ ,  $p = 0.042$ ). The remaining stimuli with more

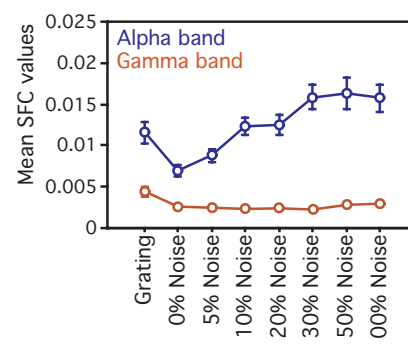


**Figure 4-42: Cross-SFC values in PMLS**

The figure gives cross-SFC values as a function of stimulus condition, where LFP and spike signals were obtained from two different electrode. SFC values for the gamma band are shown in red, data for the alpha band are shown in blue. Error bars denote  $\pm$  one standard error of the mean.

than 30% did not lead to significant changes in the coupling between LFPs and the spike signal (mean values of  $0.016 \pm 0.0002$  for 30% noise and  $0.016 \pm 0.0003$  for 100% noise).

#### 4.6.3. Discussion

The data showed that the coupling strength between unit data and LFP depends on the coherence of a visual stimulus. Whereas grating stimuli showed a strong coupling to high frequency components between 35 and 70 Hz, i.e., high SFC values, random dot stimuli showed a shift towards low frequency coupling. This shift increased with decreasing stimulus coherence when visual noise was added to the random dot pattern.

The SFC data for area 17 were in good agreement with the results from the preceding section. The SFC values resembled nicely the decrease and increase of high and low frequencies found in the LFP upon an increase in stimulus coherence. This dependence on stimulus noise was found in both auto- and cross-SFC indicating that spikes are coupled to alpha and gamma frequency components over smaller and larger cortical distances. However, the absolute values in the cross-SFC were lower showing that the coupling was not uniformly distributed over the whole cortical area but decreased with the distance between electrodes as it has also been shown for synchronization of spikes [42]. The results found were also in agreement with the correlation analysis described in section 4.4. The broadening of the center peak in the correlograms was accompanied by a transition in the spike coupling from high to low LFP frequencies. These SFC data might be taken as further evidence for the role of alpha frequencies in the processing of distributed information. The response elicited by the locally defined grating showed a strong coupling to gamma frequencies whereas the response to the random dots was dominated by lower frequency coupling which increases with a decreasing coherence of the stimulus.

Whereas area 17 showed a dependence of coupling between spikes and LFP on stimulus coherence for low and high frequency components, area PMLS showed this type of dependence only for

the coupling to low frequencies. Coupling in the high frequency region did not change with the level of stimulus coherence. Gamma coupling only dropped between responses elicited by the grating and the noise free random dot pattern and stayed constant for all noise levels from 0% to 100%.

It cannot be ruled out that the weak gamma synchronization and also the weak gamma components in the LFP and consequently in the SFC might be due to anesthetics as it has also been observed in monkey area MT. Whereas awake animals show strong oscillation and synchronization in the high frequency range, anesthetized animals have a strong reduction in the occurrence of this oscillations and synchronization.

The weak coupling is further indication that different frequency ranges become important in the processing of locally distributed information. In contrast to the high frequencies coupling found for stimulation with a grating, the values for the alpha frequencies increase with decreasing stimulus coherence in both auto- and cross-SFC. They follow nicely the dependence of the LFP for different levels of stimulus decoherence. They show that the increase in alpha frequencies is a very robust finding in both the LFP and the unit data indicating that the assemblies involved in the processing become the larger the weaker the coherence of a stimulus.

The role of low frequency oscillations in the processing of locally distributed visual information is discussed in detail in the preceding two sections as well in the following discussion.

## 4.7 Summarizing Discussion

In the present study the influence of stimulus coherence on the processing of motion information in the visual system of the cat was investigated. Changes in firing rates, in synchrony as well as in the frequency distribution of the LFPs were explored. In addition, differences in tuning behavior were analyzed for gratings and random dot texture pattern.

The tuning-curve experiments in section 4.2.1 showed that multiunits in both areas 17 and PMLS were responsive to grating and random dot stimuli. This was in agreement with earlier studies [125, 14, 73] which also reported that the majority of cells in both areas responded to gratings and texture pattern. In addition, the present results showed that the response varied as a function of stimulus direction. The preferred directions for random dot and grating stimuli were comparable in both areas 17 and PMLS and the majority of multiunits showed differences of less than  $20^\circ$ . These findings are in general agreement with earlier studies that also showed that the preferred direction for the two stimuli did differ not more than  $20^\circ$  for area 17 [15] and  $30^\circ$  for area PMLS [73] for the majority of the cells. The smaller differences in area PMLS found in the present study were most likely due to different methods in calculating the preferred direction as has been discussed in section 4.2.3. The similarity in preferred directions points towards a similar mechanism in direction discrimination for gratings and random dots. Such a similar mechanism has already been proposed for area 17 by Skottun et al. [126]. However, due to the larger differences in preferred directions found in previous studies for area PMLS [73], different mechanisms have been proposed for this area. In contrast, the more accurate results in the present study are more in favor of one common instead of two different mechanisms. Further evidence for a similar mechanism comes from the fact, that the basic processing of directional selectivity is thought to be performed already at early stages of the visual system [121]. Consequently, directional selectivity in later stages of the visual pathway might be more a result of afferent input rather than from intrinsic cortical calculation. Hence, it

seems unlikely that two separate mechanisms for additional motion discrimination should exist in area PMLS whereas they are supposed to be the same in area 17. In addition, the strong correlation between the direction indices for grating and random dot pattern found in area PMLS are also in favor of a common mechanism for directional processing in this area.

The width of the tuning curves in the two areas 17 and PMLS was also investigated for the grating and the random dot stimulus. In contrast to the similarity in preferred direction, the tuning width for the two types of stimuli turned out to be different. For both areas, the random dot pattern elicited a broader tuning curve than the grating. This is most likely a result of differences in frequency space as has been discussed in detail in section 4.2.3.

Despite the difference in tuning width the analysis of tuning properties revealed that both types of stimuli had narrow enough tuning curves to calculate a preferred direction and that the differences in preferred directions were small enough to use the same direction of motion for both types of stimuli in subsequent experiments.

The dependence of firing rates on the coherence of the random dot pattern was then investigated. Both areas showed a decrease in rates with increasing levels of stimulus noise. However, for the two areas 17 and PMLS, different levels of stimulus noise were necessary to reduce rates. Whereas in area PMLS already the lowest noise level of 5% led to a decrease of firing rates, more than 20% noise were necessary to reduce firing rates in area 17. This is most likely due to different receptive field sizes. If the receptive field is sufficiently small for a given noise level, the probability for finding an incoherent dot inside this area becomes smaller one. Thus, the small fields in area 17 led to a „blindness“ to incoherent dots for low levels of noise and high stimulus decoherence was necessary to cause a reduction in firing rates as it was discussed in detail in section 4.3.3. Taking into account these differences in receptive field size, the two areas showed a similar decrease in firing rates with increasing stimulus coherence. In addition, this decrease was unaffected by the degree of direction-

al selectivity and by the width of the tuning curve. The present results provide further evidence that area PMLS is concerned with the analysis of spatially distributed visual information [110]. Whereas area 17 is working as a local detector for orientation and direction, area PMLS can provide additional information about stimulus features that can not be detected locally.

However, both areas seem not to be able to discriminate a direction of motion in a noisy pattern near threshold level based on differences in firing rates. It has been shown in psychophysical experiments that cats can discriminate a global motion within a dot pattern of 95% incoherence [98]. However, no significant differences in firing rates were detected for noise levels of more than 50% in both areas. Furthermore, motion in the null-direction did not show any significant changes in firing rates for area 17 and only between very high and the 0% noise in area PMLS. Therefore, differences in firing rates at high noise levels can not be used as a mechanism for reliable discrimination of a global motion direction within a noisy dot pattern. In contrast, a study by Newsome et al. reported that single neurons in area MT of the monkey were able to discriminate a global direction within a noise background and that the performance of single neurons will even exceed the psychophysical results of the animal. A reason for this discrepancy in the ability of neurons to signal a global direction within a noisy background between the two studies might lie in the fact that the present study was using anesthetized as opposed to awake animals. The discrimination of direction near threshold level however might require a conscious brain and might be an attentive mechanism which can not be carried out in anesthesia. This might be of special importance for area PMLS since higher areas in the visual hierarchy tend to be more sensitive to the effects of anaesthetics. This was already observed during the recordings where little changes in the animal's arousal state were accompanied by a disappearance of any stimulus driven response in this area. Similar observations have been reported for recordings in area MT of the monkey.

In addition to the decrease in firing rates changes in the temporal properties of the recorded signal were found with decreasing stimulus coherence. The results obtained from synchronization analysis of the unit data, power spectra of the LFP as well as coupling between spike signals and field potential all gave a consistent picture of decreasing power of high frequency components and increasing power of low frequency components with increasing levels of stimulus noise. In agreement with earlier studies, narrow synchronization peaks in the unit data in area 17 [42, 28, 31, 124] and PMLS [28] were found. In addition, area 17 cells showed high frequency oscillation in firing rates in the spike data for the grating stimulus which also resembled the findings of previous studies that reported oscillations in the unit data upon grating stimulation [63]. These high frequency oscillations were not found in area PMLS. High amounts of power in the high frequency region have also been found in the LFP for both area 17 and PMLS. This was more pronounced in area 17 than in area PMLS. Furthermore, spike-field coherence values showed a strong coupling between spike signal and LFP in the high frequency range indicating that the LFP and spike signal are correlated.

The coherent random dot pattern showed a broadening of the center peak in the correlograms for both areas examined. Adding stimulus noise led to a monotonic increase in the width of the peak. This increase in center peak width with increasing stimulus decoherence is in agreement with a study by Brecht et al. who also reported a decrease in the precision of synchrony with increasing stimulus coherence for cells in the superior colliculus of the cat. However, area PMLS showed the increase due to noise only when the correlograms were characterized by a narrow center peak upon stimulation with a grating. The strength of the synchronization, i.e. the ratio between correlated and uncorrelated spikes as measured by the RMA, was only little affected by different levels of stimulus coherence. In contrast to firing rates, the decrease in gamma-synchronization started at low noise levels for both areas 17 and PMLS.



This decrease in synchronization precision went along with a lack of high frequency oscillations in both areas that was found for area 17 upon grating stimulation.

So far, precise synchronous activity as well as high frequency oscillations have been proposed to act as a mechanism for feature binding for coherent objects (for review see [123]). The results of this study found for the grating stimulus are in line with this notion. They show that, in addition to binding coherent objects, synchronization can perform binding also for objects in an incoherent stimulus based on the Gestalt criterion of “Common Fate”. Further more, the present results show a further example where, in the earlier visual areas, synchronization provides additional information to that gained from firing rates. Whereas firing rates elicited in a multiunit in area 17 does not seem to be able to signal a weak level of decoherence, synchronization can achieve this by binding the information belonging to the same ensemble of dots that is globally and inhomogeneously distributed. Synchronization therefore not only plays an important role in integrating coherent visual information in order to perform object binding but is also important for the analysis of non-coherent patterns that are distributed over a wider visual space. A largely different result was found for area PMLS. Whereas firing rates reliably signal small changes in stimulus coherence, changes in synchronization are significant only for large differences in noise level.

A similar decrease in high frequency components with increasing levels of stimulus noise was also found in the power spectrum of the LFP. Here, a decrease in stimulus coherence caused a decrease in spectral power contained in the frequency range between 30 Hz and 70 Hz. This decrease was more pronounced in area 17 than in PMLS. In addition, the coupling between spikes and LFP frequencies, as measured by the spike field coherence, decreased with increasing stimulus noise. This however was only true for area 17. SFC values for area PMLS stayed constant regardless of the level of noise contained in the random dot pattern. As discussed in section 4.6.3 the low SFC values could either be due to a decoupling of spikes and

high LFP frequencies or could be representing high frequency noise contained in the LFP. This finding can be taken as further evidence that synchronization on the earlier stages in the visual cortex is translated into a more rate based code at subsequent stages of the visual hierarchy. However, it can not be ruled out that the increasing effects of anesthesia in higher areas of the visual system were responsible for the decrease in precise synchronization found in area PMLS as opposed to area 17. This has been discussed in more detail in the discussion to the respective section.

A further important result in this study was the strong increase in low frequency components in the LFP power spectrum of area PMLS. For noise levels of more than 5% a prominent alpha oscillation built up. This oscillation did not change in frequency and neither did the amplitude of this oscillation relative to the center peak decrease with increasing noise levels. In addition, the power spectrum of the LFP showed a strong increase in the low frequency region upon stimulation with incoherent stimuli. Furthermore, coupling between spikes and these low frequency components increased with increasing levels of stimulus incoherence. The increase in low frequency components in the LFP was also found for area 17 but no alpha oscillations were visible in the unit data.

It might be speculated that the occurrence of these low frequency components in both unit and LFP data is important for the integration of distributed information in area PMLS and that low frequency oscillation might be a mechanism to allow integration over a wider area of visual space than could be achieved by gamma oscillations alone. This high frequency synchronization seems to be a mechanism to perform small scale integration of spacially distributed objects as pointed out in the preceding paragraphs (e.g. [55]). Integration over even wider visual areas might be mediated by this decrease in frequency. It has been shown in a slice preparation that the spread of cortical excitation depends on the application frequency [18]. Whereas fast repetitive inputs led to a locally restrained excitation, low frequency input led to a spread over a wider area.

Electrophysiological studies *in vivo* have shown that low frequency oscillations can stay synchronized over a larger cortical distance [13, 55].

The decrease in synchronization precision in the spike data of the primary visual area is already an indication for the frequency adaptation for the task in question. Whereas the grating can be analyzed locally, the random dot pattern is a more global stimulus so that information at one point in the visual field is not enough to extract the motion of the dot assembly. Due to the proposed larger spatial integration properties in area PMLS [110], the decrease in frequency is even more pronounced than in area 17. Further arguments came from fMRI studies [101]. They suggested that increasing decoherence will lead to an activation of more neurons but at a lower rate as compared to a coherent stimulus. This larger number of neurons could be integrated by means of low frequency oscillations.

Some authors have attributed the slow alpha rhythm to top-down processes [134] as well as to a mechanism to establish intra-areal connections over longer cortical distances [133]. They claim that whereas fast gamma frequencies are important for the processing of bottom-up and novel stimuli, low frequency components are more important for mediating the flow of top-down information. This has been discussed in detail in section 4.4.3.

On the other hand, it cannot be ruled out that the increase in low frequency components is due to anaesthetic effects. Only the grating stimulus as a strong repetitive pattern might be able to sufficiently stimulate the visual system. A random dot pattern, especially with decreasing stimulus coherence, might be too weak to be analyzed by the non-attentive animal and would require an attentional mechanism. As a consequence, the low frequency components might have (i) only small physiological meaning and might be (ii) more originating in the thalamus [69]. This is in line with results by Brecht et al. [10] who reported that low frequency oscillation occurred more frequently in the anesthetized than in the awake animal. In addition, area PMLS receives its input predominantly from the Y system whereas area 17 and 18 receive their input from the X-system. These

two pathways might be differently influenced by anesthesia thus leading to the stronger synchronization in area 17 compared to area PMLS.

However, the strong coupling between spikes and low frequencies for increasing amounts of noise are in favor of a more functional role of these low frequency components. For a purely anaesthetic effect, increasing coupling between thalamically originating oscillations and cortically generated spikes seems unlikely, unless the spikes are initiated by the thalamic oscillations. Since area PMLS does not receive strong mono-synaptic input from the thalamus, the coupling of cortically generated spikes and these low frequency oscillations should decrease with increasing noise. The fact that the slow oscillations found in the present experiments are more and more coupled to spikes as the noise level increases speaks against a purely anaesthetics effect (see section 4.6.3). In addition, the monotonic increase of low frequency components and the fact that the noise free random dot pattern does not lead to strong alpha oscillations and alpha components in the LFP are further arguments pointing towards an integrative function as described above and in the discussions for the respective chapters. Nevertheless, at least some influence of the anesthetics can not be ruled out for these experiments.

## 4.8 Conclusions

The present study shows that multiunits in both areas 17 and PMLS show a comparable preferred direction for grating and random dot stimuli. In the case of area PMLS, the differences in the directions between the two stimuli turned out to be smaller than previously reported. These small differences point towards a common neural mechanism for direction discrimination in both areas. It was further shown that firing rates in area 17 and PMLS decreased with increasing levels of stimulus coherence. For area 17, this decrease started at noise levels of more than 20%. However, taking into account the differences in receptive field size for the two areas a similar decrease in firing rates for area 17 and PMLS was found. This decrease was independent of directional selectivity and the width of the tuning curve of the respective multiunit.

In addition to a decrease in firing rates, the data revealed a decrease in the synchronization precision in both areas. This decrease in area 17 started already at very low noise levels. Hence, synchronization in area 17 gives additional information that can not be obtained from measuring firing rates alone. The opposite holds for the hierarchically higher area PMLS. In this area firing rates are more sensitive to small changes in stimulus coherence than are changes in the synchronization precision.

Along with the decrease in synchrony goes an increase in low frequency oscillation in the unit data as well as in the LFP. From these results it can be proposed that this increase in the alpha frequency range might mediate an increase in the spatial and temporal integration properties of the cortex in order to deal with the analysis of a distributed visual object. Whereas gamma synchronization is important for attentive mechanisms and new stimuli, alpha oscillations might play an important role in the non attentive, large scale integration and processing of information.

However, neither changes in firing rates nor changes in synchronization seem to be able to reliably signal a global motion within a noisy random dot pattern, at least not in the anesthetized

## Chapter 4

animal. Near the discrimination threshold of 5% stimulus coherence, none of the measures showed changes that were significantly different from chance.

## **5.1 Introduction**

In many experiments concerned with the neurophysiological basis of vision rather simple visual stimuli, such as spots or luminance defined bars and gratings were used (e.g., [52, 41]). However, in order to better account for the rich visual environment in our natural world, more complex stimuli are needed. Many objects show a textured appearance and it is possible to distinguish objects of the same color or brightness based solely on their textural characteristics if they are sufficiently different. However, the presence of shadow- or surface-markings that generate clear luminance-defined boundaries does not always correspond to the boundaries of an object thus making object recognition often more difficult to perform. Differences in an object's motion direction or speed could help to overcome these difficulties since differential motion is an additional strong cue that helps to distinguish between different objects.

Motion information in general can provide a number of perceptually useful cues [78]. For instance, motion of a retinal image contains information about the self-motion of an animal throughout the world whereas motion parallax, i.e., objects at different distances are

moving with different speed, reveals the spatial layout of the environment. Motion contrast, i.e., different motion vectors for elements of a figure and elements of a background, can provide important additional cues utilized by the visual system for scene segmentation and for the reconstruction of the two- and three-dimensional structure of an object. Thus, the ability to detect kinetically defined object boundaries gives humans and animals an important additional piece of information about their environments.

When a subset of uniformly distributed dots, forming a two-dimensional object, suddenly starts moving within a uniform static assembly, the object formed by these dots becomes immediately visible and disappears as quickly when the dots stop moving. This shape-from-motion (SFM) object is solely defined by the motion vectors of its components. Psychophysical experiments have shown that humans can effectively resolve such motion-defined shapes [104, 105]. In fact, orientation discrimination can be performed equally well for edges that are either defined by luminance, by occlusion or by relative motion [113, 105]. Although the performance in orientation discrimination for all three cues is similar, the combination of more than one cue gives better results. A rotating cloud of dots with the appropriate distribution of motion vectors is also sufficient to perceive three-dimensional structure-from-motion objects and has frequently been used in psychophysical and fMRI studies [80, 100].

Despite all this psychophysical evidence, the cortical substrate underlying the detection of motion-defined boundaries as well as the area in the brain performing this task remains unclear. Positron Emission Tomography (PET) and fMRI studies have shown that an area in the right hemisphere of the human cortex, the *kinetic occipital region* (KO), responds better to kinetically defined edges than to luminance defined contours or uniformly moving random dot patterns [23, 94, 143]. Unfortunately, an analogue area in the monkey or cat brain is not yet known.



Several studies have addressed the processing of motion contrast in the monkey visual cortex. It has been shown that the motion area MT is not able to respond to boundaries defined by motion contrast but responds only to the motion of the components of a SFM stimulus [71]. A recent study, however, provided evidence that area MT of the monkey might be more important in this analysis than previously thought [8]. The authors found that firing rates of MT cells reliably signaled the perceived surface order of a bistable three-dimensional SFM stimulus, i.e., whether moving dots belong to the back or the front of the 3D object. In contrast to area MT cells, cells in higher processing areas, such as the *inferior temporal cortex* (IT), can signal shapes independently of size, position and type of the visual cue (luminance, kinetic, texture) [112, 114]. Although area IT is part of the ventral stream, it can detect kinetically defined shapes, indicating a high degree of convergence of information from the dorsal to ventral visual areas [114].

Because the information about kinetically defined contours is available and utilized in these higher visual areas of the monkey, the question remains, how and where this information is detected in the visual system. Lamme et al [64] proposed that processing of contours of SFM objects occurs as early as in the primary visual cortex. Similar results have been reported by Leventhal who showed that cue invariant selectivity for kinetic boundaries appears early in the visual system of the monkey (V1 and V2) and may represent a rather basic aspect of vision [66]. In addition, studies by Marcar et al. [72] have shown that cells in area V2 of the monkey are able to detect the orientation of kinetically defined boundaries. However, due to large differences in response latency between kinetically and luminance defined boundaries in V2 the authors concluded that this area is most likely not the area that performs the processing of edge detection but that this information is fed back from another, higher visual area.

Marcar et al. [72] propose two possible mechanisms for the detection of static kinetic boundaries in the monkey: (i) Motion information originates in areas of the dorsal stream and is fed into the

ventral stream where it is combined with the information about the luminance and color boundaries of the object. The combined information then travels to higher order areas such as IT. (ii) The initial processing of kinetic edges already takes place early in the visual system, i.e., in areas V1 or V2. In this second mechanism, there is no need for an additional involvement of the dorsal areas in the processing of kinetic edges.

In the cat, little evidence is available regarding the cortical processing of shapes defined by motion contrast. The goal of this study was, hence, to test the effects of such stimuli on neural responses in cat area PMLS. As already pointed out in section 2.3, area PMLS is part of the dorsal, or “Where” pathway of the visual system. Cells in this area have rather large receptive fields, are highly selective to moving stimuli, show a distinct directional and speed selectivity and have a preference for high temporal frequencies [96, 129, 45, 73]. Several studies [97, 110, 67] have provided convincing evidence that area PMLS in the cat is involved in the analysis of direction and speed of retinal image motion. In addition, this area shows a strongly selective response to relative motion [45], a strong bias for preferred directions away from the area centralis [103] and a sensitivity to properties of object movement in three dimensional space [140]. Therefore, it seems reasonable to suspect that area PMLS might be important in the processing of SFM stimuli.

Psychophysical experiments by Rudolph and Pasternak [110] revealed that lesions in the lateral suprasylvian (LS) cortex, which includes area PMLS, indeed lead to a strong reduction in the abilities of cats to perceive SFM stimuli. In their experiment they used a rotating three-dimensional cylinder as visual stimulus. These findings demonstrate that LS cortex plays an important role in the processing of stimuli requiring integration of motion information and is necessary either for the detection of component motion in SFM stimuli or for the recognition of the SFM stimulus itself.

The experiments in this section were designed to answer the question, whether cells in area PMLS are able to perceive the SFM bars as an object or if they were only capable of detecting their component motion, i.e., the movement of the dots making the SFM bar.

Stimuli consisting of random dot texture patterns were used to study the mechanism underlying the detection of motion contrast cues in the visual system of the cat. The stimuli are described in detail in section 3.3.3. A bar composed of dots was moving over either a blank or a random dot background. When the bar was moving over of a random dot background, it was only visible due to its self-motion. Chapter 4 as well as several other studies have demonstrated that area PMLS of the cat is sufficiently driven by texture stimuli consisting of random dot patterns (see for instance [47, 48, 15, 73]). In addition, texture patterns can have indirect influence on firing rates by modulating the response to conventional stimuli, e.g. gratings, when presented as a surrounding background pattern [45]. This influence can either be suppressive or facilitating. This influence of various backgrounds on firing rates elicited by these SFM bars was also investigated.

## 5.2 Results

### 5.2.1. Shape-From-Motion Tuning Curve

In this section the hypothesis that cells in area PMLS can analyze the direction of motion of a contour defined solely by relative motion will be tested. The stimulus was a SFM bar defined by a group of moving dots. If cells in area PMLS can analyze the movement of the contour of this shape, the direction of movement of the dots defining the SFM bar relative to the contour of the shape should not make any difference for the analysis of the motion direction, as long as the shape itself can be perceived as such. The direction of motion detected by cells in area PMLS should always be the direction of motion of the contour of the shape.

In order to test this hypothesis, a stimulus consisting of a bar that was defined by the movement of dots was used. The bar moved across the screen with a velocity of 10 degrees per second. To investigate whether the direction of the contour or the direction of the dots was detected by cells in area PMLS, two different sets of stimuli were presented in which the bar was defined by dots moving into different directions relative to the contour of the shape. The direction of movement for the object itself, however, was kept constant. In one condition, the dots were moving into the same direction as the shape, in the other condition, the dots were moving 90° counter-clockwise to the direction of motion of the contour. The latter resulted in an effective dot movement of 45° relative to the shape due to the movement of both, shape and dots. At each recording site, both stimuli were presented moving into eight different directions for the shape similar to the tuning curve experiments in section 3.3.1.

The bar moved over a static background consisting of non-moving dots with a diameter of 0.2 degrees. Firing rates were measured for each stimulus presentation. Each measurement took a total of 7 seconds. During the first 1000 ms, spontaneous activity was recorded followed by one second of presentation of the static background alone. The bar then moved over the screen for three seconds. Following the bar presentation, one second of background stimulation alone and one second of spontaneous activity were recorded. The stimulus was positioned such that it was centered over the receptive field of the cell.

Fig. 5-1 shows an example of a PMLS multiunit response elicited by this SFM tuning curve stimulus with the two different SFM stimuli moving into eight different directions over a static dot background. The left column shows PSTHs evoked by the SFM bar that was defined by dots moving into the same direction as the shape itself. In this stimulus condition, global and local direction of motion, i.e., motion of the SFM bar and the dot motion inside the bar, were the same. Each row gives the response to one direction of motion from 0° to 315° in steps of 45° as a function of time. The stimuli are sketched to the left of the column. Small arrows give the absolute di-

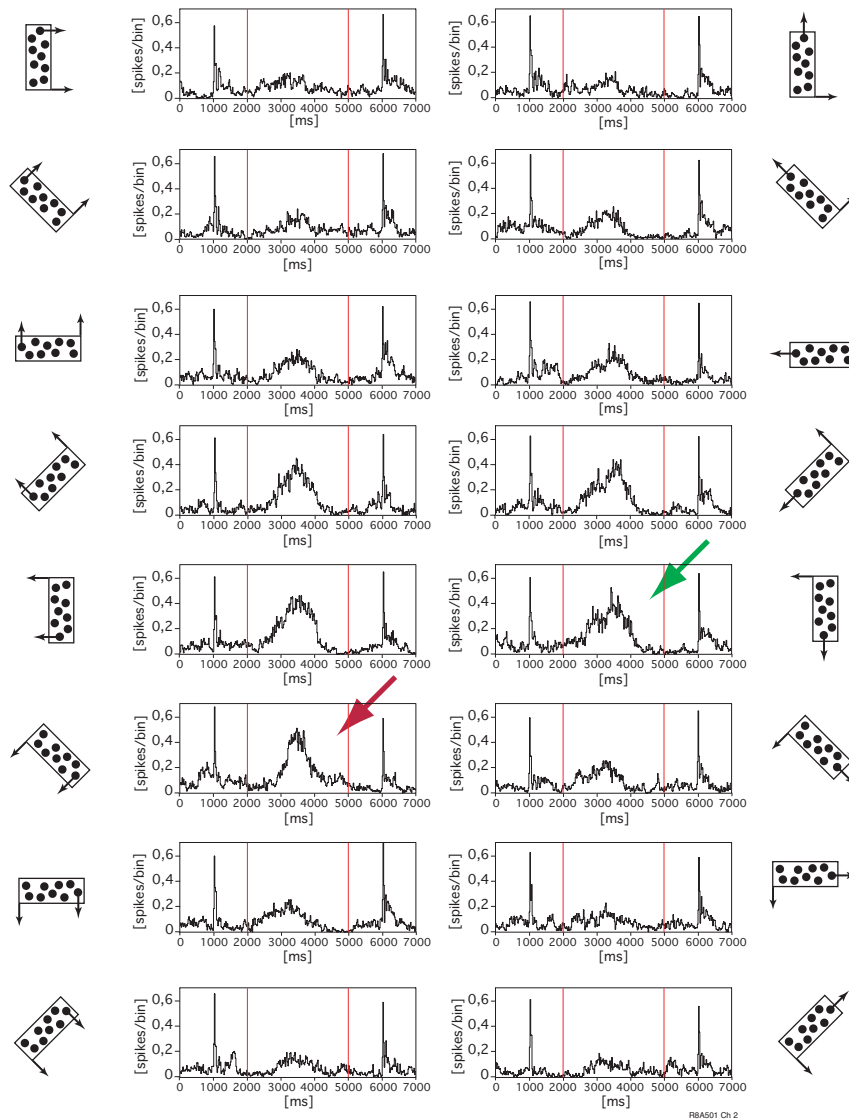


**Figure 5-1: Example of a SFM tuning curve in area PMLS**

The figure shows PSTHs for the SFM tuning curve stimulus. The left column shows responses elicited by a SFM bar where dots and shape were moving into the same direction. The right column shows responses elicited by a SFM bar with dots moving  $90^\circ$  off the direction of the shape. Time in milliseconds is plotted against spikes per time bin. Red lines indicate the beginning and the end of stimulus presentation, respectively. The red and green arrow mark the stimulus direction that elicited the strongest response. Little drawing at each side of the PSTHs show the respective stimulus.

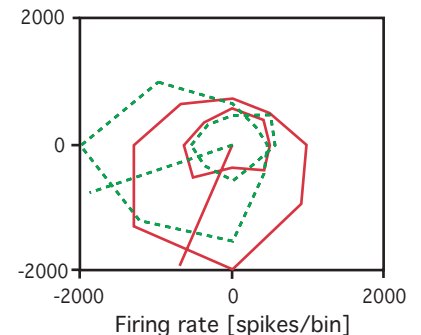
rection of motion of shape and dots, respectively. In the PSTHs, red lines at 2000 ms and 5000 ms indicate the start and end of the bar movement. Strong On- and Off-responses at 1000 ms and 6000 ms were evoked by the appearance and disappearance of the static background, respectively.

The PSTHs showed the typical response pattern of a strongly directionally tuned cell with a fairly broad tuning curve. Highest firing rates were elicited by the stimulus moving in a direction around  $225^\circ$  (red arrow). Adjacent directions at  $180^\circ$  and  $270^\circ$  showed weaker firing rates whereas stimulation in the null direction of this multiunit ( $45^\circ$ ) showed almost no increase in firing rate above spontaneous activity. The calculated preferred direction of this multiunit was  $250^\circ$  (see section 3.4.1 for details on the algorithm).

The second column in Fig. 5-1 shows the firing rates elicited by the SFM tuning curve stimulus consisting of SFM bars, where the dots were moving  $90^\circ$  off the direction of movement of the contour, i.e., the global motion was different from the local motion. Red vertical lines mark the appearance and disappearance of this bar. Drawings on the right side of the column show a picture of the respective stimulus condition. The PSTHs looked similar to the condition where dots and shapes were moving into the same direction as described above, showing the same pattern of a strongly directional cell. However, the maximum firing rate was now elicited by the SFM bar moving into a direction of  $180^\circ$  (green arrow) and was turned  $45^\circ$  compared to the condition in which dots and bars were moving into the same direction. Adjacent stimulus directions showed smaller firing rates and stimulation into the null direction of the cells led to almost no response upon stimulation with the SFM bar. The calculated preferred direction for this cell was  $201^\circ$ , showing a difference of  $49^\circ$  compared to the SFM bar with shape and dots moving into the same direction.

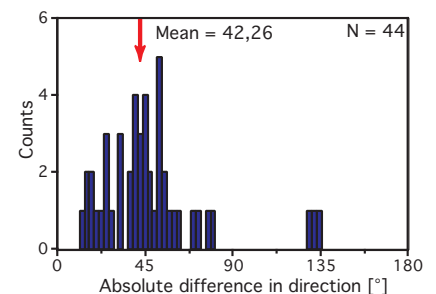
The corresponding polar plots for the two bars are shown in Fig. 5-2. The red polygon shows firing rates as a function of stimulus direction for the condition in which shape and dots were moving into the same direction. The green polygon represents the condition with bar and dots moving with a relative angle of  $45^\circ$ . The resulting polar plot was rotated approximately  $45^\circ$  relative to the previous condition. The straight red and green line indicate the calculated preferred direction of  $250^\circ$  and  $201^\circ$ , respectively. The little polygons drawn in the center of the graph represent spontaneous activity recorded from 0 ms to 1000 ms.

Fig. 5-3 shows the distribution of differences between the two types of SFM bars. Multiunits had to show a direction index of at least 0.1 for the SFM stimulus with dots and shape moving into the same direction in order to be included into the analysis. 47 out of 97 multiunits (48%) fulfilled this criterion. From this sample, cells with an absolute difference of more than the mean plus two times the standard deviation were excluded (3 cells). For the remaining 44



**Figure 5-2: Polar plot for the example shown in Fig. 5-1.**

The figure shows superimposed the two tuning curves as a polar plot representation. The red curve corresponds to the left column of Fig. 5-1, i.e. dots and shape moving into the same direction. The green curve shows the polar plot for the PSTHs shown in the right column in Fig. 5-1, i.e., dots moving  $90^\circ$  off the direction of the shape. Straight lines give the two preferred directions, the small polygons in the center represent spontaneous activity.



**Figure 5-3: Histogram of difference in preferred direction**

The histogram plots the absolute differences in preferred direction for the two different SFM tuning curve stimuli. The red arrow marks the mean of the distribution at  $42.26^\circ$ .

multiunits, the mean of the distribution was at  $42,258 \pm 2,547^\circ$ . This value is marked by a red arrow in Fig. 5-3. A one sample paired t-test showed a highly significant difference between the preferred direction of the two stimulus conditions ( $t(43) = 16.54$ ,  $p < 0.0001$ ).

The rotation of the tuning curve of  $42^\circ$  showed that cells in area PMLS are not able to signal the motion of the contour of the SFM bar. They can only signal the component motion which changed by  $45^\circ$  between the two types of stimuli used in this section.

### 5.2.2. Processing of Contours in Shape-From-Motion Stimuli

The large set of SFM stimuli has been divided into five groups: i) SFM bars on a static random dot background (Fig. 5-4 and 5-5), ii) SFM bars on a random dot background moving into the null direction of the cell (Fig. 5-6 and 5-7), iii) SFM bars on a background partially masked by a black square (Fig. 5-8 and 5-9), iv) SFM bars on a background containing visual noise (Fig. 5-10 and 5-11) and v) SFM bars on a background moving into other than the preferred direction (Fig. 5-12 to 5-15).

The examples given below for each group show neural responses of a multiunit in area PMLS elicited by the different SFM stimuli. The graphs show spiking probability per unit time as a function of time. Little drawings to the right of each PSTH show a sketch of the respective stimulus. The different stimulus conditions were described in detail in section 3.3.3. For all conditions, the background appeared at 1000 ms after the start of the recording. After 2000 ms, the SFM bar was shown and moved over the screen for 3000 ms. The background disappeared after 6000 ms of the recording time. Spontaneous activity was recorded from 0 ms to 1000 ms and from 6000 ms to 7000 ms, respectively. The bars were always moving into the preferred direction of the cell which was determined by the tuning curve experiment described in section 4.2.

The averaged responses per unit time for the different sets of stimulus conditions are shown in Figs. 5-5, 5-7, 5-9, 5-11, 5-14 and 5-15. For each stimulus condition, the average firing rate per unit time elicited by the background pattern was subtracted from the average

firing rate per unit time elicited by the bar moving over the receptive field. The time window in which data were averaged for the SFM bar was visually determined by the start and end of the response elicited by the solid contrast bar moving over a blank screen (Fig. 5-4, Panel A). Background activity was averaged between 1000 ms and 2000 ms for each stimulus. To be included into the quantitative analysis, multiunits had to show a direction index of at least 0.1 (see section 4.2 for details). In addition, tuning curves were visually inspected and only multiunits with a narrow tuning curve were chosen. 37 out of 187 multiunits (20%) fulfilled these criteria. All statistics were performed using Fischer's PLSD.

#### *Effects of static random dot backgrounds on firing rates*

Panel A in Fig. 5-4 shows an example response of a solid bar defined solely by luminance contrast (contrast bar). This stimulus was used as a reference to ensure the visual responsiveness of the multiunits and to determine the time window for subsequent stimuli. A strong response was evoked when the bar entered the receptive field and quickly vanished when the bar left the responsive area. In this example, the window, in which the stimulus was moving over the receptive field, was chosen from 2800 ms to 4500 ms. Firing rates elicited by SFM bars in consecutive conditions were summed over this time window. To investigate the effect of different backgrounds on cell responses, the following two panels added random dot backgrounds to the solid bar stimulus. While a static background alone (Fig. 5-4, B, 1000 to 2000 ms) elicited no response in the multiunit, the response strength of a solid bar moving over this background was comparable to the response evoked by a contrast bar alone (Fig. 5-4, A). However, firing rates increased more rapidly and decayed faster to the level of spontaneous activity as compared to the previous stimulus. Panel C shows the response to a contrast bar moving over a random dot background that was moving into a direction opposite to the direction of the bar (i.e., null direction). Because multiunits never have a direction index of one and, therefore, always show some response into the null direction, the background motion led to slightly increased firing rates. Nevertheless, rates increased,

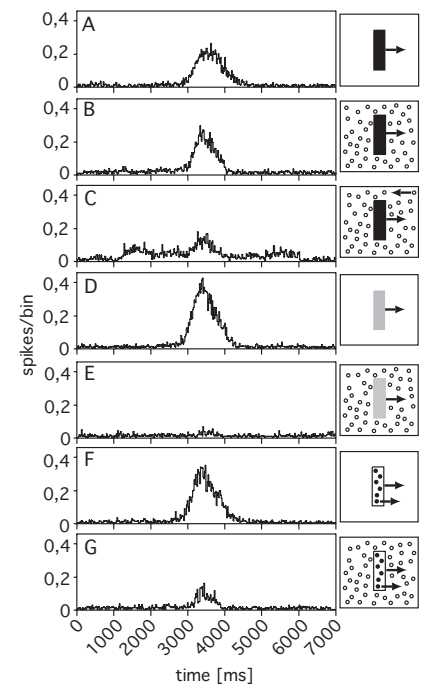


**Figure 5-4: Example for the first set of SFM stimuli**

PSTHs for different stimulus bars moving over different backgrounds. Time in milliseconds is plotted against spikes per bin. The pictures to the right of each PSTH give a sketch of the respective stimulus. Bars in all stimulus sets are moving into the preferred direction of the cell. **A** Contrast bar on a blank background; **B** contrast bar on a static random dot background; **C** contrast bar on a background moving into the null direction; **D** luminance adjusted bar on a blank background; **E** Luminance adjusted bar on a static random dot background. **F and G** The dots building the bar were moving into the preferred direction of the cells on a blank background (**F**) and on a static random dot background (**G**).



when the contrast bar entered the receptive field. However, the moving dot background had an inhibitory effect on firing rates which increased to less than half of the response elicited by the previous two stimuli.

To rule out the possibility that differences in firing rates between SFM bars and solid contrast bars were only due to differences in average luminance of the two stimuli, the luminance of the solid contrast bar was adjusted such that it matched the average luminance of the random dot pattern and the SFM bar (Panel D and E). This luminance-adjusted bar was presented on two different backgrounds. Whereas a blank background led to a strong response comparable to the response elicited by the high luminance contrast bar (5-4, D), firing rates almost decreased to the level of spontaneous activity when the bar was moving over the static random dot background. Panels F and G in figure 5-4 now show responses elicited by the SFM bar consisting of dots moving into the same direction as the dots of the shape. These bars were presented on a blank (F) and on a static random dot background (G). When the texture generated bar was moving over a blank screen, the response was comparable to the one elicited by a solid contrast bar moving over the same type of background (5-4, A). In contrast, a static random dot background led to a strong decrease in firing rates (5-4, G).

Fig. 5-5 shows the average firing rates for luminance defined solid contrast bars and the two SFM bars on different backgrounds (A to G). Insets at the bottom of each bar show sketches of the respective stimuli. 2-way ANOVA revealed significant differences within this set of stimuli (ANOVA,  $F(6, 246) = 5.521$ ,  $p < 0.0001$ ). The two leftmost bars in the figure (A and B) show the average firing rates elicited by a high contrast bar moving over a blank and a static random dot background, respectively. No significant differences between the two conditions were found ( $CD = 0.035$ ,  $p = 0.5876$ ). For condition C, the background was set into motion and was moving into the null-direction of the cell. This background motion led to a significant decrease in firing rates elicited by the contrast bar with respect to the previous two stimuli (all  $CD < 0.04$ , all  $p < 0.01$ ). Dif-

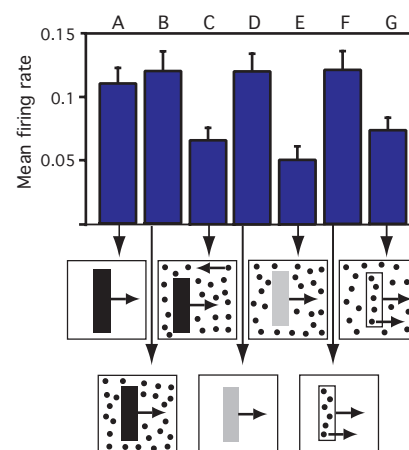


**Figure 5-5: Average response elicited by the first set of SFM stimuli**

Statistical analysis for the stimulus group shown in Fig. 5-4. The figure shows the average net firing rate for each stimulus. Error bars give  $\pm$  one standard error of the mean. Pictures below each bar give the respective stimulus.

ferences in luminance had only little effect on firing rates in the absence of a random dot background. When the luminance adjusted bar (D) moved over a blank screen, firing rates were not significantly different from those elicited by the high luminance contrast bar moving over the same type of background (B) ( $CD = 0.037$ ,  $p = 0.614$ ). However, when the bar moved over a static random dot pattern (Fig. 5-5, panel E), the reduction in luminance led to firing rates that were significantly reduced compared to the previous condition (D). They were also significantly smaller than those elicited by the high luminance contrast bar moving over a static background (B) (all  $CD < 0.036$ , all  $p < 0.0002$ ). Condition F and G in figure 5-5 show a random dot texture bar moving over a blank (F) and a static random dot background (G). The response elicited by movement over a blank screen was comparable to the response elicited by the two contrast bars with different luminance (A and D). These three stimulus conditions were not statistically different (all  $CD < 0.036$ ,  $p = 0.59$  when tested against condition A,  $p = 0.97$  when tested against condition D). When the random dot texture bar moved over a static random dot background (G) it was visible only due to its motion contrast and became a SFM bar. The response elicited by this stimulus decreased significantly compared to condition F ( $CD = 0.034$ ,  $p = 0.009$ ). This reduction in response strength of the SFM bar was also highly significant compared to the high luminance contrast bar moving over this type of background ( $CD = 0.034$ ,  $p = 0.008$ ). In contrast, the average firing rate elicited by the luminance adjusted contrast bar moving over the static background (E) was not significantly different to the SFM bar ( $CD = 0.035$ ,  $p = 0.2021$ ).

#### *Effects of moving RD backgrounds*

The second group of stimuli consisted of four SFM bars moving over random dot backgrounds with different directions of motion (Fig. 5-6). All bars were moving into the preferred direction of the multiunit. This group of stimuli was intended to look at the strength of the influence of a random dot background on SFM bars and the saliency of these stimuli compared to the contrast bar from the preceding section. A random dot background moving into the same di-

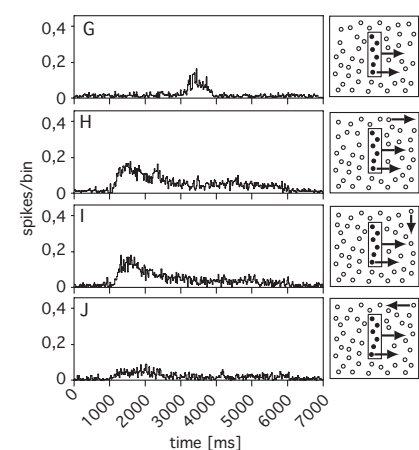


**Figure 5-6: Example for the second set of SFM stimuli**

PSTHs for different SFM bars moving over different backgrounds. The figure layout is as in figure 5-4. In this set, dots building the bar and the bar itself are moving into the preferred direction of the cells. **G** The dots building the bar were moving into the preferred direction of the cells over a static random dot background **H** SFM bar on a random dot background moving into the preferred direction; **I** SFM bar on a random dot background moving 270° off the preferred direction; **J** SFM bar on random dot background moving into the null direction.

rection as the SFM stimulus would render the bar invisible. Consequently, no changes in firing rates are expected when the bar is moving over the receptive field. This stimulus condition is shown in panel H of Fig. 5-6. The increase in response at 1000 ms which decreased during the next 2000 ms was due to the cells' responses to the moving background pattern. As predicted, the movement of the bar did not lead to an increase in firing rates relative to background activity as it has been found for the SFM bar moving over a static random dot pattern (Fig. 5-6, panel G). In stimulus I the direction of motion for the background pattern was changed. The dots were now moving perpendicular to the direction of motion of the SFM bar and thus perpendicular to the preferred direction of the multiunit. Therefore, this background motion should not elicit a strong neural response. However, due to the broad tuning properties of multiunits in area PMLS, an increase in firing rates between 1000 ms and 2000 ms was found. Although a bar moving over this type of random dot background is visible to the human observer, this multiunit in area PMLS seems not to be able to detect this stimulus. The SFM bar did not lead to an increase in firing rates when entering the receptive field at 2800 ms. An increase in neural response for the SFM bar was neither found when the background was moving into the null direction of the multiunit (5-6, panel J). Only the background elicited a response upon its appearance whereas no change in firing rates could be seen when the bar entered the receptive field.

Fig. 5-7 shows the average data for this second group of stimuli. Significant differences in firing rates between the stimuli were found (ANOVA,  $F(3,147) = 56.59$ ,  $p < 0.0001$ ). Presenting a SFM bar over a moving random dot background (H to J) always led to a reduction in firing rates relative to a movement over the static random dot pattern (G). P-values were always less than 0.0001 for background movement in the same (H), the orthogonal (I) and the opposite direction (J) when tested against the static background condition (G) ( $CD < 0.02$ ). Between these three stimuli with different background direction, significant differences were found between condition H (background moving into the same direction as the

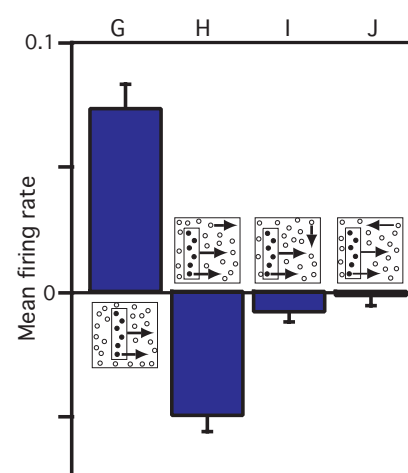


**Figure 5-7: Average response elicited by the second set of SFM stimuli**

Statistical analysis for the stimulus group shown in Fig. 5-6. The layout of the figure is as in Fig. 5-5.

SFM bar) and conditions I and J (background moving opposite and orthogonal to the bar direction, respectively) ( $CD < 0.020$ ,  $p$  always  $< 0.0001$ ). Negative net firing rate resulting from the in-phase movement of the background in condition H were responsible for these differences between condition H and condition I and J. Negative net firing rates were calculated, when the response elicited by the background pattern was larger than those elicited by the bar moving over the receptive field. In condition H, the large background rates were due to the strong non-stationary response of the background pattern moving into the preferred direction of the multiunits. Although the strong ON-response of the background was already excluded from the response, the average rate of the first 1000 ms of background movement subtracted from the firing rates elicited by the SFM bar nevertheless led to the negative net firing rates. Conditions with a background moving in the null direction (J) and orthogonal to the bar movement (I) were not significantly different ( $CD = 0.020$ ,  $p = 0.5445$ ).

#### *Effect of masking*

The next four stimuli (Fig. 5-8, panel K to N) were designed to investigate, how masking the background motion over the area of the receptive field changes firing rates elicited by the SFM bar. The question should be answered, if only a part of the receptive field, the entire receptive field or an area much bigger than the receptive field has to be masked in order to restore firing rates in area PMLS. In all four conditions, the background pattern was moving into the null-direction of the multiunit. The response of a SFM bar moving over this background is shown in panel J of Fig. 5-8. Two masks of different size were used. The mask used for the stimulus shown in panel K of Fig. 5-4 consisted of a black square area in the center of the receptive field that was much smaller than the receptive field size and had a side length equal to the width of the SFM bar. This black mask led to a slight increase in firing rates when the SFM bar moved over this area but response strength was still strongly reduced compared to the SFM stimulus moving over a blank screen. The larger mask (Fig. 5-8, Panel L) had a side length equal the length of the SFM bar

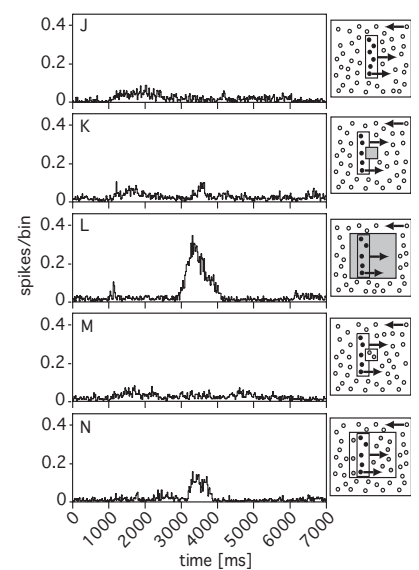


**Figure 5-8: Example for the third set of SFM stimuli**

PSTHs for different SFM bars moving over random dot backgrounds moving into the null direction of the multiunit. The layout is as in figure 5-4. Dots building the bar and the bar itself are again moving into the preferred direction of the cells. J SFM bar on random dot background moving into the null direction; K to N SFM bar moving over random dot background moving into the null direction. This background is covered with a small black mask (K), a large black mask (L), a small mask filled with static random dots (M) and a large mask with static dots (N).

and was covering an area approximately the size of the receptive field. This mask almost removed the inhibitory effect of the background motion and led to firing rates comparable to those elicited by the SFM bar without background. Panel M and N were similar to K and L except that the masking area in the center of the stimulus was now filled with static dots of the same size and density as used for bars and background. This led to a static random dot background inside the area. These masks were less efficient in restoring firing rates. Only the larger one covering an area approximately the size of the receptive field was hiding enough of the background pattern to restore firing rates when the SFM bar was moving over the receptive field. Firing rates were on the same order of magnitude as for the SFM bar moving over the static random dot pattern.

Fig. 5-9 shows the average effect of masking the background motion over the receptive field. 2-way ANOVA gave highly significant differences ( $F(3,142)=34.066$ ,  $p < 0.0001$ ). Conditions K and L show average firing rates for the condition in which the background moving into the null direction was overlaid by a black mask. A small masking window of a size equal to the width of the SFM bar led to a small increase in response when the bar was moving over the receptive field of the cell. This difference was not significant compared to the unmasked stimulus (J) ( $CD = 0.026$ ,  $p = 0.15$ ). Increasing the masking size so that it was equal to the length of the bar led to a strong increase in response strength which was highly significant with respect to the stimulus without a background mask (J) ( $CD = 0.026$ ,  $p < 0.0001$ ). This bigger mask brought the firing rates back to a response level that was not significantly different from the SFM bar moving over a blank screen (F) ( $CD = 0.027$ ,  $p = 0.0896$ ). Masking the moving random dot background with a static dot pattern instead of a black mask also led to a change in firing rates (M and N). Again, the smaller masking size did not have any significant effect on firing rates ( $CD = 0.027$ ,  $p = 0.53$  tested against condition J) whereas the bigger mask led to a significant increase in firing rates relative to the stimulus without background mask ( $CD = 0.027$ ,  $p < 0.0001$ ). Firing rates elicited by the stimulus moving over this bigger

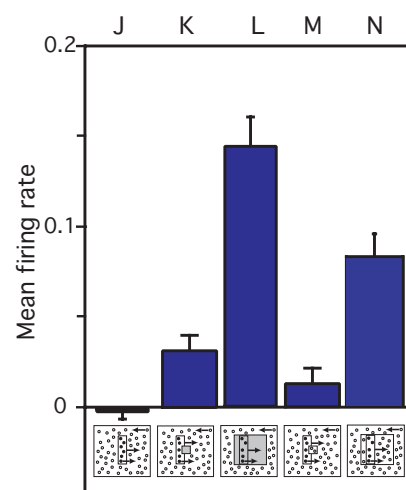


**Figure 5-9: Average response elicited by the third set of SFM stimuli**

Statistical analysis for the stimulus group shown in Fig. 5-8. The layout of the figure is as in Fig. 5-5.

mask were not significantly different from firing rates elicited by the SFM bar moving over a static random dot background (G) ( $CD = 0.027$ ,  $p = 0.7299$ ).

### *Effects of visual noise*

Experiments described in section 4.3 showed that visual noise introduced into a moving random dot stimulus leads to a decrease in the firing probability of multiunits. The three stimulus conditions O, P and Q in this section were designed to investigate the influence of visual noise on firing rates elicited by the SFM bar. Based on the results from section 4.3, a strong effect of visual noise was expected only for higher noise levels of 20% and more whereas noise of 5% to 20% should have rather little effects on firing rate in area PMLS. To test this prediction, 5%, 10% and 20% of noise were added to a static random dot background while the SFM bar was moving into the preferred direction of the multiunit. The type of noise was identical to the noise used in the experiments described in chapter 4 except that the dots that were not randomly repositioned did not move. For the human observer, the SFM bar was easily perceivable even at 20% stimulus noise. On the multiunit level, however, already a low level of five percent visual noise led to a total reduction of firing rates which did not increase above the level of spontaneous activity. The same held for higher noise levels of 10% and 20%. In this example, the 20% noise stimulus caused a little period of increased firing rate that could have been due to fluctuation in the spontaneous activity or due to chunking within the random dots of the SFM bar.

The average values for condition O to Q are given in Fig. 5-11. All three noise levels led to a total reduction of the response elicited by the SFM bar moving over the receptive field of the cell. Differences between the three noise levels were not significant (ANOVA,  $F(2,104) = 0.567$ ,  $p = 0.5688$ ).

### *SFM bar with different directions of dot motion*

So far, both the dots making up the SFM bar and the shape were moving into the preferred direction of the cell. To investigate whether cells in area PMLS are only able to analyze the component motion

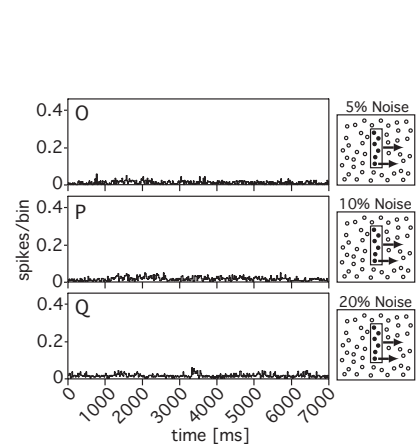


**Figure 5-10: Example for the fourth set of SFM stimuli**

PSTHs for different SFM bars moving over random dot backgrounds with different levels of stimulus noise. The layout is as in figure 5-4. Dots building the bars and the shapes of the SFM bars are moving into the preferred direction of the cell. The static random dot background contains 5% (O), 10% (P) and 20% (Q) static flicker onset noise.

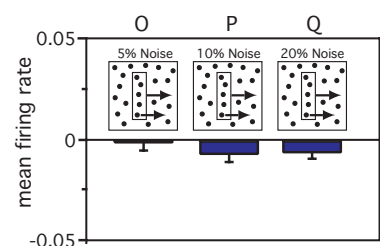


**Figure 5-11: Average response elicited by the fourth set of SFM stimuli**

Statistical analysis for the stimulus group shown in Fig. 5-10. The layout of the figure is as in Fig. 5-5.

or if they are able to detect the motion of the shape, dots building the SFM bar in this section were moving into directions that differed from the direction of the bar itself. Since the kinetically defined contour was still moving into the preferred direction of the multiunit, the different motion of the dots should not make any difference in the response of the cell if area PMLS is able to analyze kinetic boundaries.

In particular, in the stimulus shown in panel R of Fig. 5-12, dots were rotated 90° counterclockwise and moved orthogonal to the direction of the shape. Because of the motion of the bar itself, this led to an effective dot direction of 45° relative to the background. The response elicited by this stimulus was comparable to the response elicited by stimulus D, where dots and shape were moving in phase over a static random dot background. To correct for the self motion of the bar, the stimulus in panel S shows a SFM bar with dots moving 135° off the direction of motion of the shape resulting in an effective direction of 90°. When moving over a static background, this stimulus elicited a weaker neural response than the previous SFM bar with an effective dot motion of 45°. An even stronger reduction in firing rate was found when the dots building the SFM bar were moving opposite to the direction of the shape and thus moving into the null direction of the multiunit. The response to this stimulus moving over a static background is shown in Fig. 5-12, panel T. Only a weak increase is seen when the bar moved over the receptive field.

When the static dot background was replaced by a random dot pattern also moving perpendicular to the direction of the SFM bar but rotated 90° clockwise (e.g. bar 0°, background dots 270°), the response seen in the previous three stimulus conditions vanished (Fig. 5-13). Only background activity was visible in the PSTHs which was due to the broad tuning of the multiunits. No additional firing rates were elicited by the SFM bar moving over the receptive field regardless of whether the dots building the bar were moving in phase with the shape (Panel I), with a relative angle of 45° (panel U) or in the null direction of the multiunit (V).

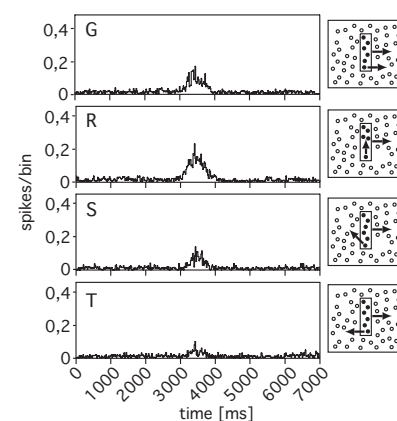


**Figure 5-12: Example for the fifth set of SFM stimuli**

PSTHs for different SFM bars moving over different static random dot backgrounds. The layout is as in figure 5-4. All bars in this stimulus set were moving into the preferred direction of the cell. **G** The dots building the bar were moving into the preferred direction of the cells over a static random dot background **R** The dots building the bar were moving 90° off the preferred direction; **S** The dots building the bar were moving 135° off the preferred direction. **T** dots building the bar are moving into the null direction.

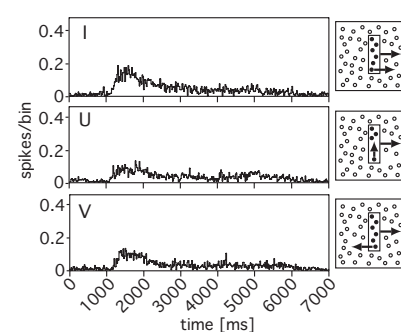


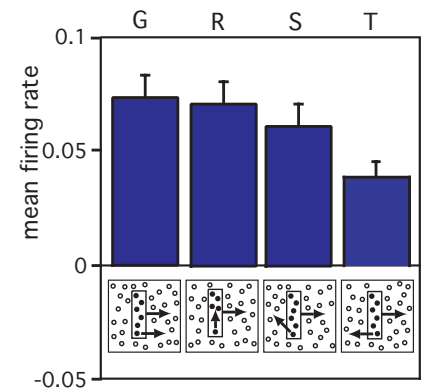
**Figure 5-13: Example for the sixth set of SFM stimuli**

PSTHs for different SFM bars moving over different backgrounds. The layout is as in figure 5-4. The SFM bar is moving into the preferred direction of the cell. **I** SFM bar on a random dot background moving 270° off the preferred direction; **U** same as R but with a background pattern that is moving 270° off the preferred direction of the cell; **V** same as T, but with a background moving 270° off the preferred direction of the cell.

The average data for this subset of SFM stimuli are shown in Fig. 5-14. A 2-way ANOVA showed significant differences between the four stimulus conditions ( $F(3, 136)=2,773$ ,  $p = 0.044$ ). The changing directions of the dots inside the bar led to a decrease in firing rates elicited by the SFM bar. Stimulus G shows again the SFM bar with dots and shape moving into the same direction. Stimulus R shows a SFM bar whose dots are moving orthogonal to the bar which led to an effective dot direction of  $45^\circ$  relative to the preferred direction of the multiunit. The response elicited by this stimulus was not significantly different from the response elicited by the SFM bar where dots and shape were moving into the same direction (G) ( $CD = 0.024$ ,  $p = 0.8276$ ). In condition S, the dots making up the bar are moving  $135^\circ$  relative to the direction of the shape, hence leading to an effective movement of  $90^\circ$  relative to the preferred direction of the multiunit. Although the average values were reduced, the firing rates elicited by this stimulus were also neither significantly different from the rates elicited by the stimulus with relative motion of  $45^\circ$  shown above (condition R) ( $CD = 0.026$ ,  $p = 0.1234$ ) nor from the stimulus where dots and shape are moving into the same direction (G) ( $CD = 0.026$ ,  $p = 0.0814$ ).

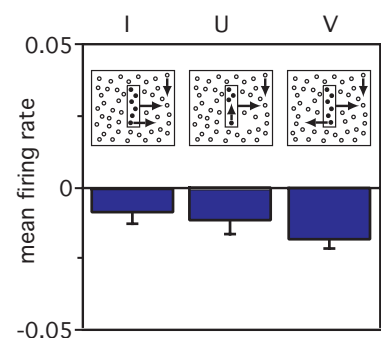
In stimulus T, the dots making up the bar were now moving into the opposite direction as the shape of the bar (null direction). Hence, the dots did not move relative to the screen and only the shape was moving over the static random dot background. This stimulus condition led to a further decrease in firing rates. Relative to condition G and R, this difference became significant ( $CD = 0.026$ ,  $p = 0.0169$  tested against condition G and  $p = 0.0285$  against condition R).

Fig. 5-15 shows the average responses elicited by the SFM bars moving over a random dot background that consisted of dots that were moving  $270^\circ$  relative to the direction of the bar movement. In condition I the dots inside the bar were moving into the same direction as the bar itself. In condition U these dots were moving  $90^\circ$  from the direction of movement of the shape whereas they were moving into the null direction in condition V. A 2-way ANOVA showed no



**Figure 5-14: Average response elicited by the fifth set of SFM stimuli**

Statistical analysis for the stimulus group shown in Fig. 5-12. The layout of the figure is as in Fig. 5-5.



**Figure 5-15: Average response elicited by the sixth set of SFM stimuli**

Statistical analysis for the stimulus group shown in Fig. 5-13. The layout of the figure is as in Fig. 5-5.



significant differences within this group of stimuli (ANOVA,  $F(2, 109) = 1.199$ ,  $p = 0.3054$ ). The negative net firing rates were again due to the background response as discussed for condition H.

### 5.3 Discussion

The results showed that multiunits in area PMLS did respond to both luminance defined contrast bars and SFM stimuli. The response strength depended on the combination of stimulus and background pattern and on the relative directions of motion between background and stimulus.

#### *Response strength without background*

Similar firing rates were found when the different stimulus bars moved over a blank background. Firing rates were the same for high and low luminance contrast bars as well as for the random dot bars. None of these responses were significantly different. Similar results have been reported for area MT in the anesthetized monkey [89]. In that study, short oriented line segments were used instead of dots. The study showed that the responses to a texture defined and a solid bar were comparable when presented on a blank screen.

The results provide further evidence that area PMLS serves as a primary motion area that responds reliably to the movement of a stimulus. The exact nature of a stimulus, e.g., contrast bar or assembly of small dots, seems to be less important. It further illustrates the integration property of this area as discussed in detail in the preceding chapter. Whereas a contrast bar is a spatially coherent stimulus with no discontinuities, the analysis of a random dot bar requires integration of a non-continuous signal over a wider space of the visual field. Since firing rates are independent of the type of stimulus, the different requirements on integration make no difference to the cells in this area PMLS. These results are in good agreement with the results from section 4.3 that firing rates elicited by the dot patterns did not decrease compared to a grating. Hence, the ability to integrate a

non-continuous stimulus such as a random dot bar makes area PMLS a good candidate for the processing of kinetically defined contours.

*Effects of static random dot backgrounds on firing rates*

The effect of a static random dot background on firing rates was tested for the different types of stimuli. The static dot pattern had the same dot density and average luminance as the random dot bars. The results showed that such background had no effect on firing rates elicited by a high luminance contrast bar moving over the receptive field. This finding is in agreement with results from a similar study in monkey area MT [89], which showed that adding a static texture surround to a moving solid contrast bar did also not reduce the response, compared to movement over a blank screen.

However, when the luminance of the contrast bar was adjusted such that it matched the average luminance of the random dot background, the static background pattern led to a reduction of firing rates by more than 50%. A decrease in firing rates was also found when the random dot bar moved over the static background, thus becoming a SFM bar. A reduction of about 75% was found. Similar results have been reported for area MT in the monkey [89], where response strength for a texture bar was reduced compared to a high contrast bar, both moving over a static background. The fact that the response elicited by the random dot bar moving over a blank screen was not reduced compared to the contrast bar showed that the decrease in response strength for the SFM bar moving over a static background was due to the background pattern and was not a result of the textured nature of the stimulus bar.

The present estimation of the suppressive effect of different backgrounds was based on the assumption that firing rates elicited by the foreground stimulus and the background add linearly. Since the contrast for the random dot bar and for the luminance-adjusted bar was rather low, it is valid to assume that saturation of cortical cells was avoided. Hence, the responses to the two stimuli most likely add in a linear way. However, it might be possible that the high

contrast bar saturated cells in area PMLS, which would result in a non-linear addition of rates, i.e., adding the response of the bar alone to the response of the dots alone will result in a higher firing rate than the response elicited by the combination of the two stimuli. This might lead to an overestimation of the suppression elicited by the background.

The neural process underlying the reduction in firing rates for the random dot bar moving over a static texture background remains unclear. One possibility is lateral inhibition. Lateral inhibition serves as a contrast enhancement mechanism at the edges of a visual stimulus. Compared to the high contrast bar, the low luminance contrast bar and the random dot bar might show less lateral inhibition when moving over a static random dot background. The effect would be more pronounced at the edges of a luminance defined bar than for a bar consisting of random dots that do not build a sharp border. When the stimuli are moving over a dark background, the strong luminance contrast might compensate for the less clearly defined edges of the random dot bar. This could lead to similar firing rates for these three types of bars. Another possibility is a mechanism similar to the filling-in mechanism of non-continuous figures, e.g. *Kanizsa* figures, that renders the random dot bar solid in area PMLS. This would explain comparable firing rates for the random dot bar and for the luminance-adjusted bar since the filling-in would lead to similar luminance for both stimuli. Hence, both bars would show comparable decreases in lateral inhibition when moving over a random dot background, which in turn would lead to a reduction of firing rates and would make it more difficult for the system to detect the moving bar.

#### *Effects of moving RD backgrounds*

In contrast to a static random dot background that did not affect the firing rates elicited by a high luminance contrast bar, a random dot background moving into the null direction of the multiunit led to a strong reduction of rates. This suppression was found for the majority of cells recorded in area PMLS.

Von Grünau et al. reported a strong inhibitory influence of a moving background on the response elicited by a moving stimulus for area PMLS cells [45]. In another study, strong suppressive influence of a moving texture background on the response elicited by a contrast bar in area 17 was reported [46]. The suppression increased with a decrease in contrast between the bar and the dot background. Moving texture background also exerts a powerful inhibitory influence on firing rates elicited by a moving bar in area 18 [93]. The background motion suppressed the responses of these cells. In addition, directional selectivity of cells in area 18 was modulated as it has also been reported for area 17 [46]. A suppressive influence of background motion on responses to bar stimuli has also been found in monkey areas V1 and V2. However, the suppression was weaker than in the visual areas of the cat [93]. Gulyas et al. found suppressive influence of a moving texture background also in geniculate cells of the cat [46]. It is possible that cortical suppression is mediated via geniculate afferents to the primary visual areas. According to the authors, this suppression could either be produced by local inhibitory connections within the LGN or by an inhibitory loop involving the striate cortex. Therefore it is possible that the inhibitory effects found in area PMLS might result from afferent inputs from lower visual areas instead of being a result of an intrinsic computation within this area. These inputs could either originate in the LGN and be sent directly to area PMLS or connect via area 21a, which has strong afferent connections to the motion area. However, lateral inhibition could also serve as a direct computational mechanism within area PMLS. More studies will be necessary to resolve this issue.

Another aspect concerning the neural mechanism underlying the suppressive effect of a moving background is the region in the visual field from which the suppression arises. Hammond and MacKay reported that the area, from which a background can influence a response, is much larger than the classical receptive field of a cell in area 17 [50]. Similar results have been reported by von Grünau et al. for area PMLS [45]. This question is discussed in more detail below.

Whereas a static random dot background already had an inhibitory effect on firing rates elicited by a SFM bar, a moving background led to an almost vanishing response. Similar results have been reported in monkey area MT for a texture bar defined by oriented line segments [89]. The degree of reduction was independent of the direction of the background relative to the bar.

The vanishing response in area PMLS was surprising, since motion contrast between a texture bar and a moving random dot background is much stronger than for a static dot background. This is in contrast to the case of luminance, where the visual system tends to enhance the luminance contrast between visual objects. The present result could be explained by assuming that area PMLS might signal only the strongest direction of motion inside the receptive field, which, in the case of a moving background, is the motion of the background pattern. This motion information might then be fed into the ventral stream for further processing. Here information from area 17 and 18 might be combined with the motion information from area PMLS. Since the receptive fields in area 17 and 18 are smaller, the cells can signal a motion direction from a more restricted area of the visual field than cells in area PMLS and could signal the motion information of the random dot bar. Thus, area PMLS would not contribute to the object recognition but would signal only the strongest motion vectors contained in a visual stimulus, i.e., the motion of the moving background pattern. This would imply that the convergent process must retain the retinotopy in order to distinguish the motion information coming from the different areas. This could result in a good motion contrast enhancement. This convergent processes proposed here would also be in line with a mechanism postulated for the monkey as discussed below.

#### *Effects of visual noise*

In order to test the saliency of the moving random dot bar, static flicker onset noise was introduced into the static random dot background pattern. For this experiment, 5%, 10% and 20% of stimulus noise was used. It turned out that already 5% of noise led to a complete disappearance of firing rates elicited by the SFM bar moving

over the receptive field of the multiunit. Hence, even low amounts of noise have similar effects on firing rates as the moving random dot backgrounds.

This finding is surprising since, based on a subjective judgment, these low amounts of stimulus noise did not disturb the perception of the SFM bar for a human observer. In addition, it has been shown in section 4.3 that small amounts of noise introduced into a moving dot pattern led only to small changes in firing rates in area PMLS. In contrast to the random dot pattern used in section 4.3, the SFM bar did not cover the entire excitatory receptive field. The width of the bar was chosen such that the field was covered only partially at any given point in time. The information about the motion of the SFM bar had therefore to be computed from only a part of the receptive field that was much smaller than the part used for the bigger random dot stimulus in the preceding chapter. This might lead to a weaker motion signal. In addition, parts of the excitatory receptive field were not covered by the stimulus carrying the motion information but detected the flicker noise, only. The combination of a weak motion signal and noise distractors could then lead to the strong reduction in firing rates found for the flicker onset noise under these stimulus conditions.

It has been shown that area PMLS is important for the perception of three-dimensional SFM stimuli [110]. However, this area itself does not seem to be able to detect such a stimulus (see below). Thus, it might serve as an important source of information about stimulus motion that is used in subsequent brain areas involved in motion analysis. If area PMLS would only feed basic motion information into the ventral stream of the visual system, as has been proposed for area MT in the monkey, the vanishing response at even very low levels of noise would significantly impair the detection of SFM stimuli. Distraction, however, is common in the natural world and it seems surprising to have such a sensitive mechanism for the detection of structures from motion. The question remains, which parameters determine the responsiveness of cells to SFM stimuli moving over a noisy background. Further electrophysiological sin-

gle- and multiunit studies with this type of stimuli would be necessary to resolve this issue. In addition, fMRI studies with humans and monkeys could give further evidence, how area MT behaves when stimulated with a noisy SFM stimulus.

It can, however, not be ruled out, that the effect of anesthesia plays again an important role in the reduction of firing rates for low levels of stimulus noise. Most of the electrophysiological studies in monkey area MT and psychophysical studies in the cat described in the literature have been performed with awake, behaving animals. The detection of SFM bars moving over a noisy background might therefore require an attentive mechanism and is missed in the present experiments.

#### *Effect of masking*

When the effect of masking the moving background pattern was investigated, a square mask of a size equal to the width of the SFM bar was not sufficient to reduce the suppressive effect of the moving random dot background. Such mask did not lead to significant changes in firing rates compared to the unmasked condition. Since area PMLS has rather large receptive fields [96], the masks were not sufficient to cover the excitatory receptive field and cancel the inhibitory effect of the background. If, however, the mask had a size equal to the length of the SFM bar, the suppressive influence of the background vanished. Depending on the pattern of the masks, firing rates elicited by the SFM bar were equal to those elicited by movement over a blank or a static random dot background, respectively. Under these conditions, the size of the mask was approximately equal to the size of the receptive field of the multiunit. This would mean that, for this stimulus, firing rates were not affected by areas outside the receptive area of the cells as has been proposed previously [45, 11]. Studies in monkey area MT showed that cells can be modulated by different directions of motion of patterns lying completely outside the classical receptive field [3, 138]. Several other studies also reported the influence of areas outside the receptive fields on firing rates in area PMLS (see for instance 45). From the

present results it can conclude that only the excitatory receptive field seems to be important for the modulation of firing rates upon stimulation with a random dot bar. It can of course not be ruled out, that the mask covered an area slightly bigger than the receptive field of the multiunit. However, long-range effects seem unlikely.

*SFM bars with different directions of dot motion*

In order to find further evidence in favor of or against the hypothesis that cells in area PMLS can analyze the motion of the contour of a SFM bar, SFM bars with different relative dot motion inside the bar but equal direction of motion of the shape itself were shown. If area PMLS analyzes the motion of the contour instead of the motion of the component dots, firing rates should be the same for all these conditions since the kinetically defined boundary always moved into the same direction. However, firing rates elicited by the different SFM bars decreased when the dots building the bars moved more and more off the direction of the shape. These differences did not become significant for dot motion of  $90^\circ$  and  $135^\circ$ . Only dots moving in the opposite direction of the shape showed a significant reduction in rates. Nevertheless, together with the results from the SFM tuning curve experiment, these results suggest that area PMLS is not able to process the direction of a kinetically defined contour but only analyzes the direction of motion of its components.

One reason for the high firing rates for dot motions  $90^\circ$  and  $135^\circ$  off the preferred direction of the cells were the tuning properties in area PMLS. The broad tuning always led to a response even when the multiunit was stimulated perpendicular to its preferred direction (see also section 4.2). Furthermore, in addition to the contour built by different motion vectors of dots and background, a further cue for the visual system to detect the moving kinetic boarder is the appearance and disappearance of dots at the edges of the SFM bar. This additional local visual cue could serve as a stimulus that could elicit further responses in area PMLS cells. It has been shown for area MST of the monkey that the appearance and disappearance of dots at a luminance defined edge can lead to a neural response in



singleunit recordings [136]. In that experiment, a solid disk on a moving dot background elicited a neural response that was not found when the moving random dot pattern or the disk were shown in isolation. The response vanished if the borders of the disk hiding the dots were blurred. This effect depended on the direction of the moving background. In the present experiment, the occlusion cue vanished for the 135° condition because the dots were not disappearing at the boarder of the bar and it reversed direction for the 180° stimulus. In addition, no differences were found between the 0° and the 90° direction based on occlusion related cues since the occlusion of the boarder remained the same for both conditions. Hence, the reduction in firing rates in the present experiments could also partially be due to the disappearance of this occlusion-related cue. Further experiments will be necessary to investigate the saliency of an occlusion defined border in area PMLS.

#### *SFM tuning curve stimulus*

The results from the tuning curve stimulus consisting of SFM bars also indicated, that cells in area PMLS predominantly process the direction of the component motion of a SFM stimulus rather than the motion of the shape itself. This was demonstrated by the rotation of the preferred direction of the multiunit by 45° when the component motion was rotated by 90° without changing the direction of motion of the shape itself.

The results that cells in area PMLS do not detect kinetically defined boundaries are in good agreement with results obtained in monkey area MT [71, 64, 72]. It has been reported that cells in area MT respond only to the motion vector of the component dots moving over their receptive fields [71]. These cells were unable to code the orientation of kinetically defined boundaries. However, monkeys are able to perceive motion defined stimuli [114]. Cells in the inferior temporal cortex (IT) respond to gratings defined solely by relative motion [114]. In these experiments, response strength did not depend on whether the gratings were defined by luminance, by texture or by motion difference but latencies were shorter for the lu-

minance-defined edge as compared to the kinetically defined boundaries. Thus, IT cells seem to contribute to the cue invariant coding of different types of boundaries [114].

In addition, it has been shown that area V2 in the monkey is able to analyze the orientation of kinetically defined edges [72]. However, despite the ability to signal the orientation of kinetically defined edges, the authors suggested that due to the long latencies of the neural response representing the kinetically defined edges as compared to luminance defined contours, area V2 is most likely not detecting these kinetic edges. Their results suggest that responses in area V2 might rather be modulated by a top-down feedback connection from higher visual areas, presumably from the dorsal stream. Since responses in area IT show the same latency of 80 ms to 120 ms for luminance and kinetically defined edges, the authors proposed that the information about these differently defined edges is combined in an area in the visual system higher than V2 so that it is transmitted to area IT without any time delay.

In contrast to the present results indicating that cells in area PMLS are not able to detect SFM stimuli and despite the evidence coming from studies in monkey area MT [71, 64, 72], a study by Pasternak et al. [110] showed that lesions in the lateral suprasylvian (LS) cortex led to a reduction in the ability of awake, behaving cats to perceive three-dimensional SFM stimuli. From these experiments the authors concluded that the LS area plays an important role in either the perception of the component motion necessary to perceive SFM stimuli or in the recognition of SFM motion itself. [110]. In addition, they found deficits in the integration of local motion signals similar to the results described in section 4.3. and deficits in direction discrimination [97]. Taken together, these results led to the conclusion that the deficits in perceiving SFM stimuli upon lesions in the LS area may be due rather to a deficit in speed discrimination than to the fact that the LS area is responsible for the recognition of SFM structures. On the other hand, Vaina et al. [142] reported that brain damaged patients showing severe deficits in speed discrimi-

nation can still perceive SFM stimuli, providing evidence that this mechanism might be independent of the mechanism necessary for speed discrimination, at least in the human visual cortex.

If PMLS is not the area in the cat that is perceiving the SFM stimulus, the question remains, where this stimulus is detected in the visual cortex. As mentioned above, psychophysical studies [110] have shown that cats are clearly able to perceive SFM stimuli. Based on fMRI experiments in humans one could speculate that a higher area in the visual pathways might be responsible for the detection of these types of stimuli. Unfortunately, the homologous to area KO, which has been identified to respond to kinetically defined boundaries in humans [23, 94, 143], as well as area IT that responded to shapes defined by motion contrast in monkeys [114] are not known in the cat. It might be that, similar to the monkey, the motion signals detected in area PMLS enter the ventral stream of the visual system where they are further processed in order to lead to the necessary information the cortex needs to perceive a SFM stimulus. This would explain why lesions in area PMLS lead to a strong impairment in the detection of 3-D cylinders [110]. However, further experiments are needed to gain more insight into the question of how and where in the visual cortex SFM stimuli are perceived.

## 5.4 Conclusion

The present results provide good evidence that area PMLS is most likely not the area perceiving SFM objects. Although this area seems to be important for the perception of this type of stimuli, the processing most likely takes place in a different area. Cells in area PMLS are more responsible for the detection of the component motion inside a SFM stimulus. The results further showed that already low levels of noise in the background pattern of a SFM stimulus are able to disturb the detection of the component motion.

In addition the results showed that background motion leads to a vanishing neural response upon stimulation with a SFM bar. The influence of the background could be controlled by masking an area of the background pattern that was equivalent to the size of the receptive field of the cells. From these results it is concluded that the component detection in area PMLS is not influenced by areas lying outside the classical receptive field.

## CHAPTER 6    **Outlook**

---

In the history of science, great advances in technical and theoretical methods have always led to new experiments that have been impossible before. Examples in the field of neuroscience are the invention of the patch-clamp technique by Erwin Neher and Bert Sakman that enabled us to measure the current flow through a single ion channel, or the development of voltage sensitive dyes for optical measurements. Together with advances in other fields of science, like the development of easy to use and fast pulsed laser systems and the development of very sensitive detectors, this led to a rapid development in our knowledge about the molecular and cellular mechanisms of the brain. Recent development in the field of functional magnetic resonance imaging, like the use of high magnetic fields of 4 T to 7 T and the improvements in coil and sequences design, have led to enormous improvements in functional imaging.

In addition to these advances on the technical side, new methods and possibilities in the manipulation of the genetic code open a completely new field in neuroscience. Knock-out mice missing certain types of receptors or ion channels can give new important insight into the function of these proteins for special brain areas and

into the processes mediated by certain channels and receptors (see for instance [79]). However, this approach is extremely difficult to control. A knockout of one receptor gene might block or activate whole cascades of mechanisms that will lead to effects we cannot explain today. In addition, many mutants are lethal. Nevertheless, the current improvements in mutagenesis, no doubt, will open the door for many new experiments that will lead to further advances in the neural sciences.

One especially interesting and promising development in the field of electrophysiology are the improvements in techniques for highly parallel *in vivo* recordings of extracellular signals. Although there are still some laboratories experimenting with a single electrode, the last two years showed a clear trend towards the use of tens of electrodes at the same time. Today, recordings with 100 electrodes in parallel are possible. These electrodes can be positioned in a vertical grid that will allow to investigate neural processing within one cortical column. They can also be positioned in a vertical matrix. This constellation is useful for looking at mechanisms within a single cortical layer that spans several columns at a time. In addition to the very high temporal resolution inherent in the electrophysiological recordings, these new advances in the available number of electrodes lead to an additional high spatial resolution in the recorded signals. This will allow experiments that investigate the behavior of firing rates, oscillation and synchronization in both, time *and* space domain. For instance, the location of current sources and sinks can be analyzed and can reveal the locations in the cortical layers where oscillations might originate. With this information it will be possible to construct cortical space-time maps showing the increase and decrease of oscillations in time for a given perceptual task. In the case of our random dot experiments, the origin of the strong alpha oscillations could be investigated using these highly parallel recording techniques. The parallel recordings will further allow to investigate non-linear relationships and higher-order correlation in cognitive processes. While the small number of available data today made these kinds of analysis tedious and a meaningful statistical interpre-

tation difficult, the huge amount of data from massive parallel recordings will allow many theoretical approaches that are impossible today. As a consequence, the availability of these data could lead to a paradigm shift away from the single neurons as the important computational unit in the brain towards a point of view where cell assemblies and inherent properties of the network become the important carriers of the computational power of the brain.

However, the new data also need new analytical tools in order to deal with the huge amount of information. The approaches used so far, e.g., calculating a correlogram and fitting the resulting correlation function in order to extract parameters like RMA or center peak width, often need an additional visual inspection. Due to the low signal-to-noise ratio in many experiments, the fit is often not reliable enough, giving too many false positive or false negative results. Hence, this widely used method for correlation analysis will quickly come to its limits when the number of electrode pairs for the correlation analysis increases, as it will be the case with 60 to 100 electrodes. In addition, the close proximity of cells recorded with the new available multielectrode systems will most likely violate the condition of independence required in most of the statistical tests employed in neuroscience. In addition, as of today, there exist no reliable and fast enough methods for computing higher order correlations from electrophysiological data. All these questions will open many possibilities for further theoretical research.

Until a detailed knowledge about the cellular mechanism underlying the temporal coding of neural signals is not available, many more experiments are necessary to further correlate perception with neural parameters. Many of these experiments will have to be performed with awake, behaving animals. Only these experiments will allow to establish a clear link between perception, behavior and neural parameters. For instance, can the strong alpha oscillation found in the present study in area PMLS also be found in the awake animal or is it only an epiphenomenon of anesthesia? It would further be interesting to see, if the changes in the temporal structure of the neural activity found upon stimulation with random

dot pattern with increasing levels of stimulus noise is better correlated with perception and psychophysical results when the animal can pay attention to this visual stimulus. A similar problem exists for the shape-from-motion stimulus. Experiments performed with awake animals will be necessary to decide, whether the detection of shape-from-motion stimuli will also need an attentive mechanism and was thus missed in our experiments.



Part of this thesis have been published in the following poster abstracts:

Kluge T., Fickel U., Goebel R. and Engel A.K., 1999, "Synchronization induced by moving random-dot patterns in cat striate and extrastriate cortex", CNS, San Francisco, USA.

Kluge T., Fickel U., Goebel R. and Engel A.K., 2000, "Influence of moving random-dot patterns on synchrony in cat striate and extrastriate cortex", FENS, Brighton, UK.

Engel A.K., Kluge T., Fickel U. and Goebel R., 2000, "Responses and Temporal Patterning with Motion-Contrast Stimuli in Cat Extrastriate Visual Cortex", Soc. Neurosci. Abstr., 2000.

Kluge T., Fickel U., Singer W. and Engel A.K., 2000, "Effects of random-dot stimuli on synchrony in cat extra-striate visual cortex", Soc. Neurosci. Abstr., 2000.

Kluge T., Fickel U., Singer W. and Engel A.K., 2001, "Effects of random-dot stimuli on synchrony in cat striate and extrastriate visual cortex", DNG, Göttingen.

Engel A.K., Kluge T. and Goebel R., 2001, "Processing of motion-contrast stimuli in cat visual area PMLS", DNG, Göttingen.



## BIBLIOGRAPHY

---

- 1 Adelson, E. H. & Movshon, J. A. (1982)  
Phenomenal coherence of moving visual patterns. *Nature* 300, 523-525.
- 2 Abeles, M. (1982)  
Role of the cortical neuron: integrator or coincidence detector? *Isr J Med Sci*, 18(1), 83-92.
- 3 Allman, J., Miezin, F. & McGuinness, E. (1985)  
Stimulus specific responses from beyond the classical receptive field: neurophysiological mechanisms for local-global comparisons in visual neurons. *Annu Rev Neurosci* 8, 407-430
- 4 Baker, S. N., Kilner, J. M., Pinches, E. M. & Lemon, R. N. (1999)  
The role of synchrony and oscillations in the motor output. *Exp Brain Res* 128, 109-117
- 5 Barlow, H. B. (1972)  
Single units and sensation: a neuron doctrine for perceptual psychology? *Perception* 1, 371-394
- 6 Bauer, R. & Jordan, W. (1993)  
Different anisotropies for texture and grating stimuli in the visual map of cat striate cortex. *Vision Res* 33, 1447-1450.
- 7 Bortz, J. (1999)  
*Statistik für Sozialwissenschaftler*, Springer Verlag, Berlin

## Bibliography

- 8 Bradley, D. C., Chang, G. C. & Andersen, R. A. (1998)  
Encoding of three-dimensional structure-from-motion by primate area MT neurons. *Nature*, 392(6677), 714-7.
- 9 Brecht, M., Singer, W. & Engel, A. K. (1998)  
Correlation analysis of corticotectal interactions in the cat visual system. *J Neurophysiol* 79, 2394-2407.
- 10 Brecht, M., Goebel, R., Singer, W. & Engel, A. K. (2001)  
Synchronization of visual responses in the superior colliculus of awake cats. *Neuroreport* 12, 43-47
- 11 Bretzner, F., Aitoubah, J., Shumikhina, S., Tan, Y. F. & Molotchnikoff, S. (2000)  
Stimuli outside the classical receptive field modulate the synchronization of action potentials between cells in visual cortex of cats. *Neuroreport* 11, 1313-1317
- 12 Britten, K. H., Shadlen, M. N., Newsome, W. T. & Movshon, J. A. (1992)  
The analysis of visual motion: a comparison of neuronal and psychophysical performance. *J Neurosci*, 12(12), 4745-65.
- 13 Bullock, T. H. (1988).  
Compound potentials of the brain, ongoing and evoked: perspectives from comparative neurology. *Dynamics of Sensory and Cognitive Processing by the Brain*, E. Basar, ed., Springer Verlag, Berlin.
- 14 Casanova, C. (1993)  
Responses of cells in cat's area 17 to random dot patterns: influence of stimulus size. *Neuroreport* 4, 1011-1014.
- 15 Casanova, C., Savard, T., Nordmann, J. P., Molotchnikoff, S. & Minville, K. (1995)  
Comparison of the responses to moving texture patterns of simple and complex cells in the cat's area 17. *J Neurophysiol* 74, 1271-1286.
- 16 Castelo-Branco, M., Neuenschwander, S. & Singer, W. (1998)  
Synchronization of visual responses between the cortex, lateral geniculate nucleus, and retina in the anesthetized cat. *J Neurosci*, 18(16), 6395-410
- 17 Castelo-Branco, M., Goebel, R., Neuenschwander, S. & Singer, W. (2000)  
Neural synchrony correlates with surface segregation rules. *Nature*, 405(6787), 685-9
- 18 Contreras, D. & Llinas, R. (2001)  
Voltage-sensitive dye imaging of neocortical spatiotemporal dynamics to afferent activation frequency. *J Neurosci*, 21(23), 9403-13.
- 19 Danilov, Y., Moore, R. J., King, V. R. & Spear, P. D. (1995)  
Are neurons in cat posteromedial lateral suprasylvian visual cortex orientation sensitive? Tests with bars and gratings. *Vis Neurosci* 12, 141-151.

- 20 Di Prisco, G. V. & W. J. Freeman (1985)  
Odor-related bulbar EEG spatial pattern analysis during appetitive conditioning in rabbits. *Behav Neurosci* 99(5): 964-78.
- 21 Dreher, B., Wang, C., Turlejski, K. J., Djavadian, R. L. & Burke, W. (1996)  
Areas PMLS and 21a of cat visual cortex: two functionally distinct areas. *Cereb Cortex* 6, 585-599.
- 22 Dreher, B., Wang, C. & Burke, W. (1996)  
Limits of parallel processing: excitatory convergence of different information channels on single neurons in striate and extrastriate visual cortices. *Clin Exp Pharmacol Physiol* 23, 913-925.
- 23 Dupont, P., De Bruyn, B., Vandenberghe, R., Rosier, A. M., Michiels, J., Marchal, G., Mortelmans, L. & Orban, G. A. (1997)  
The kinetic occipital region in human visual cortex. *Cereb Cortex*, 7(3), 283-92.
- 24 Eckhorn, R., Bauer, R., Jordan, W., Brosch, M., Kruse, W., Munk, M., Reitboeck, H. J. (1988)  
„Coherent oscillations: a mechanism of feature linking in the visual cortex? Multiple electrode and correlation analyses in the cat. *Biol Cybern* 60, 121-130.
- 25 Eckhorn, R., Frien, A., Bauer, R. & Woelbern, T. (1994)  
Oscillation frequencies (40 - 90 Hz) in monkey visual cortex depend on stimulus size and velocity. *Eur. J. Neurosci.*, 112.106.
- 26 Eggermont, J. J., Smith, G. M. & Bowman, D. (1993)  
„Spontaneous burst firing in cat primary auditory cortex: age and depth dependence and its effect on neural interaction measures. *J Neurophysiol* 69, 1292-1313.
- 27 Engel, A. K., König, P., Gray, C. M. & Singer, W. (1990)  
Stimulus-dependent neuronal oscillation in cat visual cortex; inter-columnar interactions as determined by cross-correlation analysis. *Eur. J. Neurosci.* 2, 558-606.
- 28 Engel, A. K., Kreiter, A. K., König, P. & Singer, W. (1991)  
Synchronization of oscillatory neuronal responses between striate and extrastriate visual cortical areas of the cat. *Proc Natl Acad Sci U S A*, 88(14), 6048-52.
- 29 Engel, A. K., König, P., Kreiter, A. K. & Singer, W. (1991)  
„Interhemispheric synchronization of oscillatory neuronal responses in cat visual cortex. *Science* 252, 1177-1179.
- 30 Engel, A. K., König, P., Kreiter, A. K., Schillen, T. B. & Singer, W. (1992)  
Temporal coding in the visual cortex: new vistas on integration in the nervous system. *Trends Neurosci*, 15(6), 218-26.
- 31 Engel, A. K., Roelfsema, P. R., Fries, P., Brecht, M. & Singer, W. (1997)  
Role of the temporal domain for response selection and perceptual binding. *Cereb Cortex*, 7(6), 571-82.

## Bibliography

- 32 Engel, A. K., Fries, P. & Singer, W. (2001)  
Dynamic predictions: oscillations and synchrony in top-down processing. *Nat Rev Neurosci*, 2(10), 704-16
- 33 Felleman, D. J. & Van Essen, D. C. (1991)  
Distributed hierarchical processing in the primate cerebral cortex. *Cereb Cortex*, 1(1), 1-47.
- 34 Freedman, D. J., Riesenhuber, M., Poggio, T. & Miller, E. K. (2001)  
„Categorical representation of visual stimuli in the primate prefrontal cortex. *Science* 291, 312-316.
- 35 Friedman-Hill, S., Maldonado, P. E. & Gray, C. M. (2000)  
Dynamics of striate cortical activity in the alert macaque: I. Incidence and stimulus-dependence of gamma-band neuronal oscillations. *Cereb Cortex* 10, 1105-1116.
- 36 Frien, A. & Eckhorn, R. (2000)  
Functional coupling shows stronger stimulus dependency for fast oscillations than for low-frequency components in striate cortex of awake monkey. *Eur J Neurosci*, 12(4), 1466-78.
- 37 Fries, P., Reynolds, J. H., Rorie, A. E. & Desimone, R. (2001)  
Modulation of oscillatory neuronal synchronization by selective visual attention. *Science*, 291(5508), 1560-3
- 38 Fries, P., Neuenschwander, S., Engel, A. K., Goebel, R. & Singer, W. (2001)  
Rapid feature selective neuronal synchronization through correlated latency shifting. *Nat Neurosci* 4, 194-200
- 39 Fries, P., Schroder, J. H., Roelfsema, P. R., Singer, W. & Engel, A. K. (2002)  
Oscillatory neuronal synchronization in primary visual cortex as a correlate of stimulus selection. *J Neurosci* 22, 3739-3754.
- 40 Gray, C. M. & J. E. Skinner (1988)  
Centrifugal regulation of neuronal activity in the olfactory bulb of the waking rabbit as revealed by reversible cryogenic blockade. *Exp Brain Res* 69(2): 378-86
- 41 Gray, C. M. & Singer, W. (1989)  
Stimulus-specific neuronal oscillations in orientation columns of cat visual cortex. *Proc Natl Acad Sci U S A*, 86(5), 1698-702.
- 42 Gray, C. M., Konig, P., Engel, A. K. & Singer, W. (1989)  
Oscillatory responses in cat visual cortex exhibit inter-columnar synchronization which reflects global stimulus properties. *Nature*, 338(6213), 334-7.
- 43 Gray, C. M., Engel, A. K., Konig, P. & Singer, W. (1992)  
Synchronization of oscillatory neuronal responses in cat striate cortex: temporal properties. *Vis Neurosci* 8, 337-347

- 44 Gray, C. M. (1999)  
The temporal correlation hypothesis of visual feature integration: still alive and well. *Neuron* 24, 31-47, 111-125.
- 45 von Grünau, M. & Frost, B. J. (1983)  
„Double-opponent-process mechanism underlying RF-structure of directionally specific cells of cat lateral suprasylvian visual area. *Exp Brain Res* 49, 84-92.
- 46 Gulyas, B., Orban, G. A., Duysens, J. & Maes, H. (1987)  
The suppressive influence of moving textured backgrounds on responses of cat striate neurons to moving bars. *J Neurophysiol*, 57(6), 1767-91.
- 47 Hammond, P. & MacKay, D. (1975)  
Differential Responses of Cat Visual Cortical Cells to textured Stimuli. *Exp. Brain Res.*, 22, 427-430.
- 48 Hammond, P. & MacKay, D. M. (1977)  
Differential responsiveness of simple and complex cells in cat striate cortex to visual texture. *Exp Brain Res*, 30(2-3), 275-96.
- 49 Hammond, P. (1978)  
Directional tuning of complex cells in area 17 of the feline visual cortex. *J Physiol* 285, 479-491.
- 50 Hammond, P. & MacKay, D. M. (1981)  
Modulatory influences of moving textured backgrounds on responsiveness of simple cells in feline striate cortex. *J Physiol*, 319, 431-42.
- 51 Hebb, D.O. (1949)  
*The Organization of Behavior*. Wiley, New York
- 52 Hubel, D. & Wiesel, T. (1962).  
Receptive Fields, Binocular Interaction and Functional Architecture in the Cat's visual Cortex. *J.Physiol (Lon)*, 160, 106-154
- 53 Hughes, H. C. & Sprague, J. M. (1986)  
„Cortical mechanisms for local and global analysis of visual space in the cat. *Exp Brain Res* 61, 332-354 (1986).
- 54 Joly, T. J. & Bender, D. B. (1997)  
Loss of relative-motion sensitivity in the monkey superior colliculus after lesions of cortical area MT. *Exp Brain Res*, 117(1), 43-58.
- 55 Juergens, E., Eckhorn, R., Frien, A. & Woelbern, T. (1996)  
Restricted coupling range of fast oscillations in striate cortex of awake monkey. *Brain and Evolution*, E. Elsner and H.-U. Schnitzler, eds., Thieme, Berlin/New York.

## Bibliography

- 56 Kalil, R. E., Tong, L. L. & Spear, P. D. (1991)  
„Thalamic projections to the lateral suprasylvian visual area in cats with neonatal or adult visual cortex damage. *J Comp Neurol* 314, 512-525. .
- 57 Kandel, E., Schwartz, J. & Jessell, T. (2000)  
*Principles of Neural Science*, McGraw-Hill Companies
- 58 Katsuyama, N., Tsumoto, T., Sato, H., Fukuda, M. & Hata, Y. (1996)  
Lateral suprasylvian visual cortex is activated earlier than or synchronously with primary visual cortex in the cat. *Neurosci Res* 24, 431-435.
- 59 Köhler, W. (1930)  
*Gestalt Psychology*. Bell and Sons, London
- 60 König, P. (1994)  
A method for quantification of synchrony and oscillatory properties of neuronal activity. *J. Neurosci.* 19, 130-137.
- 61 König, P., Engel, A. K. & Singer, W. (1996)  
Integrator or coincidence detector? The role of the cortical neuron revisited. *Trends Neurosci*, 19(4), 130-7.
- 62 Koffka, K. (1936),  
*Principles of Gestalt Psychology*. Routledge and Kegan Paul, London
- 63 Kruse, W. & Eckhorn, R. (1996)  
Inhibition of sustained gamma oscillations (35-80 Hz) by fast transient responses in cat visual cortex. *Proc Natl Acad Sci U S A* 93, 6112-6117.
- 64 Lamme, V. A., van Dijk, B. W. & Spekreijse, H. (1993)  
Contour from motion processing occurs in primary visual cortex. *Nature* 363, 541-543.
- 65 Lestienne, R. (2001)  
Spike timing, synchronization and information processing on the sensory side of the central nervous system. *Prog Neurobiol* 65, 545-591.
- 66 Leventhal, A. G., Wang, Y., Schmolesky, M. T. & Zhou, Y. (1998)  
Neural correlates of boundary perception. *Vis Neurosci*, 15(6), 1107-18.
- 67 Li, B., Chen, Y., Li, B. W., Wang, L. H. & Diao, Y. C. (2001)  
Pattern and component motion selectivity in cortical area PMLS of the cat. *Eur J Neurosci*, 14(4), 690-700.
- 68 Logothetis, N. K., Pauls, J., Augath, M., Trinath, T. & Oeltermann, A. (2001)  
Neurophysiological investigation of the basis of the fMRI signal. *Nature* 412, 150-157.
- 69 Lopes da Silva, F. (1991)  
Neural mechanisms underlying brain waves: from neural membranes to networks. *Electroencephalography & Clinical Neurophysiology*. 79(2): 81-93.



- 70 Maldonado, P. E., Godecke, I., Gray, C. M. & Bonhoeffer, T. (1997).  
„Orientation selectivity in pinwheel centers in cat striate cortex. *Science* 276, 1551-1555.
- 71 Marcar, V. L., Xiao, D. K., Raiguel, S. E., Maes, H. & Orban, G. A. (1995)  
Processing of kinetically defined boundaries in the cortical motion area MT of the macaque monkey. *J Neurophysiol* 74, 1258-1270.
- 72 Marcar, V. L., Raiguel, S. E., Xiao, D. & Orban, G. A. (2000)  
Processing of kinetically defined boundaries in areas V1 and V2 of the macaque monkey. *J Neurophysiol* 84, 2786-2798.
- 73 Merabet, L., Minville, K., Ptito, M. & Casanova, C. (2000)  
Responses of neurons in the cat posteromedial lateral suprasylvian cortex to moving texture patterns. *Neuroscience* 97, 611-623.
- 74 Mima, T., Oluwatimilehin, T., Hiraoka, T. & Hallett, M. (2001)  
Transient interhemispheric neuronal synchrony correlates with object recognition. *J Neurosci*, 21(11), 3942-8.
- 75 Morrone, M. C., Di Stefano, M. & Burr, D. C. (1986)  
Spatial and temporal properties of neurons of the lateral suprasylvian cortex of the cat. *J Neurophysiol* 56, 969-986.
- 76 Movshon, J. A., Thompson, I. D. & Tolhurst, D. J. (1978)  
Spatial and temporal contrast sensitivity of neurones in areas 17 and 18 of the cat's visual cortex. *J Physiol* 283, 101-120
- 77 Mulligan, K., Kim, J. N. & Sherk, H. (1997)  
Simulated optic flow and extrastriate cortex. II. Responses to bar versus large-field stimuli. *J Neurophysiol* 77, 562-570
- 78 Nakayama, K. (1985).  
„Biological image motion processing: a review. *Vision Res* 25, 625-660.
- 79 Nase, G., Hormuzdi, S. G., Monyer, H., Singer, W. & Engel, A. K. (2001)  
Stimulus induced correlation patterns in visual cortex of connexin-36-deficient mice. *Society for Neuroscience Abstracts*.
- 80 Naumer, M., Bonte, M., Grether, M., Muckli, L., Engel, A., Zanella, F., Singer, W. & Goebel, R. (2001)  
Three dimensional structure-from-motion activates shape-specific areas in the ventral visual processing stream. Conference Abstract.
- 81 Nelson, J. I., Salin, P. A., Munk, M. H., Arzi, M. & Bullier, J. (1992)  
„Spatial and temporal coherence in cortico-cortical connections: a cross-correlation study in areas 17 and 18 in the cat. *Vis Neurosci* 9, 21-37.

## Bibliography

- 82 Neuenschwander, S. & Singer, W. (1996)  
Long-range synchronization of oscillatory light responses in the cat retina and lateral geniculate nucleus. *Nature*, 379(6567), 728-32.
- 83 Newsome, W. T., Mikami, A. & Wurtz, R. H. (1986)  
„Motion selectivity in macaque visual cortex. III. Psychophysics and physiology of apparent motion. *J Neurophysiol* 55, 1340-1351
- 84 Newsome, W. T. & Pare, E. B. (1988)  
A selective impairment of motion perception following lesions of the middle temporal visual area (MT). *J Neurosci*, 8(6), 2201-11.
- 85 Newsome, W. T., Britten, K. H. & Movshon, J. A. (1989)  
Neuronal correlates of a perceptual decision. *Nature*, 341(6237), 52-4.
- 86 Niida, T., Stein, B. E. & McHaffie, J. G. (1997)  
Response properties of corticotectal and corticostriatal neurons in the posterior lateral suprasylvian cortex of the cat. *J Neurosci* 17, 8550-8565.
- 87 Niimi, K. & Sprague, J. M. (1970)  
Thalamo-cortical organization of the visual system in the cat. *J Comp Neurol*, 138(2), 219-50.
- 88 Nowak, L. G., Munk, M. H., Nelson, J. I., James, A. C. & Bullier, J. (1995)  
„Structural basis of cortical synchronization. I. Three types of interhemispheric coupling. *J Neurophysiol* 74, 2379-2400.
- 89 Olavarria, J. F., DeYoe, E. A., Knierim, J. J., Fox, J. M. & van Essen, D. C. (1992)  
Neural responses to visual texture patterns in middle temporal area of the macaque monkey. *J Neurophysiol* 68, 164-181.
- 90 Orban, G. A., Kennedy, H. & Maes, H. (1981)  
Response to movement of neurons in areas 17 and 18 of the cat: direction selectivity. *J Neurophysiol* 45, 1059-1073
- 91 Orban, G. A. (1984)  
*Neuronal Operations in the Visual Cortex*, Springer Verlag, Berlin.
- 92 Orban, G. A., Gulyas, B. & Vogels, R. (1987)  
Influence of a moving textured background on direction selectivity of cat striate neurons. *J Neurophysiol* 57, 1792-1812
- 93 Orban, G. A., Gulyas, B. & Spileers, W. (1988)  
Influence of moving textured backgrounds on responses of cat area 18 cells to moving bars. *Prog Brain Res* 75, 137-145.
- 94 Orban, G. A., Dupont, P., De Bruyn, B., Vogels, R., Vandenberghe, R. & Mortelmans, L. (1995)  
A motion area in human visual cortex. *Proc Natl Acad Sci U S A*, 92(4), 993-7.

- 95 Palmer, S.E. (1999)  
Vision Science - Photons to Phenomenology, MIT Press, Cambridge, Massachusetts
- 96 Palmer, L. A., Rosenquist, A. C. & Tusa, R. J. (1978)  
The retinotopic organization of lateral suprasylvian visual areas in the cat. *J Comp Neurol* 177, 237-256.
- 97 Pasternak, T., Horn, K. M. & Maunsell, J. H. (1989).  
Deficits in speed discrimination following lesions of the lateral suprasylvian cortex in the cat. *Vis Neurosci*, 3(4), 365-75.
- 98 Pasternak, T., Albano, J. E. & Harvitt, D. M. (1990)  
„The role of directionally selective neurons in the perception of global motion. *J Neurosci* 10, 3079-3086.
- 99 Pasternak, T., Tompkins, J. & Olson, C. R. (1995)  
The role of striate cortex in visual function of the cat. *J Neurosci* 15, 1940-1950.
- 100 Paradis, A. L., Cornilleau-Peres, V., Droulez, J., Van De Moortele, P. F., Lobel, E., Berthoz, A., Le Bihan, D. & Poline, J. B. (2000)  
Visual perception of motion and 3-D structure from motion: an fMRI study. *Cereb Cortex*, 10(8), 772-83.
- 101 Rainer, G., Augath, M., Trinath, T. & Logothetis, N. K. (2001)  
Nonmonotonic noise tuning of BOLD fMRI signal to natural images in the visual cortex of the anesthetized monkey. *Curr Biol*, 11(11), 846-54.
- 102 Rakic, P. (2002)  
Neurogenesis in adult primate neocortex: an evaluation of the evidence. *Nat Rev Neurosci*, 3(1), 65-71.
- 103 Rauschecker, J. P., von Grunau, M. W. & Poulin, C. (1987)  
„Centrifugal organization of direction preferences in the cat's lateral suprasylvian visual cortex and its relation to flow field processing. *J Neurosci* 7, 943-958.
- 104 Regan, D. (1989)  
Orientation discrimination for objects defined by relative motion and objects defined by luminance contrast. *Vision Res*, 29(10), 1389-400.
- 105 Regan, D. & Hamstra, S. J. (1992)  
Dissociation of orientation discrimination from form detection for motion-defined bars and luminance-defined bars: effects of dot lifetime and presentation duration. *Vision Res*, 32(9), 1655-66.
- 106 Rees, G., Friston, K. & Koch, C. (2000)  
A direct quantitative relationship between the functional properties of human and macaque V5. *Nat Neurosci*, 3(7), 716-23

## Bibliography

- 107 Roelfsema, P. R., Engel, A. K., Konig, P. & Singer, W. (1997)  
Visuomotor integration is associated with zero time-lag synchronization among cortical areas. *Nature*, 385(6612), 157-61.
- 108 Rossi, A. F., Desimone, R. & Ungerleider, L. G. (2001)  
Contextual modulation in primary visual cortex of macaques. *J Neurosci* 21, 1698-1709.
- 109 Roy, S. A., Dear, S. P. & Alloway, K. D. (2001)  
Long-range cortical synchronization without concomitant oscillations in the somatosensory system of anesthetized cats. *J Neurosci* 21, 1795-1808.
- 110 Rudolph, K. K. & Pasternak, T. (1996)  
Lesions in cat lateral suprasylvian cortex affect the perception of complex motion. *Cereb Cortex*, 6(6), 814-22.
- 111 Rudolph, K. & Pasternak, T. (1999)  
Transient and permanent deficits in motion perception after lesions of cortical areas MT and MST in the macaque monkey. *Cereb Cortex*, 9(1), 90-100.
- 112 Sary, G., Vogels, R. & Orban, G. A. (1993)  
Cue-invariant shape selectivity of macaque inferior temporal neurons. *Science* 260, 995-997.
- 113 Sary, G., Vogels, R. & Orban, G. A. (1994)  
Orientation discrimination of motion-defined gratings. *Vision Res*, 34(10), 1331-4.
- 114 Sary, G., Vogels, R., Kovacs, G. & Orban, G. A. (1995)  
Responses of monkey inferior temporal neurons to luminance-, motion-, and texture-defined gratings. *J Neurophysiol* 73, 1341-1354.
- 115 Schanze, T. & Eckhorn, R. (1997).  
„Phase correlation among rhythms present at different frequencies: spectral methods, application to microelectrode recordings from visual cortex and functional implications *Int J Psychophysiol* 26, 171-189
- 116 Schieber, M. H. (2002)  
Training and synchrony in the motor system. *J Neurosci* 22, 5277-5281
- 117 Schröder, J-H (2001)  
Auswahlmechanismen im Sehsystem der Katze. Dissertation Universität Bremen
- 118 Sejnowski, T. R. (1986)  
„Open questions about computation in cerebral cortex in *Parallel Distributed Processing* (eds. McClelland, J. L. & Rumelhart, D. E.) (MIT Press, Cambridge, 1986).
- 119 Shadlen, M. N. & Newsome, W. T. (1994)  
„Noise, neural codes and cortical organization. *Curr Opin Neurobiol* 4, 569-579.

- 120 Shadlen, M. N. & Movshon, J. A. (1999)  
Synchrony unbound: a critical evaluation of the temporal binding hypothesis. *Neuron* 24, 67-77, 111-125.
- 121 Shmuel, A. & Grinvald, A. (1996)  
„Functional organization for direction of motion and its relationship to orientation maps in cat area 18 *J Neurosci* 16, 6945-6964
- 122 Singer, W. & Gray, C. M. (1995)  
Visual feature integration and the temporal correlation hypothesis. *Annu Rev Neurosci*, 18, 555-86.
- 123 Singer, W., Engel, A., Kreiter, A., Munk, M., Neuenschwander, S. & Roelfsema, P. (1997)  
Neuronal assemblies: necessity, signature and detectability. *Trends in Cognitive Sciences*, 1(7), 252-261.
- 124 Singer, W. (1999)  
Neuronal synchrony: a versatile code for the definition of relations? *Neuron* 24, 49-65, 111-125.
- 125 Skottun, B. C., D. H. Grosof, et al. (1988)  
Responses of simple and complex cells to random dot patterns: a quantitative comparison. *J Neurophysiol* 59(6): 1719-35.
- 126 Skottun BC, Zhang J, Grosof DH (1994)  
On the directional selectivity of cells in the visual cortex to drifting dot patterns. *Vis Neurosci*. 1994 Sep-Oct;11(5):885-97
- 127 Smith, D. C. & Spear, P. D. (1979)  
Effects of superior colliculus removal on receptive-field properties of neurons in lateral suprasylvian visual area of the cat. *J Neurophysiol*, 42(1 Pt 1), 57-75.
- 128 Snowden, R. J., S. Treue, et al. (1992)  
The response of neurons in areas V1 and MT of the alert rhesus monkey to moving random dot patterns. *Exp Brain Res* 88(2): 389-400.
- 129 Spear, P. D. & Baumann, T. P. (1975)  
„Receptive-field characteristics of single neurons in lateral suprasylvian visual area of the cat. *J Neurophysiol* 38, 1403-1420.
- 130 Spear, P. D. & Baumann, T. P. (1979)  
Effects of visual cortex removal on receptive-field properties of neurons in lateral suprasylvian visual area of the cat. *J Neurophysiol*, 42(1 Pt 1), 31-56.
- 131 Steriade, M. & R. R. Llinas (1988).  
The functional states of the thalamus and the associated neuronal interplay. *Physiol Rev* 68(3): 649-742

## Bibliography

- 132 von Stein, A., Chiang C., König, P. (1999)  
The role of alpha and gamma frequency interactions in top-down processing in the cat. *Soc. Neurosci. Abstr.* 24.
- 133 von Stein, A. & J. Sarnthein (2000)  
Different frequencies for different scales of cortical integration: from local gamma to long range alpha/theta synchronization. *Int J Psychophysiol* 38(3): 301-13.
- 134 von Stein, A., C. Chiang, et al. (2000)  
Top-down processing mediated by interareal synchronization. *Proc Natl Acad Sci U S A* 97(26): 14748-53.
- 135 Sterling, P. (1983)  
Microcircuitry of the cat retina. *Annu Rev Neurosci* 6: 149-85.
- 136 Sugita, Y. & Tanaka, K. (1991)  
Occlusion-related cue used for analysis of motion in the primate visual cortex. *Neuroreport*, 2(12), 751-4.
- 137 Swindale, N. V. (1998)  
Orientation tuning curves: empirical description and estimation of parameters. *Biol Cybern*, 78(1), 45-56.
- 138 Tanaka, K., Hikosaka, K., Saito, H., Yukie, M., Fukada, Y. & Iwai, E.. (1986)  
Analysis of local and wide-field movements in the superior temporal visual areas of the macaque monkey. *J Neurosci* 6, 134-144
- 139 Tetzlaff, R. personal communication
- 140 Toyama, K., Komatsu, Y., Kasai, H., Fujii, K. & Umetani, K. (1985)  
Responsiveness of Clare-Bishop neurons to visual cues associated with motion of a visual stimulus in three-dimensional space. *Vision Res*, 25(3), 407-14.
- 141 Tusa, R. J., Palmer, L. A. & Rosenquist, A. C. (1978)  
The retinotopic organization of area 17 (striate cortex) in the cat. *J Comp Neurol*, 177(2), 213-35.
- 142 Vaina, L. M., Lemay, M., Bienfang, D. C., Choi, A. Y. & Nakayama, K. (1990)  
Intact "biological motion" and "structure from motion" perception in a patient with impaired motion mechanisms: a case study. *Vis Neurosci*, 5(4), 353-69.
- 143 Van Oostende, S., Sunaert, S., Van Hecke, P., Marchal, G. & Orban, G. A. (1997)  
The kinetic occipital (KO) region in man: an fMRI study. *Cereb Cortex*, 7(7), 690-701.
- 144 van Praag, H., Schinder, A. F., Christie, B. R., Toni, N., Palmer, T. D. & Gage, F. H. (2002)  
Functional neurogenesis in the adult hippocampus. *Nature*, 415(6875), 1030-4.

- 145 Wang, Y., L. Wang, et al. (1995)  
How is direction selectivity organized in the extrastriate visual area PMLS of the cat?  
*Neuroreport* 6(15): 1969-74.
- 146 Watamaniuk, S. N., Sekuler, R. & Williams, D. W. (1989)  
„Direction perception in complex dynamic displays: the integration of direction information. *Vision Res* 29, 47-59.
- 147 Weliky, M., Bosking, W. H. & Fitzpatrick, D. (1996)  
„A systematic map of direction preference in primary visual cortex. *Nature* 379, 725-728.
- 148 Wertheimer, M. (1923)  
„Untersuchungen zur Lehre von der Gestalt, *Psychol. Frosch.* 4: 301 - 305
- 149 Williams, D. W. & Sekuler, R. (1984)  
„Coherent global motion percepts from stochastic local motions. *Vision Res* 24, 55-62.
- 150 Worgotter, F. & Eysel, U. T. (1987)  
Quantitative determination of orientational and directional components in the response of visual cortical cells to moving stimuli. *Biol Cybern*, 57(6), 349-55.

## Bibliography



## LIST OF FIGURES

Figure 1-1: Gestalt criterion .....	3
Figure 1-2: Example of Common Fate .....	3
Figure 2-1: Anatomy of a pyramidal cell .....	8
Figure 2-2: Crossing at the chiasma .....	10
Figure 2-3: The visual system of the cat .....	11
Figure 2-4: Input to area PMLS .....	13
Figure 3-1: Experimental Setup .....	21
Figure 3-2: Mapping of receptive fields .....	23
Figure 3-3: Tuning curve stimulus .....	24
Figure 3-4: Grating and RD stimulus .....	24
Figure 3-5: The coherence stimulus .....	25
Figure 3-6: SFM stimulus set I .....	27
Figure 3-7: SFM stimulus set II .....	28
Figure 3-8: SFM stimulus set III .....	28
Figure 3-9: SFM stimulus set IV .....	29
Figure 3-10: SFM stimulus set V .....	29
Figure 3-11: SFM stimulus set VI .....	29
Figure 3-12: Sample Correlogram .....	38
Figure 4-1: Tuning curves for area 17 .....	57
Figure 4-2: Polar plot of a random dot and grating tuning curve .....	57
Figure 4-3: Differences in preferred direction in area 17 .....	58
Figure 4-4: Direction indices in area 17 .....	59
Figure 4-5: Width indices for area 17 .....	59
Figure 4-6: Tuning curve for area PMLS .....	60
Figure 4-7: Polar plot for a cell in PMLS .....	60
Figure 4-8: Differences in preferred direction in area PMLS .....	61
Figure 4-9: Differences in direction indices for area PMLS .....	61
Figure 4-10: Width indices for PMLS .....	61
Figure 4-11: Firing rates as a function of decreasing coherence in area 17 .....	68
Figure 4-12: Firing rates as a function of coherence in area 17 .....	69
Figure 4-13: Fit of firing rates from A17 .....	70
Figure 4-14: Firing rates for different direction indices in area 17 .....	70
Figure 4-15: Firing rates for different width indices in area 17 .....	71
Figure 4-16: Firing rates as a function of decreasing coherence in area PMLS .....	71
Figure 4-17: Firing rates as a function of coherence in area PMLS .....	72
Figure 4-18: Fit of firing rates in PMLS .....	73
Figure 4-19: Firing rates for different direction indices in area PMLS .....	73

Figure 4-20: Firing rates for different width indices in area 17 .....	73
Figure 4-21: Firing rates as a function of coherence for areas 17 and PMLS: Stimulation in the Null direction 74	
Figure 4-22: Correlograms for different level of coherence in area 17 .....	80
Figure 4-23: Center peak width area 17 .....	81
Figure 4-24: RMA as a function of coherence .....	82
Figure 4-25: Synchronization as a function of coherence in area PMLS .....	83
Figure 4-26: Width distribution for the grating stimulus in area PMLS .....	83
Figure 4-27: Center peak width for narrow grating synchronization .....	84
Figure 4-28: RMA as a function of coherence .....	84
Figure 4-29: Center peak width for broad grating synchronization .....	85
Figure 4-30: RMA for broad grating synchronization .....	85
Figure 4-31: Frequency as a function of coherence for alpha oscillations .....	85
Figure 4-32: Relative Amplitude of the alpha oscillation .....	86
Figure 4-33: LFP power spectra for different level of coherence in area 17 .....	96
Figure 4-34: Alpha and gamma power in area 17 as a function of coherence .....	97
Figure 4-35: Analog Power Spectrum in Area PMLS .....	99
Figure 4-36: LFP Power in Area PMLS .....	99
Figure 4-37: Dataset for the SFC analysis in area 17 .....	106
Figure 4-38: Auto-SFC values in area 17 .....	107
Figure 4-39: Cross-SFC values in area 17 .....	108
Figure 4-40: Dataset for the SFC analysis in area PMLS .....	110
Figure 4-41: Auto-SFC values in PMLS .....	111
Figure 4-42: Cross-SFC values in PMLS .....	112
Figure 5-1: Example of a SFM tuning curve in area PMLS .....	131
Figure 5-2: Polar plot for the example shown in Fig. 5-1. ....	132
Figure 5-3: Histogram of difference in preferred direction .....	132
Figure 5-4: Example for the first set of SFM stimuli .....	134
Figure 5-5: Average response elicited by the first set of SFM stimuli .....	135
Figure 5-6: Example for the second set of SFM stimuli .....	136
Figure 5-7: Average response elicited by the second set of SFM stimuli .....	137
Figure 5-8: Example for the third set of SFM stimuli .....	138
Figure 5-9: Average response elicited by the third set of SFM stimuli .....	139
Figure 5-10: Example for the fourth set of SFM stimuli .....	140
Figure 5-11: Average response elicited by the fourth set of SFM stimuli .....	140
Figure 5-12: Example for the fifth set of SFM stimuli .....	141
Figure 5-13: Example for the sixth set of SFM stimuli .....	141
Figure 5-14: Average response elicited by the fifth set of SFM stimuli .....	142
Figure 5-15: Average response elicited by the sixth set of SFM stimuli .....	142

## LIST OF ABBREVIATIONS

ANOVA	Analysis of Variance
BOLD	blood oxygenation level dependent
CD	Critical Difference
fMRI	functional magnetic resonance imaging
LFP	Local field potential
LS	lateral suprasylvian
PET	Positron Emission Tomography
PLSD	Protected least significant difference
PMLS	Posteromedial lateral suprasylvian area
PSTH	Peri-Stimulus-Time-Histogram
RMA	Relative modulation amplitude
SFM	Shape-from-Motion



## LEBENS LAUF

Geburtsdatum: 16. Januar 1972

Geburtsort: Hameln

1978-1991: Schulausbildung in Hameln

1991: Abitur am Schiller-Gymnasium Hameln

1991-1992: Zivildienst beim Rettungsdienst des Deutschen Roten Kreuzes

1992: Staatliche Prüfung zum Rettungssanitäter

1992-1994: Studium der Physik an der TU Clausthal

1995-1996: Fortsetzung des Physikstudiums an der Freien Universität Berlin.  
Spezialisierung auf das Gebiet der Molekularen Biophysik

1996-1997: Diplomarbeit am Molecular Biophysics Laboratory at Boston University

1997: Diplom in Physik an der Freien Universität Berlin.  
Titel der Diplomarbeit: „Setup of a Step Scan FTIR Experiment and Investigation of Structural Changes in the Core Structure of Bacteriorhodopsin“

1998-2002: Promotion am Max-Planck-Institut für Hirnforschung.

2002-2004: Berater bei der syspilot Industrie Consulting GmbH

seit 2004: Wissenschaftlicher Mitarbeiter bei der Seibersdorf Research GmbH,  
Bereich Neuroinformatik



## DANKSAGUNG

Mein herzlicher Dank gilt meinen Eltern, die durch die Finanzierung meines Studiums diese Dissertation überhaupt erst ermöglicht und mich auf diesem Weg immer ermutigt und unterstützt haben.

Besonderers danken möchte ich Herrn Prof. Wolf Singer sowie Herrn Prof. Andreas Engel für die Möglichkeit, diese Dissertation am Max-Planck-Institut für Hirnforschung anfertigen zu können, sowie für die zahlreichen wissenschaftlichen Diskussionen über die Arbeit. Weiterhin danke ich Herrn Prof. Ronald Tetzlaff für die Bereitschaft, diese Arbeit zu begutachten.

Ferner gilt mein Dank:

Herrn Dr. Jan-Hinrich Schröder, der mich in die Geheimnisse der Elektrophysiologie und der Synchronisationstheorie eingewiesen hat und mir bei allen kleinen und großen Problemen immer als verlässlicher Ratgeber zur Seite stand.

Frau Sandra Schwegmann, ohne die der Abschluss der Experimente unendlich viel schwerer geworden wäre und die immer jede Menge gute Laune versprüht hat.

Herrn Dr. Ralf Galuske für seine Unterstützung besonders in der zweiten Hälfte der Dissertation.

Herrn Ulrich Fickel für seine Unterstützung bei einer Vielzahl der hier beschriebenen Experimente.

Herrn Dr. Danko Nikolic für die vielen interessanten und endlosen Diskussionen, die gründliche Durchsicht der Arbeit und unsere wichtigen Erfahrungen mit *knoon*.

Frank Borchard, Dr. Matthias Munk, Dr. Sonja Grün, Michael Niessing, Gordon Pipa, Jun-Suk Kang, Gabi Schneider und Birgit Voigt für die viele gemeinsam am MPI verbrachte Zeit.

Herrn Leber, Herrn Herzberger sowie allen Mitarbeitern der EDV- und Elektronikabteilung für ihre Hilfe.

Dr. Kristiane Kiefert, Maren Kurschat sowie allen Mitarbeitern des Tierhauses für ihre Unterstützung.

meiner Frau Ute, die mir besonders in der Endphase dieser Dissertation motivierend zur Seite stand.

